Chapter 5
Electron–Atom Collisions

Abstract The theory of electron–atom collisions including excitation, ionization, and recombination is presented in the framework of Fermi's equivalent photon method, the similarity function approach, and semi-empirical analytical formulas. Collisional excitation is described via a quasi-classical consideration. Dipole-allowed, dipole-forbidden, and intercombination electron transitions are considered including intermediate coupling effects. Comparisons between different theoretical approaches and experimental data for excitation cross-sections are provided for various atoms and type of electronic transitions. Semi-empirical analytical formulas for excitation, de-exciation, ionization, and three-body recombination are given. Complex dielectronic recombination rates in dense plasmas are presented with account for density and electric field effects. Extensive numerical data for dielectronic recombination into H-, He-, and Li-like ions taking into account multi-channel Auger and radiative decay are given for all elements with nuclear charge Z_n = 2–42 together with easy to use scaled semi-empirical formulas. The theory of excited states coupling and collisional redistribution for dielectronic recombination is developed.

5.1 Fermi Equivalent Photon Method

The radiative–collisional processes appear to be a wide domain for the application of Kramers electrodynamics (KrED). These are processes in which the electron participates while moving along a classical highly curved quasi-parabolic orbit (Kogan et al. 1992). The most natural domain for the application of the KrED is the physics of multicharged ions (MCI).

According to the Fermi concept (Fermi 1924) of equivalent photons (EPh), the electromagnetic field produced by an external particle (e.g., an electron) in the vicinity of a MCI location may be interpreted as a flux of equivalent photons incident on the MCI. It can be shown that this description is applicable provided the dipole approximation for describing the interaction between the bound electron of the MCI and the incident electron of the plasma holds true. In this case, the dipole approximation describes in an universal manner all the processes of energy loss

F. B. Rosmej et al., *Plasma Atomic Physics*, Springer Series on Atomic, Optical, and Plasma Physics 104, https://doi.org/10.1007/978-3-030-05968-2_5

induced by the incident electron (either due to radiation emission during a collision with an ion or due to an inelastic non-radiative collision with an ion) as the processes of the emission of real or equivalent photons. The probability of both processes is determined by the dipole matrix element for the corresponding inelastic (radiative or non-radiative) transition of the incident electron.

The spectral intensity distribution of the EPh may be described on the basis of the classical radiation theory. In this case, the intensity of the EPh flux is simply determined by the Fourier transforms of the electron coordinates determined in turn by its classical trajectory. This approach makes it possible to treat several important radiative–collisional processes:

(a) excitation of an ion by electron impact treated as an absorption of the EPh by this ion,
(b) the same excitation as in a) but with subsequent re-emission of a real photon as a resonance fluorescence of the EPh,
(c) dielectronic recombination as a resonance fluorescence of the EPh, which results in a recombination of the incident electron.

An essential advantage of the EPh method is related to applications of purely radiative processes to the description of non-radiative processes (both, collisional and radiative–collisional). Several processes are of resonant character with respect to the absorption of the EPh by the ion and of non-resonant character, for which the intermediate state of a two-step "absorption–re-emission" process is not real and consequently is not obeying the energy conservation law (this state is formed by the process of virtual excitation with the energy $E \neq \hbar\omega_0$, where ω_0 is the frequency of a resonant transition). These non-resonant processes are known as polarization radiation (Thytovich and Oiringel 1991) and can be treated as the non-resonant scattering of the EPh by the ion. The polarization radiation is determined by the dynamical polarizability of ion in the domain of non-resonant frequencies.

For the application of the Fermi method, it is necessary that effective distances r_{eff} which are responsible for the main contribution to the inelastic collision cross-section are much greater than the characteristic size of the bound electron orbit. This requirement is especially well fulfilled for MCI. Let us illustrate this for the excitation of a $\Delta n = 0$ transition. The electron orbit size is of the order $1/Z$ (in atomic units), transition energies ΔE for $\Delta n = 0$ transitions in MCI are typically of the order of Z, and the values of r_{eff} for the corresponding cross-section can be estimated as

$$r_{\text{eff}} \sim r_{\omega=\Delta E/\hbar} \sim (Z/\Delta E^2)^{1/3} \sim Z^{-1/3} \gg Z^{-1}. \tag{5.1}$$

This inequality justifies the use of the dipole approximation for the potential V of interaction between bound and incident electrons (with space coordinate vectors $\mathbf{r}_\text{i}$ and $\mathbf{r}_\text{e}$, respectively), $V = e^2 \mathbf{r}_\text{i} \cdot \mathbf{r}_\text{e}/\mathbf{r}_\text{e}^3$. In this framework, the static Coulomb interaction between the bound and incident electrons transforms to the processes of emission and absorption of the EPh by electrons, and the corresponding probabilities are determined by the conventional dipole matrix elements.

The electric field produced by the incident electron at the location $r = 0$ of the ion is equal to

$$\mathbf{F}(0,t) = -e\mathbf{r}_e(t)/\mathbf{r}_e^3(t), \tag{5.2}$$

where the dependence $\mathbf{r}_e(t)$ describes the classical trajectory of the incident electron. Using the equation of the motion of the incident electron in the field of the MCI $m\ddot{\mathbf{r}}_e = -Ze^2\mathbf{r}_e/\mathbf{r}_e^3$, it is convenient to transform (5.2) into the form

$$F(t) = \ddot{\mathbf{r}}_e(t)m/Ze. \tag{5.3}$$

The spectral distribution for the EPh flux I_ω of the electric field of the incident electron can be expressed in terms of the Fourier transforms:

$$I_\omega = \frac{c}{4\pi^2}\frac{1}{\omega}\left\{|F_{x,\omega}|^2 + |F_{y,\omega}|^2\right\} = \frac{c\omega^3}{4\pi^2 Z^2}\left\{|x_\omega|^2 + |y_\omega|^2\right\}, \tag{5.4}$$

where x and y are the coordinates of the incident electron in the plane of its motion. The Fourier transforms of the electron space coordinates in the Coulomb field are well known (Berestetskii et al. 1982; Landau and Lifschitz 2003; Jackson 1998). Thus, we obtain

$$I_\omega = \frac{c\omega^2}{4\upsilon^4}\left\{\left[H_{i\nu}^{(1)'}(i\nu\varepsilon)\right]^2 - \frac{\varepsilon^2-1}{\varepsilon^2}\left[H_{i\nu}^{(1)}(i\nu\varepsilon)\right]^2\right\}, \tag{5.5}$$

where υ is the electron initial velocity, $H_{i\nu}^{(1)}$ is the Hankel function, ε is the orbital eccentricity;

$$\varepsilon = 1 + 2EM^2/Z^2; \quad \nu = \omega Z/\upsilon^3;\ E = m\upsilon^2/2; \tag{5.6}$$

E and M are the energy and angular momentum of the incident electron, respectively. In the limit of low EPh frequencies, $\nu \ll 1$, the main contribution to the spectral distribution of the EPh flux integrated over the electron impact parameters ρ is due to the distance from the field center trajectories, ($\rho \gg a \equiv Z/2E$), which are nearly rectilinear, with eccentricity $\varepsilon \gg 1$. In this case, (5.5) is transformed to

$$I_\omega = \left(c\omega/2\pi^2\upsilon^4\right)\left\{K_0^2(\omega\rho/\upsilon) + K_1^2(\omega\rho/\upsilon)\right\}, \tag{5.7}$$

where $K_0(x)$ and $K_1(x)$ are the Macdonald functions. Fermi (1924) used (5.7) to describe atomic excitation by a rectilinearly moving particle.

For the description of the processes resulting in a loss of a considerable part of the incident electron energy, it is necessary to consider the EPh with high frequencies, namely $\nu \gg 1$. The main contribution to the emission of such EPh comes

from the strongly curved electron trajectories, $\varepsilon - 1 \ll 1$, which are close to the field center, $\rho \ll a$. In this Kramers domain, we arrive at the result (see Chap. 3)

$$I_\omega = \pi^{-2} Z^{-2} cMG_0(\omega M^3/3Z^2) \tag{5.8a}$$

with [see also (3.47)]

$$G_0(x) = x\left[K_{1/3}^2(x) + K_{2/3}^2(x)\right]. \tag{5.8b}$$

5.1.1 *Excitation by Electron Impact as Absorption of Equivalent Photons by an Ion*

The equivalent photons method makes it possible to obtain a simple analytical description of the collisional processes and treat them as purely radiative. Within this framework, the excitation of multicharged ions (MCI) by electron impact may be clearly considered as absorption of the equivalent photons (EPh) with a resonant frequency $\omega_0 = \Delta E_{\mathrm{if}}/\hbar$. The relationship between the collisional cross-section σ_{exc} and the cross-section σ_{abs} for the absorption of the EPh can be obtained by means of equating the number of excitation events, during the time interval $\mathrm{d}t$ (caused by the collisions of the MCI with the electron flux) with a space density n_{e} and a particle velocity υ_{e} to the corresponding number of transitions caused by the absorption of the EPh produced by a single electron, i.e., $\mathrm{d}N_{\mathrm{exc}} = n_{\mathrm{e}}\upsilon_{\mathrm{e}}\sigma_{\mathrm{exc}}\mathrm{d}t$. This is multiplied by the total number of electrons in the volume $\mathrm{d}V$ corresponding to the time interval $\mathrm{d}t$, $\mathrm{d}V = 2\pi\rho\mathrm{d}\rho\upsilon_{\mathrm{e}}\mathrm{d}t$,

$$\mathrm{d}N_{\mathrm{abs}} = \int 2\pi\rho\mathrm{d}\rho n_{\mathrm{e}}\upsilon_{\mathrm{e}}\mathrm{d}t \int \mathrm{d}\omega\left(cE_\omega^2/4\pi^2\hbar\omega\right)\sigma_{\mathrm{abs}}(\omega), \tag{5.9}$$

where the expression in brackets corresponds to the spectral distribution of the EPh flux (5.4) produced by a single electron with a fixed value of the impact parameter ρ. Assuming $\sigma_{\mathrm{exc}} = \int \sigma_{\mathrm{exc}}^l \mathrm{d}l$ for the relation of the total and partial (with respect to the orbital quantum number l) cross-sections, we arrive at the result

$$\sigma_{\mathrm{exc}}^l = 2\pi(\hbar/m\upsilon_{\mathrm{e}})^2(l+1/2)\int \sigma_{\mathrm{abs}}(\omega)\left(cE_\omega^2/4\pi^2\hbar\omega\right)\mathrm{d}\omega. \tag{5.10}$$

Furthermore, the expression for the EPh flux can be taken out of the integral at the frequency ω_0 of the radiative transition in the MCI core because of its weak frequency dependence in comparison with the absorption cross-section. The resulting integral over ω gives the well-known expression

$$\int \sigma_{\mathrm{abs}}(\omega)\mathrm{d}\omega = \pi^2(c/\omega)^2 g_{\mathrm{f}} 4\omega_0^2 |d_{\mathrm{if}}|^2/3\hbar c^3, \tag{5.11}$$

where d_{if} is the dipole moment matrix element of the transition and g_{f} is the statistical weight of the upper level.

Substituting the spectral distribution (5.5) into (5.10) for the EPh flux, produced by the electron in the Coulomb field of the MCI, we finally obtain

$$\begin{aligned}\sigma^{l}_{\mathrm{exc}} = {} & \frac{8\pi^3}{3}(\hbar/m\upsilon_e)^2\omega_0^2|d_{\mathrm{if}}|^2 g_{\mathrm{f}}\upsilon_e^{-4}(l+1/2) \\ & \cdot\left\{\left[H^{(1)'}_{\mathrm{iv}}(\mathrm{i}v\varepsilon)\right]^2 - (\varepsilon^2-1)\varepsilon^{-2}\left[H^{(1)}_{\mathrm{iv}}(\mathrm{i}v\varepsilon)\right]^2\right\}.\end{aligned} \tag{5.12}$$

The transition in (5.12) to the Kramers electrodynamics (KrED) domain ($v \gg 1$) corresponds to the transition from (5.5) to (5.8). Thus, we obtain the result in the KrED domain:

$$\sigma^{l}_{\mathrm{exc}} = (8\pi/3)(\hbar/m\upsilon_{\mathrm{e}})^2(g_{\mathrm{f}}/g_{\mathrm{i}})f_{\mathrm{if}}Z^{-2}(l+1/2)^2 G_0[\omega(l+1/2)^3/3Z^2], \tag{5.13}$$

where f_{if} is the oscillator strength for the transition considered and g_{i} is the statistical weight of the lower level.

Equation (5.13) manifests explicitly the interrelation between the independence of the radiation characteristics on the energy (see also Chap. 3) and the well-known fact of the finiteness of the excitation cross-section at threshold. Thus, we face once more the phenomenon, inherent to the KrED, of the independence of the spectral distribution on the energy, which leads to a smooth transition between the discrete and continuous energy spectra for the processes with both real (from the BR to the PR) and equivalent photons (the transition from the Born approximation domain for the excitation to its threshold and further to the DR).

The total excitation cross-section is obtained by summing up the partial cross-section (5.10) over l, yielding an expression in terms of the well-known spectral distribution for the Coulomb bremsstrahlung Gaunt-factor $g(v)$ (Kogan et al. 1992)

$$\sigma^{\mathrm{if}}_{\mathrm{exc}} = \frac{8\pi^2}{\sqrt{3}}|d_{\mathrm{if}}|^2 g_{\mathrm{i}}^{-1}\upsilon_{\mathrm{e}}^{-2} g[Z\omega_0/(2E)^{3/2}]. \tag{5.14}$$

The function $g(v)$ has a simple analytic approximation:

$$g(v) \approx \frac{\sqrt{6}}{\pi}\cdot\ln\left[\left(\frac{2}{\gamma\cdot v}\right)^{1/\sqrt{2}} + \exp\left(\frac{\pi}{\sqrt{6}}\right)\right]. \tag{5.15}$$

The result (5.14) was derived earlier (Bazylev and Chibisov 1981) in a somewhat different way. It should be noted that (5.14) is valid up to the excitation threshold where Kramers EPh spectrum (5.8) does not depend on the incident

electron energy at all. In the opposite limit of a fast-incident particle, the cross-section (5.14) exhibits a logarithmic (Born-type) structure. It is this result that was derived by Fermi for atomic excitation and ionization by fast particles. Equation (5.14) is in good agreement with quantum numerical calculations as well as with experimental data (Bazylev and Chibisov 1981; Gau and Henry 1977).

It should be also noted that for the first time, the interrelation between the excitation cross-section for allowed dipole transitions and the Gaunt factor for bremsstrahlung in a Coulomb field for the general quantum case (Sommerfeld formula) was investigated by Gailitis (1963). So far we have restricted ourselves to the case of quasi-classical incident electron motion; however, the applicability of the KrED approach to the calculation of excitation cross-sections remains valid also for an arbitrary (not necessarily purely Coulombic) ionic potential (e.g., of a Thomas–Fermi ion). The description of these excitation cross-sections may be achieved by the replacement of the Coulomb EPh intensity by the corresponding EPh spectral intensity in (5.5).

5.1.2 Autoionization Decay and Dielectronic Capture

Let us recall the essence of the dielectronic recombination (DR) process. An incident electron with the energy E_i excites an ion core with an excitation energy $\Delta E = \hbar\omega_0$. In this case, if the energy E_i is smaller than ΔE, the electron is finally captured by the ion into a state with the energy $E_\mathrm{f} = -\mathrm{Ry}/n_\mathrm{f}^2$ obeying the condition

$$E_\mathrm{i} - E_\mathrm{f} = E_\mathrm{i} + 1/2n_\mathrm{f}^2 = \Delta E = \hbar\omega_0. \tag{5.16}$$

This capture results in a double excited state of the ion, namely the ion core electron is excited with energy ΔE while the captured electron occupies a highly excited level of the ion. This state of the ion can decay in two possible ways:

(i) by relaxation of the ion core electron into the initial ground state with the simultaneous ejection of the captured electron from the ion: This process is known as autoionization;
(ii) by radiative decay of the ion core electron, resulting in its return to the initial state after the emission of a photon of energy $\hbar\omega \simeq \hbar\omega_0 = \Delta E$, whereas the captured electron remains in the ion.

For illustration, Fig. 5.1 shows the relevant energy level diagram for the He-like $2l2l'$-satellites close to the H-like Lyman-alpha transition (so-called Ly_α-satellites). The energy of the $2l2l'$-satellites is approximately (in the H-like approximation) $E_\mathrm{sat} \approx 2 \cdot Z^2\mathrm{Ry}/4 = Z^2\mathrm{Ry}/2$ which is half of the ionization potential of the H-like ground state ($Z^2\mathrm{Ry}$). The series limit of the autoionizing levels $2lnl'$ is the first excited state $2l$. Radiative decay from the $2l2l'$-levels populates the single excited levels $1s2l\ ^{1,3}\mathrm{L}$, from which radiative decays (W- and Y-line) populate finally the

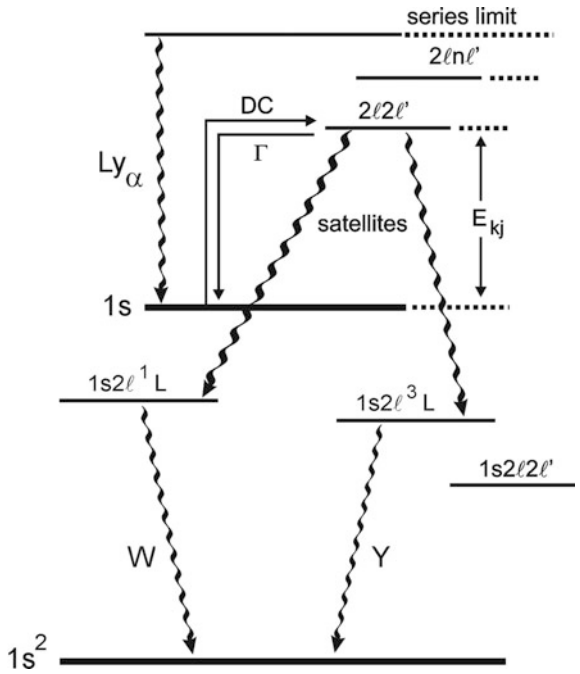

Fig. 5.1 Energy level diagram relevant for the He-like autoionizing levels $2l2l'$, so-called Ly_α-satellites

ground state $1s^2$. The chain of processes, dielectronic capture ($1s + e - 2l2l'$), radiative decay to single excited levels ($2l2l' - 1s2l + h\nu$) and radiative decay to the ground state ($1s2l\ ^{1,3}L - 1s^2 + h\nu'$), is called dielectronic recombination (DR channel) because an effective recombination has taken place (from the H-like ground state $1s$ to the He-like ground state $1s^2$).

Thus, the DR process as well as the photorecombination (PhR) process result in the capture of an incident electron and its simultaneous photon emission. The difference is that the photon is emitted by the ion core electron in the DR process rather than by the incident electron as in the PhR process. The relationship between the PhR and the DR is analogous to the interrelation between conventional and polarization bremsstrahlung (Astapenko 2013).

As a rule, the DR rate is large for ions with a complex core which possesses transitions between the levels with the same quantum number n (the transitions with $\Delta n = 0$, e.g., $2s \to 2p$ transitions in lithium-like and more complex ions). The transition energy $\Delta E = \hbar\omega_0$ for $\Delta n = 0$ and $Z \gg 1$ is of the order of $Z \cdot \mathrm{Ry}$, while the ionization energy is of the order of $Z^2 \cdot \mathrm{Ry} \gg \Delta E$. Since the energy E of the incident recombining electron is in any case smaller than the excitation energy, this implies the following inequality

$$(Z^2\mathrm{Ry}/E)^{1/2} \sim Ze^2/\hbar v \gg 1, \tag{5.17}$$

which justifies the application of a quasi-classical approach to the description of dielectronic recombination process.

An application of the proposed approach to the DR implies the treatment of a DR process as a resonance fluorescence with a complicated intermediate state which appears after the capture of the incident electron by an ion and possesses an additional channel of decay via the autoionization. The resonance fluorescence thus involves three types of quantum states:

- an initial state with total energy E_1 of a non-excited ion and an initial spectral distribution I_0 of equivalent photons;
- an intermediate state with total energy E_2 of an excited ion with a captured incident electron on a highly excited ionic level (double excited ion with an ion charge reduced by unity) and an EPh distribution I_0 reduced by one EPh of energy ω_{eq};
- a final state with total energy E_3 of a single excited ion with a charge reduced by unity, an EPh of energy ω and a EPh distribution I_0. The state energies are connected by conservation laws:

$$E_3 - E_1 = \omega - \omega_{eq}, \quad E_3 - E_2 = \omega - \omega_0. \tag{5.18}$$

The resonance fluorescence probability has the form (Heitler 1984)

$$w_{RF} = \frac{|V_{21}|^2 |V_{32}|^2}{[(\omega - \omega_{eq})^2 + \Gamma^2/4][(\omega - \omega_0)^2 + \gamma^2/4]}, \tag{5.19}$$

where V_{21} and V_{32} are the matrix elements that correspond to the absorption of an EPh at frequency ω_{eq} and the emission of a real photon at frequency ω, respectively; γ and Γ are the total probabilities (per unit time) of photon absorption and emission, i.e.,

$$\gamma(E) = 2\pi \sum_{k} |V_{32}|^2 \delta(E - E_3), \tag{5.20}$$

$$\Gamma(E) = \gamma \sum_{k_{eq}} |V_{21}|^2 \frac{1}{[(E - E_2)^2 + \gamma^2/4]}. \tag{5.21}$$

The quantities $\Gamma(E)$ and $\gamma(E)$ in (5.21) should be taken at the energy $E = E_3$, but in fact they depend only weakly on energy.

It is noteworthy to recall an implication of (5.19): For the elementary process of absorption–emission, the energies of the absorbed and emitted photons are equal (within the very small width Γ). This "memory" about the absorbed photon by the ion (atom) manifests itself in the probability (5.19) which does not reduce to the product of absorption and emission probabilities. Indeed, the first factor in the

denominator of (5.19) does not bind (approximately via the corresponding δ function) the energies of the initial (ω_{eq}) and exactly resonant (ω_0) photons, but only the energies of the initial and final (ω) photons. It is the continuity of the incident photon spectrum that reduces the resonance fluorescence to the two independent processes of absorption and subsequent emission. Thus, the DR width Γ_{DR} is formed by the width γ (5.20) and by the probability (per unit time) of the autoionization process of the intermediate state:

$$\Gamma_{DR} = \gamma + \Gamma_A \,. \tag{5.22}$$

This relation implies the possibility of the return of the recombined electron to the continuum energy state with the simultaneous equivalent photon re-emission by the ion core.

The matrix element V_{21} is determined by the oscillator strength of the radiative transition in an ion ($V_{21} \sim d_{21}$, where d_{21} is the matrix element of the dipole moment of a bound radiating electron in an ion) and is proportional to the flux density of the EPh incident on an ion. For the continuous EPh spectrum, the total probability of absorption Γ_{RF} is expressed in terms of I_0:

$$\Gamma_{RF} = 2\pi I_{0,\omega} \overline{|V_{21}|^2}, \tag{5.23}$$

where the bar ($\overline{|V_{21}|^2}$) denotes the averaging over the angles of the absorbed photon wave vector. As applied to the specific conditions of the model for the DR considered, the summation over k_{eq} in (5.21) should be supplemented by a summation over the final states of the captured electron. This procedure combined with the conservation law for the incident electron energy leads to the result:

$$\Gamma_{DR} = \Gamma_{RF} Z^2/n^3. \tag{5.24}$$

Using then the expression for the DR total probability summed over the EPh frequencies

$$\sum_{\omega} w_{DR} = \frac{\gamma \Gamma_A}{\gamma + \Gamma_A} \tag{5.25}$$

we obtain the rate of the autoionization process

$$\Gamma_A = \frac{f_{12}}{\pi n^3} l G_0 \left(\frac{\omega_0 M^3}{3Z^2} \right), \tag{5.26}$$

where f_{12} is the oscillator strength of the excited radiative transition in the ion core, and the function $G_0(x)$ is given by (5.8b). Equation (5.26) coincides with the result which may be obtained from the exact quantum calculation (Beigman et al. 1981; Sobelman and Vainshtein 2006) of autoionization rate in Kramers domain

(quasi-classical motion of the incident electron along a quasi-parabolic orbit, $Ze^2/\hbar\upsilon \gg 1$, $\rho \ll a$). The total DR rate corresponding to the capture of an electron into an ionic nl state is then given by the expression

$$\alpha_{\mathrm{DR}} = \left(\frac{2\pi}{T}\right)^{3/2} \frac{g(2)}{g(1)} \frac{(2l+1)\gamma\,\Gamma_{\mathrm{A}}}{(\gamma+\Gamma_{\mathrm{A}})} \exp\left[-\frac{\omega}{T} + \frac{\mathrm{Z}^2}{2n^2T}\right], \tag{5.27}$$

where T is the electron temperature, and $g(1)$ and $g(2)$ are the statistical weights for the ground and excited ion levels, respectively.

The result (5.26) may also be derived on the basis of the relation between the autoionization probability and the cross-section for the ion excitation by electron impact near the ionization threshold. This relation follows from the detailed balance equation for the mutually inverse processes of autoionization and electron capture into an ion nl-level with the excitation of the $1 \rightarrow 2$ transition in an ion core, i.e.,

$$(2l+1)g_2\Gamma_{\mathrm{A}}(nl) = Z^2 n^{-3} \omega g_1 \sigma_{\mathrm{exc}}(l)/\pi^2 a_0^2. \tag{5.28}$$

Substituting the KrED result (5.13) for the excitation cross-section σ_{exc}, we obtain (5.26).

All the methods for the derivation of autoionization, dielectronic capture, and dielectronic recombination are equivalent in the sense that they are based on the dipole approximation for the interaction between an incident and a bound electron. It is exactly this approximation that allows us to treat all of the processes related to an energy loss of the incident electron as processes of effective radiation of either real (bremsstrahlung and photorecombination radiation) or equivalent (excitation, dielectronic recombination, polarization bremsstrahlung, and polarization recombination) photons.

5.2 Ionization by Electron Impact

5.2.1 Thomson Formula

Ionization of atoms by electron impact is one of the most important elementary processes defining the characteristics both of laboratory and astrophysical plasmas. A consistent description of this phenomenon involves the quantum mechanical approach; however, its main qualitative features can be determined also within the framework of classical mechanics. A corresponding formula for the cross-section was first proposed by J. Thomson in 1912, even before the development of the quantum theory. The classical consideration of ionization of an atom by electron impact

$$e + A \rightarrow A^{+} + 2\,e \tag{5.29}$$

carried out by Thomson is based on the assumption of elastic scattering of the projectile by bound electrons of the target. In this case, ionization results from the transfer of energy to an atom, that is, higher than the ionization potential of the electron subshell under consideration (as a result of projectile scattering). The applicability of the classical method to estimate the atomic ionization cross-section is based on the exact coincidence of quantum mechanical and classical cross-section of elastic electron–electron scattering.

Without considering the binding of atomic electrons to the nucleus, the expression for the integrated (with respect to the angle of scattering) cross-section of collisional ionization can be represented as (Astapenko and Lisitsa 2007)

$$\sigma_{\mathrm{i}} = \int\limits_{\Delta E > I} \mathrm{d}\sigma, \tag{5.30}$$

where $\mathrm{d}\sigma$ is the differential cross-section of electron–electron scattering, ΔE is the energy transferred from a projectile, I is the atomic ionization potential. Neglecting the change of the energy of the incident electron in comparison to its initial energy, we can derive the cross-section $\mathrm{d}\sigma$ with the help of the Rutherford formula (that describes the cross-section of elastic scattering of a charged particle in the Coulomb potential):

$$\frac{\mathrm{d}\sigma^{(R)}}{\mathrm{d}\Omega} = \left(\frac{Z\,e^2}{2\,m\upsilon^2\,\sin^2(\theta/2)}\right)^2. \tag{5.31}$$

$\mathrm{d}\Omega$ is an element of the solid angle, into which a projectile is scattered, θ is the angle of scattering, and υ is the velocity of the incident electron. For electron–electron scattering, we have $Z = 1$. Assuming that the value of energy transferred to an atomic electron ΔE is equal to the recoil energy, it is easy to find that

$$\Delta E = 4\,E\,\sin^2(\theta/2). \tag{5.32}$$

For the derivation of (5.32), the relation for a transmitted pulse that neglects the binding of an atomic electron to the nucleus was used, i.e.,

$$\Delta p = 2\,m\upsilon\sin(\theta/2), \tag{5.33}$$

that follows from elementary consideration of elastic scattering (Landau and Lifschitz 2005). With the use of (5.32), it is possible to express the angle of scattering in terms of energy transferred to an atomic electron ΔE. As a result, we obtain from (5.31) for a one-electron atom

$$\mathrm{d}\sigma = \frac{\pi e^4 \,\mathrm{d}\Delta E}{E(\Delta E)^2}, \tag{5.34}$$

where $E = mv^2/2$ is the energy of the incident electron. Substituting the expression (5.34) in (5.30) and integrating over the possible values of the transferred energy ΔE, we obtain the so-called *Thomson formula* for the cross-section of collisional ionization of a one-electron atom:

$$\sigma_\mathrm{i} = \int_I^E \mathrm{d}\sigma = \frac{\pi e^4}{E}\left(\frac{1}{I} - \frac{1}{E}\right), \quad E > I. \tag{5.35}$$

If the dimensionless parameter $x = E/I$ is introduced, the right-hand side of (5.35) can be rewritten as

$$\sigma_\mathrm{i}^{(\mathrm{Th})}(E) = \frac{\pi e^4}{I^2}\frac{x-1}{x^2}, \quad x \geq 1. \tag{5.36}$$

It is clear that the value $x_\mathrm{th} = 1$ ($E_\mathrm{th} = I$) is the threshold value: At $x < 1$, the process cross-section is equal to zero since the energy of an incident electron is insufficient for ionization of an atom.

5.2.2 Similarity Function Method for the Ionization Cross-Section

Qualitatively, the Thomson formula (5.36) renders properly the features of the collisional ionization of a one-electron atom. However, from the quantitative point of view the formula is not very precise. To obtain a realistic description, it is advisable to represent the expression (5.36) as follows (Astapenko and Lisitsa 2007):

$$\sigma_\mathrm{i}^{(\mathrm{Th})}(E) = \pi a_\mathrm{I}^2 f^{(\mathrm{Th})}(E/I). \tag{5.37}$$

Here the dimensionless Thomson *similarity function* $f^{(\mathrm{Th})}(x) = (x-1)/x^2$ describing the dependence of the collisional ionization cross-section on a projectile energy and the "ionization radius" are introduced:

$$a_\mathrm{I} = \frac{e^2}{I}. \tag{5.38}$$

As one can easily see from (5.38), the ionization radius is equal to the distance between incident and atomic electrons, at which the energy of the Coulomb

interaction is equal to the atomic ionization potential. The radius a_{I} defines the cross-section $\sigma_{\mathrm{I}} = \pi a_{\mathrm{I}}^2$ that characterizes the cross-section of collisional ionization of a one-electron atom by an order of magnitude.

From formula (5.37), it follows that the projectile energy enters in the expression for the collisional ionization cross-section only in terms of the ratio E/I. This circumstance forms the basis for the similarity function method that assumes that the ratio of the ionization cross-section to the value $\sigma_{\mathrm{I}} = \pi a_{\mathrm{I}}^2$ is a universal function of the dimensionless variable $x = E/I$. Thus, the formula (5.36) is generalized by (5.37): The similarity function $f(x)$ can be determined either within the framework of a chosen theoretical or empirical approach.

The Thomson similarity function gives a value for the cross-section maximum of $1/4$ at $x_{\max} = 2$, i.e., at $E_{\max} = 2\,I$. The comparison with experimental data shows that this value $x_{\max}$ is too low. In other words, the Thomson formula shifts the true position of the cross-section maximum closer to the threshold value $E_{\mathrm{th}} = I$. In fact, the maximum of the collisional ionization cross-section is found from $E_{\max} = 3\,I$ to $E_{\max} = 4\,I$ (see the next section).

Curiously, the Thomson formula gives a value for the cross-section maximum of collisional ionization of a hydrogen atom of $\sigma_{\mathrm{i}}^{(H)}(E_{\max}) = \pi a_{\mathrm{B}}^2 \approx 0.88\ \text{Å}^2$ (a_{B} is the Bohr radius) that is equal to the area of the first Bohr orbit. According to (5.36), the energy at cross-section maximum is $E_{\max} = 2I_{1s}^{(H)} \cong 27.2\,\mathrm{eV}$, which coincides with the atomic unit of energy.

For more realistic descriptions of the cross-section of atomic ionization by electron impact, it is necessary to develop other similarity functions. For ionization potentials $I > 10$ eV, good agreement with experimental data is obtained by the Gryzinski similarity function (Gryzinski 1959, 1965a, b, c)

$$f^{(\mathrm{Gryz})}(x) = \frac{1}{x}\left(\frac{x-1}{x+1}\right)^{3/2}\left[1+\frac{2}{3}\left(1-\frac{1}{2x}\right)\ln\left(2.7+\sqrt{x-1}\right)\right] \tag{5.39}$$

derived within the framework of classical consideration but taking into account the velocity distribution function of the bound electrons. For completeness, we mention also the Eletskii–Smirnov similarity function

$$f^{(\mathrm{ES})}(x) = \frac{10\,(x-1)}{\pi\,x\,(x+8)}, \tag{5.40}$$

obtained empirically (on the basis of comparison with experimental data). It should be noted that the functions (5.39) and (5.40) are similar to each other.

The formulas (5.36), (5.37) were obtained for a one-electron atom. For the calculation of collisional ionization of multielectron atoms, the expression (5.37) should be generalized so that the contribution of different subshells of an atom (in particular the number of electrons in each subshell) to the total cross-section is taken into account. The resultant formula looks like

$$\sigma_{\mathrm{i}}(E) = \sum_{\mathrm{nl}} N_{\mathrm{nl}}\, \pi\, a_{I_{\mathrm{nl}}}^2 f(E/I_{\mathrm{nl}})\; \theta(E - I_{\mathrm{nl}}), \tag{5.41}$$

where N_{nl} is the number of equivalent electrons, I_{nl} the ionization potential of a nl-subshell (n, l are the principal and orbital quantum numbers), and $\theta(x)$ is the Heaviside step function that describes the "inclusion" of inner atomic subshells in the process at $E > I_{\mathrm{nl}}$.

The comparison with experimental data shows that the similarity functions (5.39), (5.40) give the best result for atoms with ionization potentials $I > 10$ eV (remember that $I = \min\{I_{\mathrm{nl}}\}$). In case of multielectron atoms with a moderate value of I ($10\,\mathrm{eV} > I > 6\,\mathrm{eV}$), the Born–Compton similarity function is more adequate for the description of collisional ionization (Astapenko 2001):

$$f^{(\mathrm{BC})}(x) = \frac{2.5}{\pi}\frac{1}{x}\int_1^{y_{\mathrm{m}}} \mathrm{d}y \int_{\sqrt{x}-\sqrt{x-y}}^{\sqrt{x}+\sqrt{x-y}} \frac{\mathrm{d}t}{t^2\left[t^2 + (y - t^2)^2/0.64\right]}, \tag{5.42}$$

where $y_{\mathrm{m}} = (x+1)/2$. The similarity function (5.42) is obtained in the first Born approximation for the interaction of a projectile with atomic electrons. For its derivation, the analogy between collisional ionization and Compton scattering of the projectile eigenfield by an atom was used, and the electron shell of the atom was described within the framework of the Thomas–Fermi model.

In the case that a significant contribution to the ionization process is made by atomic subshells with large orbital quantum numbers ($l = 2, 3$), the use of the similarity functions (5.42) may be insufficient. In this case, the similarity function of the so-called Binary Encounter Bethe (BEB) approximation can be used (Kim and Rudd 1994):

$$f^{(\mathrm{BEB})}(x, u) = \frac{1}{1+x+u}\left[\frac{\ln(x)}{2}\left(1 - \frac{1}{x^2}\right) + 1 - \frac{1}{x} - \frac{\ln(x)}{1+x}\right]. \tag{5.43}$$

In (5.43), the additional parameter u is introduced that represents the ratio of the average kinetic energy of a subshell to its ionization potential. It should be noted that for a hydrogen atom (in view of the virial theorem) $u = 1$. The parameter u takes into account the decrease of the cross-section of collisional ionization of atomic subshells with high orbital momenta. This decrease is connected with the fact that at equal ionization potentials, a subshell with a higher orbital moment has a smaller radius, which results in a decrease of process cross-section.

Figure 5.2 shows the similarity functions (5.39), (5.40) as well as (5.42), (5.43). A common feature of the similarity functions presented in Fig. 5.2 is their identical near-threshold dependence: $f(x) \propto x - 1$. This dependence is a consequence of the common quantum mechanical regularity connected with the behavior of the statistical weight of the final state of an ionized electron as a function of the projectile energy. On the other hand, the asymptotic behavior of the similarity functions at

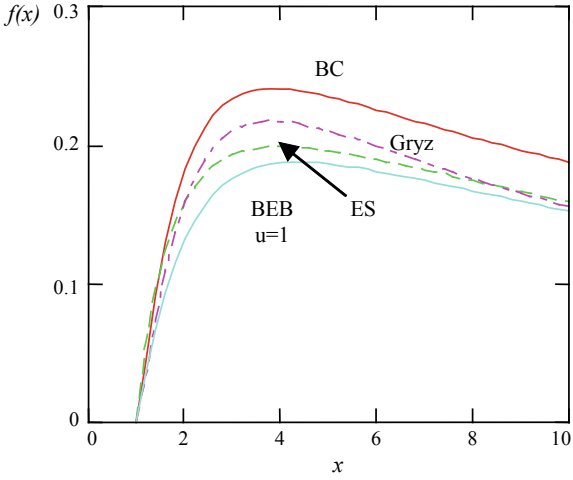

Fig. 5.2 Comparison of different similarity functions for the collisional ionization cross-section of an atom: Gryz—Gryzinski; ES—Eletskii–Smirnov; BC—Born–Compton; BEB—BEB approximation

high-incident electron energies $E \gg I$ ($x \gg 1$) is different. From formulas (5.39), (5.40) and (5.42), (5.43) and $x \gg 1$, we obtain: $f^{(\mathrm{Gryz}),\,(\mathrm{BEB})} \propto \ln(x)/x$, $f^{(\mathrm{ES}),\,(\mathrm{BC})} \propto 1/x$. The first asymptote coincides with the high-energy limit of the inelastic cross-section of the Bethe quantum mechanical theory, the second asymptote deviates from it, but provides better agreement with experimental data at not too high projectile energies.

The similarity function method favorably differs from other methods of calculation of the collisional ionization cross-section by its simplicity and reliability; it is often used for fast evaluation of the cross-sections (in particular for bulky complex configurations).

5.2.3 *Comparison with Experimental Data*

At present days, electron impact ionization cross-sections of neutral atoms have been measured for the majority of elements from the periodic table. The experimental measurements are carried out with the help of the so-called crossed-beam technique that consists of several steps:

(a) the beam of fast neutrals is produced by neutralization of fast (with an energy of several keV) ions in a chamber with low-pressure gas (about 10^{-4} torr),
(b) the ion beam is then pre-extracted from a DC gas discharge, focused, and passed through a special filter that sorts ions with respect to their velocities,
(c) the resultant beam of fast neutrals with specified energy retains the collimation of the initial ion beam, which is mandatory for high-precision measurements,
(d) the absolute neutral atom flux is measured with the help of a calibrated detector,

(e) the measurement of the collisional ionization cross-section is then carried out intersecting the neutral beam of atoms with the electron beam,
(f) ions resulting from electron–atom collisions are focused on an electrostatic analyzer extracting ions with a given charge number that are then recorded by an electron multiplier,
(g) based on the measured data, the experimental value of the ionization cross-section is finally calculated by the formula

$$\sigma_{\mathrm{i}}^{(\mathrm{exp})}(E) = \frac{J_{\mathrm{i}}(E)\, \upsilon_{\mathrm{e}}\, \upsilon_{\mathrm{n}}}{J_{\mathrm{e}}(E)\, R\, F\, \sqrt{\upsilon_{\mathrm{e}}^2 + \upsilon_{\mathrm{n}}^2}}, \tag{5.44}$$

where $J_{\mathrm{i,e}}$ are the ion and electron currents, $\upsilon_{\mathrm{n,e}}$ are the velocities of neutrals and electrons, R is the neutral flux, F is the value characterizing the degree of intersection of the neutral beam and the electron beam.

Thus, the measurement of the absolute value of the collisional ionization cross-section consists in the measurement of each value appearing in the right-hand side of (5.44).

Figure 5.3 shows the comparison of the experimental cross-section of collisional ionization of a hydrogen atom with the results of calculations by the similarity function method.

It is seen that in this case, the Eletskii–Smirnov similarity functions and the BEB approximation provide better agreement with the experiment than the Born–Compton method that considerably overestimates the cross-section. This circumstance is connected with the fact that the formulas for the Born–Compton method were obtained in the Thomas–Fermi approximation for an electron shell of an

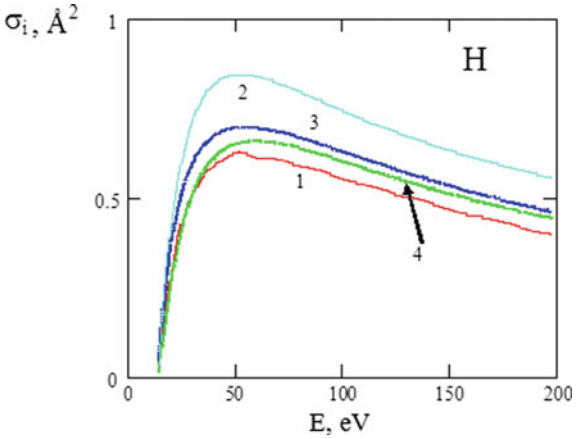

Fig. 5.3 Ionization cross-sections of a hydrogen atom by electron impact: 1—experiment, 2—Born–Compton method, 3—Eletskii–Smirnov formula, 4—BEB approximation for $u = 1$

ionized atom that is only valid for multielectron atoms. Moreover, in this case the ionization potential of a hydrogen atom (13.6 eV) is overestimated and the use of the Born–Compton similarity function is beyond its range of applicability.

From Fig. 5.3, it follows that the maximum of the ionization cross-section of a hydrogen atom by electron impact is reached at an incident electron energy $E_{\max} \approx 50$ eV in contrast to the value $E_{\max} \approx 27.2$ eV following from the Thomson formula (5.36). The value of the cross-section at the maximum is about 0.6 Å^2, which is somewhat less than the prediction of the Thomson theory (0.88 Å^2). Thus in the case of a hydrogen atom, the classical approach of J. Thomson strongly shifts the position of a maximum to a too low energy range, but gives a satisfactory value of the maximum cross-section.

It is of interest to compare the cross-section of photoionization of a hydrogen atom $\sigma_{\text{ph}}(\omega)$ with the cross-section of ionization by electron impact. The cross-section of photoionization of a hydrogen atom reaches its maximum at threshold, i.e., at a photon energy of 13.6 eV, whereas the maximum of the photoionization cross-section (0.064 Å^2) is about an order of magnitude less. Different asymptotic behavior of the cross-sections can also be noted: $\sigma_{\text{ph}}(\omega) \propto \omega^{-7/2}$, while $\sigma_{\text{i}}(E) \propto \ln(E)/E$, i.e., the photoionization cross-section decreases much more rapidly.

As an example we compare experimental data with different theories of collisional ionization of a multielectron atom. Figure 5.4 shows an example for the tellurium atom (atomic number $Z = 52$): The configurations of outer electron shells are $(4d)^{10}(5s)^2(5p)^4$, and their ionization potentials are $I_{4\text{d}} = 47$ eV, $I_{5\text{s}} = 18$ eV, $I_{5\text{p}} \cong 9$ eV. As follows from these energies and formulas (5.37)–(5.38), the cross-section maximum of collisional ionization of the 5*p*-subshell is about an order of magnitude higher than the corresponding value for the 5*s*-subshell, indicating

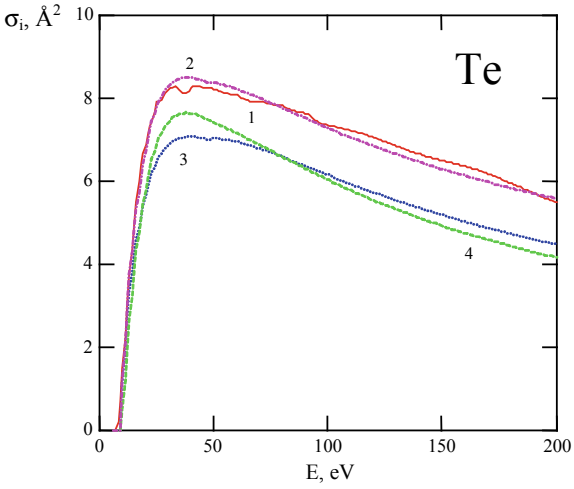

Fig. 5.4 Cross-section of ionization of a tellurium atom by electron impact: 1—experiment, 2—Born–Compton method, 3—Eletskii–Smirnov formula, 4—Gryzinsky formula

that the main contribution to the ionization process stems from the outer atomic subshell. This situation is typical: As a rule, the cross-section of collisional ionization of an atom is defined by its outer subshell since it has the smallest ionization potential.

From Fig. 5.4, it is seen that in this case the best agreement with experimental data is achieved by the Born–Compton similarity function (5.42). The Eletskii–Smirnov and Gryzinsky formulas somewhat underestimate the cross-section.

The value of the cross-section of collisional ionization of neutral atoms in the ground state varies in a relatively narrow range: from 0.5 Å^2 (for helium) to about 10 Å^2 for heavy atoms such as tellurium. Atoms in excited states with low ionization potential have large collisional ionization cross-sections that at the maximum can make up several hundreds of squared angstroms. For multiply charged positive ions with a high ionization potential, the cross-section can be rather small because $\sigma \propto 1/I \propto 1/Z^2$.

The cross-section of ionization of atoms by electron impact defines an important parameter for atomic population kinetic equations that is called the rate coefficient [typical employed units are ($\text{cm}^3\ \text{s}^{-1}$)] that is determined by the expression

$$k_\text{i}(T_\text{e}) = \int \sigma_\text{i}(E)\, \upsilon_\text{e}(E)\, F_\text{e}(E, T_\text{e})\, \text{d}E, \tag{5.45}$$

where $F_\text{e}(E, T_\text{e})$ is the energy distribution function of plasma electrons at a given temperature T_e of an electron subsystem, $\upsilon_\text{e}(E) = \sqrt{2E/m_\text{e}}$ is the velocity (non-relativistic) of an electron.

With the use of the universal expression (5.41) for the atomic ionization cross-section, it is easy to estimate the rate coefficient for a Maxwellian electron energy distribution function:

$$F_\text{e}(E, T_\text{e}) = \frac{2}{\sqrt{\pi}} \frac{\sqrt{E}}{(T_\text{e})^{3/2}} \exp\left[-\frac{E}{T_\text{e}}\right], \tag{5.46}$$

where T_e is expressed in energy units. Substituting the formulas (5.41) and (5.46) in the expression (5.45), we obtain

$$k_\text{i}(T_\text{e}) = \frac{2}{\pi} \sum_\text{nl} \sqrt{2\, m_\text{e} I_\text{nl}} \left(\frac{e^2}{I_\text{nl}}\right)^2 H(I_\text{nl}/T_\text{e}), \tag{5.47}$$

where electron temperature is included in the dimensionless function

$$H(y) = y^{3/2} \int_1^\infty f(x)\, \text{e}^{-xy}\, x\, \text{d}x, \tag{5.48}$$

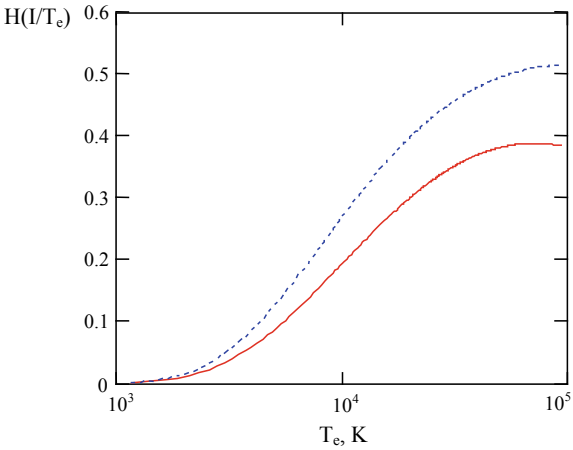

Fig. 5.5 Dependence of the function $H(I/T_e)$ [the formulas (5.47), (5.48)] on electron temperature calculated with the Eletskii–Smirnov (solid curve) and Born–Compton (dotted curve) similarity functions for a ionization potential of I = 1Ry (ionization potential of a hydrogen atom)

that depends itself on the similarity function $f(x)$. $H(y)$ reaches a maximum at about values y = 0.06–0.08, i.e., at a temperature of $T_{\max} \approx (12-15)\,I$. It should be noted that at such temperatures, an atom is already ionized. The functions $H(I/T)$ calculated with the Eletskii–Smirnov and Born–Compton similarity functions for the ionization potential of a hydrogen atom are shown in Fig. 5.5.

5.3 Analytical Empirical Formulas for Ionization, Single, and Total Recombination Rates

5.3.1 Ionization

Among a vast amount of fitting formulas and numerical calculations (Sobelman and Vainshtein 2006; Voronov 1997; Lotz 1970; Kato et al. 1991), we point out here one of the most used formulas from Lotz providing a modified explicit analytic expression for the ionization from shell "n" of an ion with charge state "Z" (i.e., $X_Z(n)+e \rightarrow X_{Z+1}(m)+e+e$) averaged over a Maxwellian electron energy distribution function:

$$I_{Z,Z+1}(n,m) \approx 6\times 10^{-8}\,P_n\left(\frac{\mathrm{Ry}}{E_{Z,Z+1}(n,m)}\right)^{3/2}\sqrt{\beta_{nm}}\,e^{-\beta_{nm}}\,\alpha(\beta_{nm})\;[\mathrm{cm}^3\,\mathrm{s}^{-1}], \tag{5.49a}$$

$$\alpha(\beta_{nm}) \approx \ln\left[1+\frac{0.562+1.4\,\beta_{nm}}{\beta_{nm}\,(1+1.4\,\beta_{nm})}\right], \tag{5.49b}$$

$$\beta_{\mathrm{nm}} = \frac{E_{\mathrm{Z,Z+1}}(n,m)}{kT_{\mathrm{e}}}. \tag{5.49c}$$

kT_{e} is the electron temperature in [eV], $E_{\mathrm{Z,Z+1}}(n,m)$ is the ionization energy in [eV] from state "n" of ion "Z" to state "m" of ion "$Z + 1$", and P_{n} is the number of equivalent electrons in the state "n". Note, that detailed ionization rate coefficients for H I, He I and He II are presented in Annex 2 and 3.

5.3.2 Three-Body Recombination in Dense Plasmas

Three-body recombination (i.e., $X_{\mathrm{Z}+1}(m) + e + e \rightarrow X_{\mathrm{Z}}(n) + e$) is the inverse process of ionization and can be approximated by the following analytical expression:

$$T_{\mathrm{Z}+1,\mathrm{Z}}(m,n) \approx 2 \times 10^{-31} \left(\frac{\mathrm{Ry}}{E_{\mathrm{Z,Z}+1}(n,m)}\right)^3 \frac{P_{\mathrm{n}}\, g_{\mathrm{Z}}(n)}{g_{\mathrm{Z}+1}(m)}\ \beta_{\mathrm{nm}}^2\, \alpha(\beta_{\mathrm{nm}})\ [\mathrm{cm}^6\,\mathrm{s}^{-1}], \tag{5.50}$$

with $\alpha(\beta_{\mathrm{nm}})$ and β_{nm} given by (5.49b, c). $g_{\mathrm{Z}+1}(m)$ is the statistical weight of the state before recombination (usually the strongly populated ground state) and $g_{\mathrm{Z}}(n)$ is the statistical weight of the recombined state. Note, that detailed three-body recombination rate coefficients for H I, He I and He II are presented in Annex 2 and 3.

Of particular interest for the calculation of the ionic fraction and radiation losses is the total three-body recombination rate, i.e., the summation over principal quantum number "n" until N_{max} in (5.50):

$$T_{\mathrm{Z}+1,\mathrm{Z}} = \sum_{n=1}^{N_{\mathrm{max}}} T_{\mathrm{Z}+1,\mathrm{Z}}(n). \tag{5.51}$$

The summation over the principal quantum number "n" in (5.51) has to be taken out with care. In fact, (5.51) assumes that all recombination into excited states finally populate the ground state via radiative cascades. At large quantum numbers, however, collisional processes become so important that that the recombination flow to an excited state might even be transferred back before it can decay to the ground state by radiative cascades. As collisional rates strongly increase with principal quantum number "n" but radiative decay rates decrease with principal quantum number "n", there exist a critical electron density $n_{\mathrm{e,crit}}$ where collisional processes are equally important as radiative decay for a given principal quantum number $n = n_{\mathrm{crit}}$. A rough guideline for the selection of the maximum principal quantum number in (5.51) is therefore

$$N_{\max} \approx n_{\text{crit}}. \tag{5.52}$$

If the atomic structure is such that the atomic ground state has the principal quantum number $n = 1$, critical electron density and critical principal quantum number are related by:

$$n_{\text{e, crit}} \geq 6 \times 10^{19}\, Z^7 \frac{(n_{\text{crit}} - 1)^{2n_{\text{crit}}-2}}{n_{\text{crit}}^3 (n_{\text{crit}} + 1)^{2n_{\text{crit}}+2}} \left(\frac{kT_{\text{e}}(\text{eV})}{Z_{\text{eff}}^2\, \text{Ry}}\right)^{1/2} \left[\text{cm}^{-3}\right]. \tag{5.53}$$

kT_{e} is the electron temperature in [eV], Z_{eff} is the effective ionic charge and Ry = 13.6 eV. With the help of (5.53), for each given electron density $n_{\text{e,crit}}$, the critical principal quantum number n_{crit} can be calculated. Equation (5.53) has a well-defined asymptote for large quantum numbers:

$$\begin{aligned} \lim_{n_{\text{crit}} \to \infty} \left\{ \frac{(n_{\text{crit}} - 1)^{2n_{\text{crit}}-2}}{n_{\text{crit}}^3 (n_{\text{crit}} + 1)^{2n_{\text{crit}}+2}} \right\} &= \lim_{n \to \infty} \left\{ \frac{1}{n_{\text{crit}}^3 (n_{\text{crit}} + 1)^4} \left(\frac{n_{\text{crit}} - 1}{n_{\text{crit}} + 1}\right)^{2n_{\text{crit}}-2} \right\} \\ &\approx \frac{0.0183}{n_{\text{crit}}^7} \end{aligned} \tag{5.54}$$

because

$$\lim_{n_{\text{crit}} \to \infty} \left\{ \left(\frac{n_{\text{crit}} - 1}{n_{\text{crit}} + 1}\right)^{2n_{\text{crit}}-2} \right\} \approx \frac{1}{54.6}. \tag{5.55}$$

Therefore, we can write

$$n_{\text{e,crit}} \approx 6 \times 10^{19} Z_{\text{eff}}^7 \frac{1}{n_{\text{crit}}^3} \frac{0.0183}{n_{\text{crit}}^4} \left(\frac{kT_{\text{e}}(\text{eV})}{Z_{\text{eff}}^2 \text{Ry}}\right)^{1/2} \approx 10^{18} \frac{Z_{\text{eff}}^7}{n_{\text{crit}}^7} \left(\frac{kT_{\text{e}}(\text{eV})}{Z_{\text{eff}}^2 \text{Ry}}\right)^{1/2} \left[\text{cm}^{-3}\right]. \tag{5.56}$$

Equation (5.56) shows that the critical electron density scales with the seventh power of the principal quantum number and with the seventh power of the effective charge. Equation (5.52) can therefore be estimated as follows:

$$n_{\text{crit}} \approx 373 \frac{Z_{\text{eff}}}{n_{\text{e,crit}}^{1/7}} \left(\frac{kT_{\text{e}}(\text{eV})}{Z_{\text{eff}}^2 \text{Ry}}\right)^{1/14}. \tag{5.57}$$

The maximum principal quantum number is not a very critical issue for radiative and dielectronic recombination, as both processes decrease rapidly with the principal quantum number itself. For the three-body recombination, however, the recombination rates increase strongly with principal quantum number and $N_{\max}$ has to be chosen with care. Monte Carlo simulations (Mansbach and Keck 1969) that

take into account the complex movement of the electron in the excitation–ionization among the numerous excited states indicate the following:

$$T_{Z+1,Z} \approx 2 \times 10^{-27} \zeta \frac{Z_{\text{eff}}^3}{(kT_e)^{9/2}} \left[\text{cm}^6\,\text{s}^{-1}\right] \tag{5.58}$$

with $\zeta = 1$. Most of the results obtained with different methods propose expressions similar to (5.58) but differ by the numerical coefficient $\zeta = 0.1$–10 (Hahn 1997; Mayorov et al. 1994). Note that if all three-body recombination rates are summed up and the upper limit is identified with the collisional ionization limit, $\zeta = 3.1$ (Hahn and Li 1996) (note that the ionization limit employed in (Hahn and Li 1996) does not depend on density).

In dense and cold plasmas, the classical three-body recombination rate is diverging because the Maxwell electron distribution function becomes very narrow. This is unphysical, because it can be shown that this violates the Pauli principle. A recent investigation based on a consistent use of the Fermi–Dirac distribution function and Pauli-blocking factors has shown (Deschaud et al. 2014, 2015) that the three-body recombination rate is then well defined for all transitions from the hot dense plasma to the warm dense matter (WDM), to the hot solid, and to the cold solid.

5.3.3 Radiative Recombination in Dense Plasmas

In a similar manner, the total radiative recombination is the sum of all radiative recombination into the ground and excited states ($N_{\max}$ is the largest principal quantum number to be taken into account):

$$R_{Z+1,Z} = \sum_{n=1}^{N_{\max}} \sum_{l=0}^{n-1} R_{Z+1,Z}(nl). \tag{5.59}$$

In the optical electron model (hydrogenic approximation), the radiative recombination can be directly represented by a sum over the orbital l-quantum numbers (Baker and Menzel 1938; Sobelman and Vainshtein 2006):

$$R_{Z+1,Z}(n) = \sum_{l=0}^{n-1} R_{Z+1,Z}(nl), \tag{5.60}$$

$$R(n) \approx 5.2 \times 10^{-14} Q_n Z_{\text{eff}} \beta_n^{3/2} \gamma(\beta_n)\,[\text{cm}^3\,\text{s}^{-1}], \tag{5.61a}$$

$$Z_{\text{eff}} = n_{\text{gr}} \cdot \sqrt{\frac{E_{Z,Z+1}(n_{\text{gr}})}{\text{Ry}}}, \tag{5.61b}$$

$$\gamma(\beta_n) \approx \ln\left[1 + \frac{0.562 + 1.4\,\beta_n}{\beta_n(1 + 1.4\,\beta_n)}\right], \tag{5.61c}$$

$$\beta_n = \frac{E_{Z,Z+1}(n)}{kT_e}, \tag{5.61d}$$

$$Q_n \approx 1 - \frac{N}{2\,n^2}. \tag{5.61e}$$

kT_e is the electron temperature in [eV], $E_{Z,Z+1}(n)$ is the ionization energy of the state "n" of ions "Z" into state "m" of ion "$Z + 1$" in [eV], Z_{eff} is the effective charge of the ion before recombination, n_{gr} is the principal quantum number of the ground state, Ry = 13.6 eV and Q_n is an angular factor which takes into account the Pauli principle (means the reduced probability to be captured into a certain level that is already partially occupied with electrons), (5.61e) is the corresponding hydrogenic approximation. For example, for radiative recombination into He-like neon (i.e., $Ne^{9+}(1s) + e \rightarrow Ne^{8+}(1s^2)$), we have $Q_n = 1 - 1/(2 \cdot 1^2) = 0.5$ and $Z_{eff} = 1 \cdot \sqrt{1195.81\,\text{eV/Ry}} = 9.4$. Note, that detailed radiative recombination rate coefficients for H I, He I and He II are presented in Annex 2 and 3.

Using (5.61) and Q_n = 1, the sum of (5.60) over the n-quantum numbers can be approximated by the following analytic expression:

$$R^{tot}(n \geq n_1) = 2.6 \times 10^{-14}\, Z_{eff}\, n_1 \beta_1^{1/2} \cdot \{\ln(1.78\beta_1) + g(\beta_1)(1 + \beta_1/n_1)\}\,\left[\text{cm}^3\,\text{s}^{-1}\right], \tag{5.62a}$$

$$\beta_1 = \frac{Z_{eff}^2\,\text{Ry}}{n_1^2 kT_e}, \tag{5.62b}$$

$$g(\beta_1) \approx \ln\left[1 + \frac{0.562 + 1.4\,\beta_1}{\beta_1\,(1 + 1.4\,\beta_1)}\right]. \tag{5.62c}$$

n_1 is the principal quantum number from which the sum is taken (usually over all higher lying excited states with $n > n_{gr}$). In practice, the calculations of the total radiative recombination rate employ detailed calculations for the recombination into the ground state and states that have the same principal quantum number as the ground state, i.e., $R(n = n_{gr})$ (either via (5.61) or more advanced detailed quantum mechanical calculations) and employ (5.62) for the excited states with an effective charge given by (5.61b). In this case, $n_1 = n_{gr} + 1$. In other words, one employs detailed calculations for the states with the same principal quantum number as the ground state and the hydrogenic approximation with effective charge for the excited states.

In the framework of the hydrogenic approximation for the contribution of the excited states, dense plasma effects can be estimated with the help of (5.52) and (5.62) assuming that all recombination is suppressed for quantum numbers larger

than the critical quantum number, i.e., $n > n_{\mathrm{crit}}$. In this case, $n_1 = n_{\mathrm{crit}}$ in (5.62) and the total radiative recombination in dense plasmas is given by

$$R^{\mathrm{tot}}_{\mathrm{dense}} \approx R^{\mathrm{tot}}(n \le n_{\mathrm{crit}}) \approx R(n = n_{\mathrm{gr}}) + \left\{R^{\mathrm{tot}}(n \ge n_{\mathrm{gr}} + 1) - R^{\mathrm{tot}}(n \ge n_{\mathrm{crit}} + 1)\right\}. \tag{5.62d}$$

5.4 Classical Consideration of Collisional Excitation of an Atom

5.4.1 Fermi Photon Equivalent Method and Oscillator Strength Method

Excitation of atoms in collisions with electrons is another example of an inelastic collisional process that plays an important role in various fields of physics and technology. In contrast to collisional ionization, when an atomic electron is excited to the continuous energy spectrum (corresponding to infinite motion), excitation of an atomic electron goes to the discrete spectrum, that is (within the framework of the classical picture), to another atomic orbit with higher energy. This phenomenon is responsible for emission of photons in plasmas resulting from a transition of an atomic excited state to the ground state. It is also one of the mechanisms to achieve population inversion in gas lasers (so-called electron beam pumping). Also the population inversion of the soft X-ray Ne-like and Ni-like lasers is based on collisional excitation in plasmas (Sobelman and Vinogradov 1985; Elton 1990). Note that X-ray laser schemes without population inversion have also been proposed (Braunstein and Shuker 2003) that is based on a complex interplay of the atomic master equations that include the atomic coherences (Loudon 2000).

Electron collisional excitation is schematically described as

$$e + A \rightarrow A^* + e, \tag{5.63}$$

where the symbol A^* denotes an atom in the excited state of a discrete spectrum. For calculation of the reaction cross-section (5.63), we will use the spectroscopic principle of correspondence between quantum physics and classical physics. According to this principle, an atom in interaction with an electromagnetic field behaves as a set of oscillators that are assigned to a pair of energy levels E_{i} and E_{j} of the atomic spectrum. Let us assume that $E_{\mathrm{i}} < E_{\mathrm{j}}$. The eigenfrequencies of these oscillators are equal to the eigenfrequency of the transition $i \rightarrow j$: $\omega_{\mathrm{ji}} = \left(E_{\mathrm{j}} - E_{\mathrm{i}}\right)/\hbar$, and the efficiency of their interaction with an electromagnetic field is defined by the *oscillator strength*:

$$f_{ji} = \frac{2\, m\omega_{ji} \left|\mathbf{d}_{ji}\right|^2}{3\, \hbar\, e^2\, g_i}, \tag{5.64}$$

where g_i is the statistical weight of the initial state. In the quantum mechanical description of the dipole moment of a transition oscillator, $\mathbf{d}_{ji}$ is a matrix element of an electric dipole moment operator calculated between states $|i\rangle$ and $|j\rangle$. In the case of excitation of an atom, $\omega_{ji} > 0$ and $f_{ji} > 0$; for an electron transition with decreasing energy ($\omega_{ij} < 0$), $f_{ij} < 0$. Since $\left|\mathbf{d}_{ji}\right| = \left|\mathbf{d}_{ij}\right|$, we obtain from (5.64) $g_i f_{ji} = -g_j f_{ij}$.

Atomic excitation $i \rightarrow j$ via collisions with an electron corresponds therefore to the interaction between the electric field of the scattered electron and the transition oscillator. Assuming a homogenous incident electron field close to the atom, it is possible to write the following equation for the radius vector of the oscillator $\mathbf{r}_{ji}$:

$$\ddot{\mathbf{r}}_{ji} + \gamma_{ji}\, \dot{\mathbf{r}}_{ji} + \omega_{ji}^2\, \mathbf{r}_{ji} = f_{ji} \frac{e}{m} \mathbf{E}(t,\, \rho), \tag{5.65}$$

where γ_{ij} is the damping constant, $\mathbf{E}(t,\, \rho)$ is the strength of the electric field that is produced by an incident electron moving along a trajectory with an impact parameter ρ relative to the atom.

Let us assume $f_{ji} \neq 0$. Corresponding transitions are called dipole (or optically)-allowed transitions. Otherwise, the transitions are called dipole or optically forbidden transitions.

The Fourier transform of (5.65) is given by:

$$\mathbf{v}_{ji}(\omega) = f_{ji} \cdot \frac{e}{m} \cdot \frac{(-i\, \omega)\, \mathbf{E}(\omega,\, \rho)}{\omega_{ji}^2 - \omega^2 - i\, \gamma_{ji}\, \omega}, \tag{5.66}$$

where $\mathbf{E}(\omega,\, \rho)$ is the Fourier component of the electric field strength of a scattered electron. In order to determine the excitation cross-section of an atom for the transition $i \rightarrow j$, we calculate the work done on a transition oscillator by an incident electron during the duration of the collision:

$$A_{ji}(\rho) = \int_{-\infty}^{\infty} e\, \mathbf{v}_{ji}(t)\, \mathbf{E}(t,\, \rho)\, \mathrm{d}t = \frac{1}{2\, \pi} \int_{-\infty}^{\infty} e\, \mathbf{v}_{ji}(\omega)\, \mathbf{E}^*(\omega,\, \rho)\, \mathrm{d}\omega. \tag{5.67}$$

The second equality of (5.67) is a Fourier representation using the relation $\mathbf{E}(-\omega,\, \rho) = \mathbf{E}^*(\omega,\, \rho)$ and the integral representation of the delta function, i.e.,

$$\int_{-\infty}^{\infty} \exp(i\, \omega\, t)\, \mathrm{d}t = 2\, \pi\, \delta(\omega). \tag{5.68}$$

It should be emphasized that the expression (5.67) is valid only for sufficiently high-impact parameters $\rho > a$, where a is the "cutoff" length. If $\rho > a$, penetration of an incident electron into an atomic core can be neglected. The analysis shows that essentially distant collisions contribute to the excitation cross-section of a dipole-allowed transition. Hereafter, we assume $A_{ji}(\rho < a) = 0$. The cutoff parameter a is of the order of several Bohr radii; its exact value depends on the atom and the specific transition.

Substituting (5.66) in (5.67) and transforming the integration over positive frequencies only, we obtain

$$A_{ji}(\rho) = f_{ji} \frac{e^2}{2m} \int_0^\infty G_{ji}^{(h)}(\omega - \omega_{ji}) \, |\mathbf{E}(\omega, \rho)|^2 \, d\omega. \tag{5.69}$$

$$G_{ji}^{(h)}(\Delta\omega) = \frac{\gamma_{ji}/2\pi}{\Delta\omega^2 + (\gamma_{ji}/2)^2} \tag{5.70}$$

is the spectral line shape of a transition for homogeneous broadening. Equation (5.70) shows that the damping constant γ_{ji} defines the spectral width of a line. The function (5.70) satisfies the asymptotic relation

$$G_{ji}^{(h)}(\Delta\omega, \gamma_{ji} \to 0) \to \delta(\Delta\omega). \tag{5.71}$$

The spectral width of the function $|\mathbf{E}(\omega, \rho)|^2$ in (5.69) is defined by the ratio υ/ρ. This value is much larger than the width of the spectral line of an atomic transition γ_{ji} for $\rho > a$ and $\upsilon > \sqrt{2\hbar\omega_{ji}/m}$. Therefore, the asymptotic formula (5.71) can be used.

The probability of excitation of the transition $i \to j$ is equal to the ratio

$$W_{ji}(\rho) = \frac{A_{ji}(\rho)}{\hbar\omega_{ji}}, \tag{5.72}$$

where $\hbar\omega_{ji} = \Delta E_{ji}$ is the atomic excitation energy. The analysis shows that $W_{ji} < 1$ for the considered range of impact parameters ρ and impact velocities υ as it should be according to the physical meaning of the probability.

The cross-section integrated with respect to the impact parameter is given by

$$\sigma_{ji} = 2\pi \int_a^\infty W_{ji}(\rho) \, \rho \, d\rho. \tag{5.73}$$

Here the upper limit of integration with respect to the impact parameter is assumed to be equal to infinity according to the classical picture. Substituting the formulas (5.72) and (5.69) in (5.73), we find in view of (5.71):

$$\sigma_{\mathrm{ji}} = \pi f_{\mathrm{ji}} \frac{e^2}{m\,\Delta E_{\mathrm{ji}}} \int_a^\infty \left|\mathbf{E}\left(\omega_{\mathrm{ji}},\, \rho\right)\right|^2 \rho\, \mathrm{d}\rho. \tag{5.74}$$

To proceed further, let us consider the *approximation of straight trajectories*. In this case, it is easy to obtain an expression for the Fourier component of an incident electron field:

$$\mathbf{E}(\omega, \rho) = \frac{2\,e}{\rho\,\upsilon} \left\{ F\left(\frac{\omega\,\rho}{\upsilon}\right) \mathbf{e}_{\mathrm{n}} - iF'\left(\frac{\omega\,\rho}{\upsilon}\right) \mathbf{e}_{\tau} \right\}, \tag{5.75}$$

where $\mathbf{e}_{\mathrm{n},\,\tau}$ are the normal and tangent (with respect to the velocity vector $\mathbf{v} = \mathrm{const}$) unit vectors and

$$F(\zeta) = \int_0^\infty \frac{\cos(\zeta\, x)}{(1+x^2)^{3/2}}\, \mathrm{d}x \tag{5.76}$$

(the prime in (5.75) denotes differentiation with respect to the argument).

Substituting (5.75)–(5.76) in (5.74), we obtain an expression for the collisional excitation cross-section as a function of the incident electron energy $E = m\upsilon^2/2$:

$$\sigma_{\mathrm{ji}}(E) = 2\,\pi f_{\mathrm{ji}} \left(\frac{e^2}{\Delta E_{\mathrm{ji}}}\right)^2 \frac{\Delta E_{\mathrm{ji}}}{E} \int_1^\infty H\left(\frac{\omega_{\mathrm{ji}}\, a\, \tilde{\rho}}{\sqrt{2\,E/m}}\right) \frac{\mathrm{d}\tilde{\rho}}{\tilde{\rho}}. \tag{5.77}$$

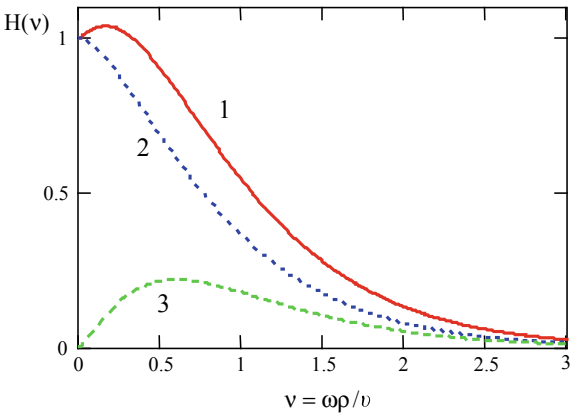

Fig. 5.6 Spectrum of the electric field of an incident electron (5.78) as a function of the dimensionless frequency: 1—total, 2—normal component of the field, 3—tangential component of the field

$$H(v) = F^2(v) + F'^2(v) \tag{5.78}$$

is the spectral function of the electric field strength of an incident electron (see Fig. 5.6). In (5.77), integration with respect to the dimensionless variable $\tilde{\rho} = \rho/a$ is introduced. From (5.77) to (5.78), it follows that the spectrum of the electric field of the scattered electron depends only on the dimensionless parameter $v = \omega\,\rho/\upsilon$.

Figure 5.6 shows that the main contribution to the spectral function $H(v)$ near its maximum is essentially only due to the normal component of the electric field of the electron. In this parameter region, the spectrum width is of the order of magnitude of the ratio υ/ρ.

It is convenient to rewrite formula (5.77) for the collisional excitation cross-section of an atom according

$$\sigma_{\mathrm{ji}}(E) = 2\,\pi f_{\mathrm{ji}} \left(\frac{e^2}{\Delta E_{\mathrm{ji}}}\right)^2 \phi\left(\frac{E}{\Delta E_{\mathrm{ji}}}, \eta\right), \tag{5.79}$$

$$\phi(x, \eta) = \frac{1}{x} \int_1^\infty H\left(\frac{\eta\,\tilde{\rho}}{\sqrt{x}}\right) \frac{\mathrm{d}\tilde{\rho}}{\tilde{\rho}} \tag{5.80}$$

is a dimensionless function that depends on the ratio $E/\Delta E_{\mathrm{ji}}$ and on the dimensionless parameter

$$\eta = \frac{1}{\sqrt{2}} \frac{a}{a_{\mathrm{B}}} \sqrt{\frac{\Delta E_{\mathrm{ji}}}{2\,\mathrm{Ry}}}, \tag{5.81}$$

where $\mathrm{Ry} = 13.6$ eV, $a_{\mathrm{B}} = 0.53 \times 10^{-8}$ cm is the Bohr radius. The numerical value η depends on the value of the cutoff length a.

The expression (5.72) for the excitation probability of an atom can be rewritten as

$$W_{\mathrm{ji}}(\rho) = \int_0^\infty \sigma_{\mathrm{ji}}^{(\mathrm{ph})}(\omega)\, \frac{\mathrm{d}N(\omega,\, \rho)}{\mathrm{d}S\,\mathrm{d}\omega}\, \mathrm{d}\omega, \tag{5.82}$$

where

$$\sigma_{\mathrm{ji}}^{(\mathrm{ph})}(\omega) = f_{\mathrm{ji}} \frac{2\,\pi^2\, e^2}{m\, c}\, G_{\mathrm{ji}}^{(h)}(\omega) \tag{5.83}$$

is the cross-section of photoabsorption of an atom for the transition $i \to j$. The expression

$$\frac{\mathrm{d}N(\omega,\,\rho)}{\mathrm{d}S\,\mathrm{d}\omega}=\frac{c}{(2\pi)^2}\frac{|\mathbf{E}(\omega,\,\rho)|^2}{\hbar\,\omega} \tag{5.84}$$

can be interpreted as the number of photons (per unit area in a unit frequency interval) contained in the electric field of an incident electron during the collision time. Based on the formulas (5.82)–(5.84), the process of atomic collisional excitation can be represented as an atomic absorption of photons forming the eigenfield of a scattered charged particle. Such photons are called equivalent photons. The knowledge of the photoabsorption cross-section (e.g., from experimental data) and the number of equivalent photons allow to obtain the transition probability according (5.82). This approach was used by E. Fermi in 1924 (even before the development of quantum mechanics) for the calculation of the atomic excitation induced by fast-charged particles (Fermi 1924). This theory is called the *Fermi equivalent photon method* (discussed in Sect. 5.1).

5.4.2 *Similarity Function Method for Collisional Excitation of an Atom*

The formulas (5.79)–(5.81) for the cross-section of collisional excitation of a dipole-allowed transition in an atom in the approximation of straight trajectories are valid for sufficiently high-incident electron energies $E \gg \Delta E_{\mathrm{ji}}$. In the vicinity of the excitation threshold, i.e., $E \approx \Delta E_{\mathrm{ji}}$, an electron loses practically its whole of kinetic energy and the approximation $\mathbf{v} = \text{const}$ becomes obviously incorrect. The analysis shows that the expression (5.79) can be extended to the whole range of incident electron energies if the function $\varphi\,(E/\Delta E_{\mathrm{ji}})$ is properly chosen. This choice can be made either empirically on the basis of comparison with experimental data or on general theoretical considerations. The basis of this approach is the assumption that the ratio

$$\varphi\left(E/\Delta E_{\mathrm{ji}} \equiv x\right)=\frac{\sigma_{\mathrm{ji}}(E)}{2\,\pi f_{\mathrm{ji}}\left(e^2/\Delta E_{\mathrm{ji}}\right)^2} \tag{5.85}$$

is a universal function of the dimensionless variable $x = E/\Delta E_{\mathrm{ji}}$ only. Equation (5.85) expresses the essence of the *similarity function method* for the calculation of the cross-section of collisional excitation of an atom. Quantum mechanical consideration shows that the similarity function $\varphi(x)$ should satisfy two asymptotic relations:

$$\varphi(x \to 1) \propto \sqrt{x-1} \text{ and } \varphi(x \gg 1) \propto \frac{\ln(x)}{x}. \tag{5.86}$$

In view of (5.86), $\varphi(x)$ can be approximated by Astapenko et al. (2000)

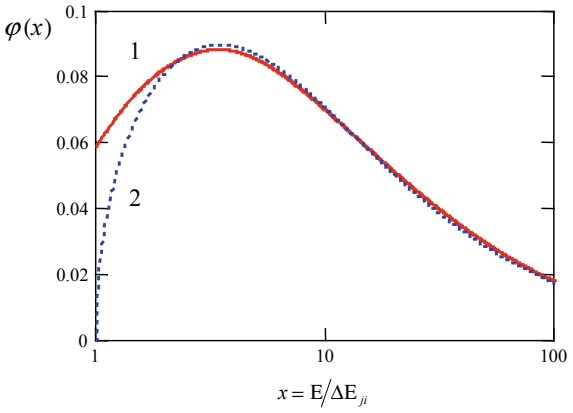

Fig. 5.7 Empirical similarity function (1) and the similarity function calculated in the approximation of straight trajectories (2) for the cross-section of collisional excitation of a dipole-allowed transition in an atom

$$\varphi(x) = \frac{\ln\left(1 + a\sqrt{x-1}\right)}{x+b}. \tag{5.87}$$

The values of the parameters a and b can be obtained from experimental data: $a \approx 0.5$, $b \approx 3$. Let us note the difference of the near-threshold behavior of the similarity function for the excitation of an atom, i.e., $\varphi(x \approx 1) \propto \sqrt{x-1}$ from the corresponding dependence for ionization of an atom by electron impact, i.e., $f(x \approx 1) \propto x - 1$.

It is of interest to compare the similarity function (5.87) with the expression obtained in the approximation of straight trajectories (5.80), (5.78). This comparison for $\eta = 1.7$ is given in Fig. 5.7. From this figure, it follows that for $x > 3$ both functions practically coincide. In particular, the position of maxima $x_{\max} \cong 3.45$ and the maximum values $\varphi_{\max} \cong 0.09$ coincide. A noticeable difference exists only in the near-threshold region $1 < x < 2$, where the approximation of straight trajectories is inadequate.

Therefore, the cross-section of collisional excitation of a dipole-allowed transition in an atom for arbitrary energies of an incident electron, including the near-threshold region, can be represented as

$$\sigma_{\mathrm{ji}}(E) = 2\,\pi\,\sigma_{\mathrm{a}} f_{\mathrm{ji}} \left(\frac{2\,\mathrm{Ry}}{\Delta E_{\mathrm{ji}}}\right)^2 \varphi\left(\frac{E}{\Delta E_{\mathrm{ji}}}\right), \tag{5.88}$$

where the similarity function $\varphi(x)$ is given by the formula (5.87). Note that (5.88) is expressed in atomic units ($e = 1$, $E_{\mathrm{a}} = 2\,\mathrm{Ry} \cong 27.2$ eV, and $\sigma_{\mathrm{a}} = a_{\mathrm{B}}^2 \cong 2.8 \times 10^{-17}$ cm^2). In view of the above values for $x_{\max}$, $\varphi_{\max}$, the formula (5.88) gives for the maximum cross-section

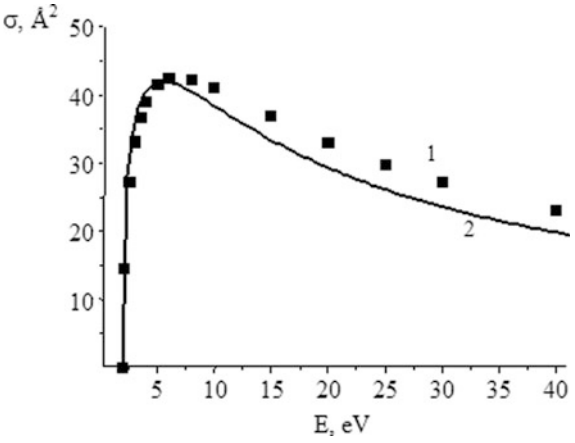

Fig. 5.8 Cross-section of excitation of a lithium atom by electron impact for the transition $2s \rightarrow 2p$: 1—experimental data of the American National Standards Institute (NIST 2019), 2—calculation by the similarity function method according (5.88)

$$\sigma_{\mathrm{ji}}\left(E_{\max} = 3.45\,\Delta E_{\mathrm{ji}}\right) \cong 0.63 \times 10^{-16} f_{\mathrm{ji}} \left(\frac{\mathrm{Ry}}{\Delta E_{\mathrm{ji}}}\right)^2 [\mathrm{cm}^2]. \tag{5.89}$$

Thus, the cross-section of collisional excitation of a dipole-allowed transition is directly proportional to the transition oscillator strength and inversely proportional to the squared excitation energy. A characteristic value for the transition energies in a neutral atom is 1–10 eV. The oscillator strengths vary in a more wide range: from 10^{-6} to 2. At $f_{\mathrm{ji}} < 10^{-6}$, an electron transition in an atom can be considered to be forbidden. The maximum value $f_{\mathrm{ji}} \cong 2$ is reached for transitions with no change in a principal quantum number in atoms of alkaline-earth elements.

Figure 5.8 shows the experimental (curve 1) and calculated (curve 2) excitation cross-sections for the transitions $2s \rightarrow 2p$ in the lithium atom. Because there is no change in principal quantum number, the oscillator strength is rather high ($f_{2\mathrm{p}\rightarrow 2\mathrm{s}} = 0.75$) and the excitation energy rather low ($\Delta E_{2\mathrm{p}\rightarrow 2\mathrm{s}} \approx 1.85$ eV). Therefore, the maximum value of the cross-section is rather large: $\sigma_{\max} \cong 4.3 \times 10^{-15}$ cm^2. The position of the maximum corresponds to an energy of about 7.5 eV. Figure 5.8 demonstrates rather good agreement between theory and experiment, especially in the vicinity of threshold.

5.4.3 Analytical Empirical Formulas for Excitation and De-excitation Rates

5.4.3.1 Dipole Excitation and De-excitation of Ions

For dipole-allowed transitions (i.e., $\Delta l = \pm 1$), one of the most used general formulas has been proposed by Van Regemorter (1962). The corresponding excitation rates (integration of the cross-section over a Maxwellian energy distribution function) can be cast in the following analytical form:

$$\langle \upsilon\sigma(\alpha \to \alpha') \rangle := C_{\alpha\alpha'} = 3.15 \times 10^{-7} f_{\alpha\alpha'} \left(\frac{\mathrm{Ry}}{\Delta E_{\alpha\alpha'}} \right)^{3/2} \cdot \sqrt{\beta} \cdot \mathrm{e}^{-\beta} \cdot p^{(Z>0)}(\beta), \quad (5.90a)$$

$$\Delta E_{\alpha\alpha'} = E_\alpha - E_{\alpha'}, \quad (5.90b)$$

$$\beta = \frac{\Delta E_{\alpha\alpha'}}{T_\mathrm{e}}. \quad (5.90c)$$

$f_{\alpha\alpha'}$ is the oscillator strength for the dipole transition from state α to state α', and $p^{(Z>0)}(\beta)$ is an effective Gaunt factor. The required oscillator strength $f_{\alpha\alpha'}$ is easily obtained from the spontaneous transition probability $A_{\alpha'\alpha}$

$$f_{\alpha\alpha'} = \frac{1}{4.339 \times 10^7 \left(E_\alpha - E_{\alpha'}\right)^2} \frac{g_{\alpha'}}{g_\alpha} A_{\alpha'\alpha} \quad (5.91)$$

with E_α and E_α expressed in [eV], g_α and $g_{\alpha'}$ are the statistical weights of the lower and upper states, respectively. Note that (5.91) expresses the absorption oscillator strength in terms of the spontaneous emission coefficient. The effective Gaunt-factor $p(\beta)$ can be approximated by an analytical expression:

$$p^{(Z>0)}(\beta) = 0.2757\, \mathrm{e}^{-1.3\beta} \left(\beta - \frac{\beta^2}{4} - \ln(\beta) - 0.5772 \right) + 0.2\left(1 - \mathrm{e}^{-4.5\beta}\right). \quad (5.92)$$

This formula provides the correct asymptotic behavior for low and high energies and an accuracy better than 5% for all values of β.

De-excitation rates are obtained from the principle of detailed balance, i.e.,

$$C_{\alpha'\alpha} = C_{\alpha\alpha'} \frac{g_\alpha}{g_{\alpha'}} \exp(\beta) \quad (5.93)$$

providing

$$C_{\alpha'\alpha} = 3.15 \times 10^{-7} f_{\alpha\alpha'} \frac{g_\alpha}{g_{\alpha'}} \left(\frac{\mathrm{Ry}}{\Delta E_{\alpha\alpha'}}\right)^{3/2} \cdot \sqrt{\beta} \cdot p(\beta). \tag{5.94}$$

Equation (5.94) demonstrates that de-excitation rates do not contain the exponential factor from the Maxwellian average. For low temperatures, i.e., for parameters $\beta > 10$, the effective Gaunt-factor approaches $p^{(Z>0)}(\beta) \to 0.2$ (approaching a finite value for the Gaunt factor is due to the attraction of the electron via the Coulomb potential of the atoms, i.e., the electron practically falls into the potential of the ion and excites the ion) and we find formally the following asymptotic expressions:

$$C_{\alpha\alpha'} \to 6.3 \times 10^{-8} f_{\alpha\alpha'} \left(\frac{\mathrm{Ry}}{\Delta E_{\alpha\alpha'}}\right)^{3/2} \sqrt{\beta} \cdot \exp(-\beta) \propto \frac{\mathrm{e}^{-\Delta E_{\alpha\alpha'}/T_\mathrm{e}}}{\sqrt{T_\mathrm{e}}}, \tag{5.95}$$

$$C_{\alpha'\alpha} \to 6.3 \times 10^{-8} f_{\alpha\alpha'} \frac{g_\alpha}{g_{\alpha'}} \left(\frac{\mathrm{Ry}}{\Delta E_{\alpha\alpha'}}\right)^{3/2} \sqrt{\beta} \propto \frac{1}{\sqrt{T_\mathrm{e}}}. \tag{5.96}$$

It should be noted that (5.95), (5.96) provide only approximate values because for low temperatures, the Born approximation is not valid anymore and normalization of the transition probability becomes of importance. Equations (5.95) and (5.96) demonstrate that for small temperatures, the excitation rate vanishes whereas the de-excitation rate is rather large. Therefore, in low-temperature recombining plasmas, the collisional processes are dominated by the de-excitation of the populated levels. For high temperatures, i.e., $\beta < 10$, we find the following asymptotic expressions:

$$C_{\alpha\alpha'} \to 8.7 \times 10^{-8} f_{\alpha\alpha'} \left(\frac{\mathrm{Ry}}{\Delta E_{\alpha\alpha'}}\right)^{3/2} \sqrt{\beta} \cdot \ln(1/\beta) \propto \frac{\ln T_\mathrm{e}}{\sqrt{T_\mathrm{e}}}, \tag{5.97}$$

$$C_{\alpha'\alpha} \to 8.7 \times 10^{-8} f_{\alpha\alpha'} \frac{g_\alpha}{g_{\alpha'}} \left(\frac{\mathrm{Ry}}{\Delta E_{\alpha\alpha'}}\right)^{3/2} \sqrt{\beta} \cdot \ln(1/\beta) \propto \frac{\ln T_\mathrm{e}}{\sqrt{T_\mathrm{e}}}. \tag{5.98}$$

Therefore, for high temperatures (i.e., hot electrons), excitation and de-excitation rates have the same asymptotic behavior and are identical except the ratio of the statistical weights.

5.4.3.2 Dipole Excitation and De-excitation of Neutral Atoms

Dipole excitation and de-excitation by collisions between electrons and neutral atoms can likewise be described by the formulas (5.90), (5.91), (5.93), however, with a modified effective Gaunt factor. The following analytical formula is proposed:

$$p^{(Z=0)}(\beta) = \left\{ \begin{array}{ll} \text{if } \beta \leq 0.4: & 0.27566 \cdot \left(\beta - \dfrac{\beta^2}{4} + \dfrac{\beta^3}{12} - \ln(\beta) - 0.57722 \right) \\ \text{else} & 0.066 \dfrac{\sqrt{\beta+2}}{\beta+0.127} \end{array} \right\}. \tag{5.99}$$

These formulas provide the correct asymptotic behavior for low and high energies and an accuracy better than 3% for all values of β.

For low temperature, we find formally the following asymptotic expressions:

$$C_{\alpha\alpha'} \rightarrow 2.1 \times 10^{-8} f_{\alpha\alpha'} \frac{g_\alpha}{g_{\alpha'}} \left(\frac{\mathrm{Ry}}{\Delta E_{\alpha\alpha'}} \right)^{3/2} \frac{\exp(-\beta)}{\sqrt{\beta}} \propto \sqrt{T_\mathrm{e}} \cdot \exp(-\Delta E_{\alpha\alpha'}/T_\mathrm{e}), \tag{5.100}$$

$$C_{\alpha'\alpha} \rightarrow 2.1 \times 10^{-8} f_{\alpha\alpha'} \frac{g_\alpha}{g_{\alpha'}} \left(\frac{\mathrm{Ry}}{\Delta E_{\alpha\alpha'}} \right)^{3/2} \frac{1}{\sqrt{\beta}} \propto \sqrt{T_\mathrm{e}}\,. \tag{5.101}$$

It should likewise be noted here that (5.100), (5.101) provide only very approximate values because for low temperatures, the Born approximation is not valid, and normalization of the transition probability becomes of importance. Equations (5.100), (5.101) indicate that, unlike for the case of electron excitation of ions, the excitation and de-excitation rates vanish both for low temperatures. For high temperatures, the following asymptotes are obtained:

$$C_{\alpha\alpha'} \rightarrow 8.7 \times 10^{-8} f_{\alpha\alpha'} \left(\frac{\mathrm{Ry}}{\Delta E_{\alpha\alpha'}} \right)^{3/2} \sqrt{\beta} \cdot \ln(1/\beta) \propto \frac{\ln T_\mathrm{e}}{\sqrt{T_\mathrm{e}}}, \tag{5.102}$$

$$C_{\alpha'\alpha} \rightarrow 8.7 \times 10^{-8} f_{\alpha\alpha'} \frac{g_\alpha}{g_{\alpha'}} \left(\frac{\mathrm{Ry}}{\Delta E_{\alpha\alpha'}} \right)^{3/2} \sqrt{\beta} \cdot \ln(1/\beta) \propto \frac{\ln T_\mathrm{e}}{\sqrt{T_\mathrm{e}}}. \tag{5.103}$$

Comparing (5.102), (5.103) with (5.97), (5.98), we find that the high-temperature asymptotes of neutral atoms and ions are identical.

Finally we note that numerous variants of the effective Gaunt factors $p^{(Z>0)}(\beta)$ and $p^{(Z=0)}(\beta)$ are proposed in the literature, see, e.g., (Fischer et al. 1996). They practically do all not differ very much.

5.5 Excitation of Dipole-Forbidden Transitions in Atoms

5.5.1 Intercombination Transitions

The previous section considered collisional excitation of dipole-allowed transitions in atoms that can be described classically with the use of the concept of a transition oscillator. For dipole-forbidden transitions, this approach is not applicable because $f_{ji} = 0$. In this case, the interaction between an incident electron and an atom/ion is of *non-dipole* nature.

Dipole-forbidden transitions can be of two types: (1) no change in an atomic spin and (2) with a change in an atomic spin. In the first case, there is no dipole moment of a transition because of non-fulfillment of selection rules (in pure *LS*-coupling) for the orbital quantum number L: $\left|L_j - L_i\right| > 1$ or $L_i = L_j = 0$. Excitation for these atomic transitions is due to *direct* Coulomb interaction of an incident electron with quadrupole or other more higher multipole moments.

The dependences of the cross-section of collisional excitation of transitions of the first type on the incident electron energy E in the near-threshold region ($x = E/\Delta E_{ji} \approx 1$) and for high energies ($x \gg 1$) are the same as for dipole-allowed transitions [see (5.86)]. In view of this fact, the most simple approximation of the excitation cross-section of a dipole-forbidden transition *with no change in spin* can be represented as

$$\sigma_{ji}\left(x = E/\Delta E_{ji}\right) = c\frac{\sqrt{x-1}}{a + x^{3/2}}, \tag{5.104}$$

where a, c are the parameters that define the incident electron energy at the cross-section maximum ($E_{max} = \Delta E_{ji}\, x_{max}$) and the value of the cross-section maximum σ_{max} itself. It should be noted that formula (5.104) can be used for an approximate description of the cross-section of a dipole-allowed transition. As a rule, the maximum cross-section σ_{max} for dipole-forbidden transitions with no change in atomic spin is much less than a corresponding dipole-allowed transition. The maximum of the cross-section of dipole-forbidden transitions is shifted to the region of lower energies in comparison with dipole-allowed transitions (in the majority of cases $1.5 < x_{max} < 2$, whereas with increasing excitation energy x_{max} decreases).

Now let us consider collisional excitation of dipole-forbidden transitions with a change in atomic spin, the so-called *intercombination* transitions (see also Sect. 1.2.2). In this case, excitation of an atom occurs due to *exchange* interaction between incident and atomic electrons. Exchange interaction is essentially of quantum mechanical nature. At a qualitative level, the process can be described as follows. An incident electron transfers a considerable part of its energy ΔE to an atomic electron that is in a state with energy E_i. As a result, the incident electron is captured into an atomic orbit with an energy $E_j > E_i$, and the atomic electron is ionized. Thus, the incident and atomic electrons seem to exchange their roles that are based on the indistinguishability of electrons.

The energy transfer, at which exchange excitation of an atom at the transition $i \to j$ occurs, is determined by the inequality

$$E + \left|E_j\right| \le \Delta E \le E + |E_i|. \tag{5.105}$$

We note that bound states of atomic electrons correspond to negative energies $E_{i,j} < 0$. The simple classical consideration is valid far from threshold $x \gg 1$ when [according to (5.105)] the energy transferred from an incident electron to an atomic electron is much larger than the excitation energy: $\Delta E \gg \Delta E_{ji}$. Therefore, exchange interaction is more strong than direct interaction if $\Delta E = \Delta E_{ji}$. It occurs at small distances from the atomic nucleus (of the order of the size of an excited electron orbit), in contrast to the electron–dipole interaction for the excitation of dipole-allowed transitions that occur at long distances from an atom.

According to the above-developed physical picture of cross-section calculation, it is possible to use the expression (5.34) for the cross-section of electron energy transfer in Rutherford scattering. Integrating this formula within the limits determined by the relation (5.105), we find

$$\sigma_{ji}^{(\mathrm{inter})}\left(E \gg \Delta E_{ji}\right) = \frac{\pi e^4}{E} \frac{\Delta E_{ji}}{\left(E + \left|E_j\right|\right)\left(E + |E_i|\right)}. \tag{5.106}$$

It is convenient to rewrite this equation in terms of the dimensionless variable $x = E/\Delta E_{ji}$. From (5.106), it follows then the asymptotic expression for the intercombination transition cross-section in the high-energy domain, i.e., $E \gg |E_i|$:

$$\sigma_{ji}^{(\mathrm{inter})}(E \gg |E_i|) = \frac{\pi e^4}{\left(\Delta E_{ji}\right)^2} \frac{1}{x^3}. \tag{5.107}$$

Therefore at high-incident electron energies, the excitation cross-section of an intercombination transition decreases more rapidly than the cross-section with no change in spin (5.104). This fact is connected with the necessity of transfer of a large quantity of energy in exchange interaction [see the relations (5.105)] resulting in intercombination excitation.

In the near-threshold region of energies, i.e. $x = E/\Delta E_{ji} \approx 1$, the same asymptotic is valid for the intercombination cross-section as for the dipole case [$\sigma \propto \sqrt{x-1}$, see (5.86)]. Combining the limiting cases [see analogy for the derivation of (5.104)], the following simple approximation can be obtained for the excitation cross-section of an intercombination transition in an atom by electron impact (Astapenko et al. 2000):

$$\sigma_{ji}^{(\mathrm{inter})}\left(x = \frac{E}{\Delta E_{ji}}\right) = c\frac{\sqrt{x-1}}{a + x^{7/2}}, \tag{5.108}$$

where a and c are the parameters characterizing the transition under consideration. The obtained expression is valid in a wide range of projectile energies up to relativistic values. Figure 5.9 shows the cross-section of collisional excitation of the intercombination transition $3s\ ^1S \rightarrow 3p\ ^3P$ in a magnesium atom calculated by (5.108) for $c = 2 \times 10^{-14}$ cm^2 and $a = 10$ together with experimental data.

In the initial state, there are two valence electrons with antiparallel spins in the 3*s*-subshell of a magnesium atom, i.e., the total spin is zero. In a collision with an incident electron, one of the 3*s*-*valence* electrons is excited to the 3*p*-subshell due to exchange interaction with a spin flip, resulting in a total atomic spin of one. From Fig. 5.9, it is seen that the cross-section is rather large and that $x_{\max} = E_{\max}/\Delta E_{ji} \approx 1.85$, which is considerably less than for the case of a dipole-allowed transition, when $x_{\max} \cong 3.45$. It follows from it that the large value of the cross-section maximum is caused by a relatively low value of the excitation threshold ($\Delta E_{ji} \cong 2.7$ eV).

5.5.2 *Intermediate Coupling Effects*

The asymptotic behavior of the intercombination cross-sections for high-energy is strictly valid only in the *LS*-coupling scheme. In general, however, intermediate coupling admixes spin-allowed cross-sections to the exchange cross-section thereby changing entirely the asymptotic behavior. As has been shown by Vainshtein (Sobelman and Vainshtein 2006), the excitation cross-section can be expressed in terms of products of radial cross-sections and angular factors. In the intermediate coupling scheme, this can be formulated for the mixed states a_0 and a_1 in the following way:

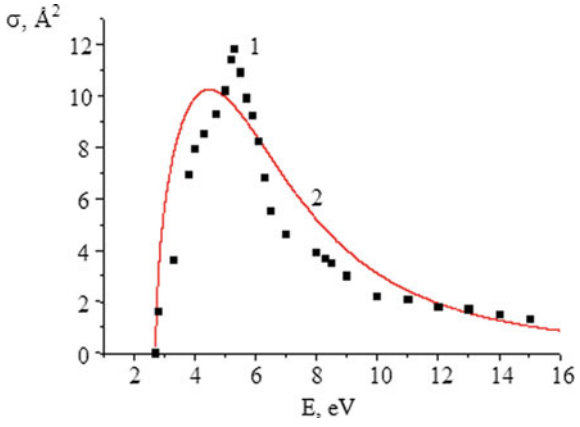

Fig. 5.9 Excitation cross-section by electron impact of the intercombination transition $3s\ ^1S \rightarrow 3p\ ^3P$ in a magnesium atom: 1—experimental data (NIST 2019), 2—model cross-section (5.108)

$$\sigma_{a_0 a_1} = \sum_{\kappa} \left\{ Q^d_\kappa(a_0,a_1)\sigma^d_\kappa(n_0 l_0, n_1 l_1) + Q^e_\kappa(a_0,a_1)\sigma^e_\kappa(n_0 l_0, n_1 l_1) + Q^e_{\kappa+1}(a_0,a_1)\sigma^e_{\kappa+1}(n_0 l_0, n_1 l_1) \right\} . \tag{5.109}$$

$\sigma^d_\kappa(n_0 l_0, n_1 l_1)$, $\sigma^e_\kappa(n_0 l_0, n_1 l_1)$, and $\sigma^e_{\kappa+1}(n_0 l_0, n_1 l_1)$ are the radial parts of the one-electron cross-sections of direct and exchange contributions of multiplicity κ (the multiplicity can vary in the interval $\kappa = \kappa_{\min}, \kappa_{\min}+2, \ldots, \kappa_{\max}$ with $\kappa_{\min} = |l_0 - l_1|$ and $\kappa_{\max} = l_0 + l_1$), $Q^d_\kappa(a_0,a_1)$, $Q^e_\kappa(a_0,a_1)$, and $Q^e_{\kappa+1}(a_0,a_1)$ are the corresponding angular factors of direct and exchange terms. If the mixed state is represented by

$$\Psi(a) = \sum_{\mathrm{LS}} \langle a \mid a_{\mathrm{LS}} \rangle \Psi(a_{\mathrm{LS}}), \tag{5.110}$$

where $\langle a \mid a_{\mathrm{LS}} \rangle$ are the mixing coefficients, the angular factors are given by

$$Q^d_\kappa = \frac{2l_0+1}{2J_0+1} \cdot b^2_\kappa(a_0,a_1), \tag{5.111}$$

$$Q^e_\kappa = \frac{2l_0+1}{2J_0+1} \cdot \left(\frac{b^2_\kappa(a_0,a_1)}{4} + \sum_{\mathrm{x}} b^2_{\kappa,\mathrm{x}}(a_0,a_1) \right). \tag{5.112}$$

The respective amplitudes in intermediate coupling can be expressed in terms of the known mixing coefficients and amplitudes in *LS*-coupling:

$$b_{\kappa,\mathrm{x}}(a_0,a_1) = \sum_{L_0 S_0 L_1 S_1} \left\langle a_0 \mid a_{0,L_0S_0} \right\rangle b^{(LS)}_{\kappa,\mathrm{x}}(a_{0,L_0S_0}, a_{1,L_1S_1}) \left\langle a_{1,L_1S_1} \mid a_1 \right\rangle, \tag{5.113}$$

$$b_{\kappa}(a_0,a_1) = \sum_{L_0 S_0 L_1 S_1} \left\langle a_0 \mid a_{0,L_0S_0} \right\rangle b^{(LS)}_{\kappa}(a_{0,L_0S_0}, a_{1,L_1S_1}) \left\langle a_{1,L_1S_1} \mid a_1 \right\rangle. \tag{5.114}$$

$b^{(LS)}_\kappa(a_{0,L_0S_0}, a_{1,L_1S_1})$ and $b^{(LS)}_{\kappa,\mathrm{x}}(a_{0,L_0S_0}, a_{1,L_1S_1})$ are the amplitudes in *LS*-coupling that have analytical solution in terms of the $3j$ and $6j$ symbols, the quantum numbers of the atomic core $L_\mathrm{P}S_\mathrm{P}$ and of the optical electron l_0 and l_1, the number of equivalent electrons m, and the fractional parentage coefficient $G^{L_0S_0}_{L_\mathrm{P}S_\mathrm{P}}$:

$$b^{(LS)}_\kappa(a_{0,L_0S_0}, a_{1,L_1S_1}) = \delta_{S_0S_1} \cdot (-1)^{J_1-S_0} \cdot [J_0J_1] \cdot \begin{Bmatrix} \kappa & J_0 & J_1 \\ S_0 & L_1 & L_0 \end{Bmatrix} \cdot \tilde{b}^{(LS)}_\kappa(L_0L_1), \tag{5.115}$$

$$b^{(LS)}_{\kappa,\mathrm{x}}(a_{0,L_0S_0}, a_{1,L_1S_1}) = \sqrt{3/2}\cdot(-1)^{S_\mathrm{P}-S_1+1/2+L_1}\cdot[J_0J_1S_0S_1x]\cdot \begin{Bmatrix} \kappa & J_0 & x \\ S_0 & L_1 & L_0 \end{Bmatrix}\begin{Bmatrix} x & J_1 & 1 \\ S_1 & S_0 & L_1 \end{Bmatrix}\begin{Bmatrix} 1 & S_0 & S_1 \\ S_\mathrm{P} & 1/2 & 1/2 \end{Bmatrix}\cdot \tilde{b}^{(LS)}_{\kappa}(L_0L_1), \tag{5.116}$$

$$\tilde{b}^{(LS)}_{\kappa}(L_0L_1) = \sqrt{m}\cdot(-1)^{L_\mathrm{P}}\cdot[L_0L_1]\cdot \begin{Bmatrix} \kappa & L_0 & L_1 \\ L_\mathrm{P} & l_1 & l_0 \end{Bmatrix}\cdot G^{L_0S_0}_{L_\mathrm{P}S_\mathrm{P}}, \tag{5.117}$$

$$[J_0J_1\ldots] = [(2J_0+1)\cdot(2J_1+1)\cdot\ldots]^{1/2}. \tag{5.118}$$

Table 5.1 Intermediate coupling angular coefficients and fitting parameters for rate coefficients

Transition	Q^d	Q^e	A^d/A^e	χ^d/χ^e	D^d/D^e
$1s^2\ {}^1S_0 - 1s2s\ {}^1S_0$					
LS-coupling	2	0.5			
$Z_\mathrm{n} = 9$	2	0.5	3.31/2.09	0.782/0.608	0.350/0.00
$Z_\mathrm{n} = 18$	2	0.5	3.40/2.18	0.641/0.665	0.30/0.00
$Z_\mathrm{n} = 42$	2	0.5	3.33/2.48	0.933/1.18	1.00/0.05
$1s^2\ {}^1S_0 - 1s2s\ {}^3S_1$					
LS-coupling	0	1.5			
$Z_\mathrm{n} = 9$	0	1.5	2.13/1.83	0.0651/0.587	-0.80/0.00
$Z_\mathrm{n} = 18$	0	1.5	2.83/2.07	0.287/0.657	-0.40/0.00
$Z_\mathrm{n} = 42$	0	1.5	3.33/2.48	0.933/1.18	1.00/0.05
$1s^2\ {}^1S_0 - 1s2p\ {}^1P_1$					
LS-coupling	2	0.5			
$Z_\mathrm{n} = 9$	2.00	0.5	5.90/12.7	0.378/1.08	4.50/0.00
$Z_\mathrm{n} = 18$	1.97	0.5	8.91/12.6	0.217/1.07	2.10/0.00
$Z_\mathrm{n} = 42$	1.52	0.5	9.35/14.3	0.392/1.69	3.25/0.05
$1s^2\ {}^1S_0 - 1s2p\ {}^3P_0$					
LS-coupling	0	1.67×10^{-1}			
$Z_\mathrm{n} = 9$	0	1.67×10^{-1}	6.19/13.5	0.386/1.07	4.50/0.00
$Z_\mathrm{n} = 18$	0	1.67×10^{-1}	9.03/13.0	0.222/1.06	2.15/0.00
$Z_\mathrm{n} = 42$	0	1.67×10^{-1}	9.35/14.3	0.392/1.69	3.25/0.05
$1s^2\ {}^1S_0 - 1s2p\ {}^3P_1$					
LS-coupling	**0**	0.5			
$Z_\mathrm{n} = 9$	$\mathbf{6.27 \times 10^{-4}}$	0.5	6.19/13.5	0.386/1.07	4.50/0.00
$Z_\mathrm{n} = 18$	$\mathbf{3.21 \times 10^{-2}}$	0.5	9.02/13.0	0.221/1.07	2.15/0.00
$Z_\mathrm{n} = 42$	$\mathbf{4.85 \times 10^{-1}}$	0.5	9.35/14.3	0.392/1.69	3.25/0.05
$1s^2\ {}^1S_0 - 1s2p\ {}^3P_2$					
LS-coupling	0	8.33×10^{-1}			
$Z_\mathrm{n} = 9$	0	8.33×10^{-1}	6.19/13.5	0.386/1.07	4.50/0.00
$Z_\mathrm{n} = 18$	0	8.33×10^{-1}	9.06/1.29	0.218/1.06	2.10/0.00
$Z_\mathrm{n} = 42$	0	8.33×10^{-1}	9.35/14.3	0.392/1.69	3.25/0.05

The fitting coefficients for $Z_\mathrm{n} = 42$ can be used for any ion with $Z_\mathrm{n} > 10$. The precision of the fitting coefficients β, χ, D is typically better than 10% in a large temperature interval of $1/8 < \beta < 64$

It is difficult to obtain general expressions for the cross-sections in intermediate coupling because the calculation of the mixing coefficients $\langle a \mid a_{LS}\rangle$ requests numerical calculations of the atomic structure and the sums in (5.109), (5.111)–(5.114) are rather cumbersome.

In order to provide some insight into the intermediate coupling effects on excitation cross-sections, let us consider the excitation of the He-like excited levels $a_1 = 1s2l\,LSJ$ from the ground state $a_0 = 1s^2\ {}^1S_0$. In this case, formulas (5.109)–(5.114) can be considerably simplified ($n_0 = 1;\ l_0 = 0;\ n_1 = 2;\ l_1 = 0, 1;\ \kappa = 1$):

$$\sigma_{a_0 a_1} = Q^d_\kappa \sigma^d_\kappa(n_0 l_0, n_1 l_1) + Q^e_\kappa \sigma^e_\kappa(n_0 l_0, n_1 l_1). \tag{5.119}$$

Table 5.1 shows the angular Q-factors for LS-coupling and intermediate coupling for various elements. The angular factors for the intercombination transition $1s^2\ {}^1S_0 - 1s2p\ {}^3P_1$ show that in LS-coupling the contribution of the direct cross-section is zero ($Q^d = 0$) and gradually increases with increasing nuclear charge (see bold values in Table 5.1). For molybdenum (Z_n = 42), the intermediate coupling effect is so strong that the angular factor reaches a value of $Q^d = 0.485$ which is about one-third of the angular factor for the resonance transition $1s^2\ {}^1S_0 - 1s2p\ {}^1P_1$. Therefore, the high-energy asymptote is entirely dominated by the direct cross-section rather than by the exchange cross-section, i.e.,

$$\sigma(1s^2\ {}^1S_0 - 1s2p^3P_1) = Q^d_1 \sigma^d_1(1,0;2,1) + Q^e_1 \sigma^e_1(1,0;2,1) \underset{E \gg \Delta E}{\rightarrow} Q^d_1 \sigma^d_1(1,0;2,1). \tag{5.120}$$

For completeness, Table 5.1 provides also the fitting parameters for the explicit calculation of the corresponding rate coefficients averaged over a Maxwellian distribution function.

The adopted fitting formulas are as follows:

$$\frac{C_{ij}}{(\mathrm{cm}^3\,\mathrm{s}^{-1})} = \frac{10^{-8}}{Z^3}\left(\frac{E_j}{E_i}\right)^{3/2}\sqrt{\beta}\cdot\exp\left(-\frac{\Delta E_{ij}}{T_e}\right) \cdot\left\{\frac{Q^d\cdot A^d\cdot(\beta+1+D^d)}{\beta+\chi^d} + \frac{Q^e\cdot A^e\cdot(\beta+D^e)}{\beta+\chi^e}\right\}, \tag{5.121}$$

$$\beta = \frac{Z^2\mathrm{Ry}}{T_e}, \tag{5.122}$$

$$\Delta E_{ij} = E_i - E_j, \tag{5.123}$$

where Z is the spectroscopic symbol and Ry = 13,606 eV. Let us consider an example for molybdenum and the intercombination transition $1s^2\ ^1S_0 - 1s2p\ ^3P_1$ for an electron temperature of T_e = 20,000 eV: $Z = 42 - 2 + 1 = 41$, $E_{i=1s^2\ ^1S_0} = 23,810.6\,\text{eV}$, $E_{j=1s2p\ ^3P_1} = 5903.7\,\text{eV}$, $\Delta E_{ij} = 17,906.9\,\text{eV}$, $\beta = 1.277$: $C_{ij} \approx 1.5 \times 10^{-13}\,\text{cm}^3\,\text{s}^{-1}$. This is the intermediate coupling cross-section whereas in pure LS-coupling $C_{ij}^{LS} \approx 2.6 \times 10^{-14}\,\text{cm}^3\,\text{s}^{-1}$. This example demonstrates not only the importance of intermediate coupling on the high-energy asymptotes of cross-sections and rates but also its impact on the total rate coefficient for rather moderate temperatures (β—values of the order of one). We note that the fitting coefficients in Table 5.1 do not include resonance contributions. These contributions are most pronounced for the excitation of the $1s2s\ ^3S_1$ state (some 10%) and the $1s2p\ ^3P_2$ state (about 10%). For applications in plasma atomic physics, resonance contributions can be rather well included in atomic kinetics via explicit inclusion of multiple excited autoionizing states as suggested by Cowan (1980, 1983).

It should be noted that the decreasing of the cross-section σ_κ with decreasing κ is not connected with any small parameter. This differs radically from the interaction of an atom with an electromagnetic field where higher multipoles contain the factor $(Z \cdot \alpha)^{2\kappa+1}$ making each successive term smaller by a factor of about $5 \times 10^{-5} \cdot Z^2$. In the case of electron–atom collisions, such small parameter does not exist. Numerical calculations show that the multipole cross-section $\sigma_{\kappa+2}$ is usually about ten times smaller than σ_κ (Sobelman and Vainshtein 2006) but might be in some cases have even larger contributions than the lowest one (Rosmej 2000). Finally we note that unlike radiative transitions, non-dipole transitions (e.g., monopole, quadrupole) can have rather large cross-section values and are not at all negligible for high-precision calculations.

For rapid calculations of large transition arrays, the Regemorter approach provides a reasonable estimate of the collisional cross-sections for the total emission group. For similar purposes, the plane wave Born PWB approximation attracts interest up to present days, because this approach can be easily incorporated in atomic structure codes and allows to estimate also monopole and quadrupole transitions and shows a correct high-energy behavior (which is difficult to obtain in more complex numerical methods like the R-matrix and the convergent-close-coupling method). The pathological behavior at threshold of the PWB approximation can be removed by the empirical Robb–Cowan approach (Cowan 1981) that has recently been improved by the so-called Elwert–Sommerfeld correction factor (Kilcrease and Brookes 2013).

Other important corrections to the first-order cross-sections have been proposed by Vainshtein (Sobelman and Vainshtein 2006): one-channel normalization, K-matrix, inclusion of exchange and intermediate coupling effects (note that the above fitting parameters of Table 5.1 are based on numerical calculations of the one-channel normalized Coulomb–Born approximation including exchange and intermediate coupling effects). For example, it has been demonstrated for neutral helium HeI (Beigman et al. 2000) that the application of the K-matrix method to

pure Born cross-sections results in rather good agreement with the numerically very complex convergent-close-coupling calculations CCC. Detailed electron collisional exciation and deexciation rate coefficients (including intercombination transitions) for H I, He I and He II are presented in Annex 2 and 3.

Finally we note that the application of PWB collisions strengths to line polarization provides reasonable numerical values as essentially ratios of cross-sections enter to the line polarization formulas (Cowan 1981; Percival and Seaton 1958).

5.6 Analytical Empirical Formulas for Dielectronic Recombination in Dense Plasmas

Dielectronic recombination is a combination of dielectronic capture and subsequent radiative stabilization competing with multi-channel autoionization. In non-LTE plasmas, excited states coupling, angular momentum changing collisions, collisional depopulation and ionization potential depression strongly alter the stabilization processes. A consistent description of non-LTE dielectronic recombination involves therefore atomic kinetics and electric field perturbations of the atomic structure and related matrix elements (Rosmej et al. 2020).

5.6.1 Autoionization, Dielectronic Capture, and Dielectronic Recombination

Dielectronic recombination can easily be calculated from the autoionizing rate of a certain atomic state with the help of the principle of detailed balance. The first step is the application of the principle of detailed balance to dielectronic capture, i.e.,

$$n_{\mathrm{j}}^{Z} \cdot \Gamma_{\mathrm{jk}}^{Z,Z+1} = n_{\mathrm{k}}^{Z+1} \cdot n_{\mathrm{e}} \cdot \langle \mathrm{DC} \rangle_{\mathrm{kj}}, \tag{5.124}$$

where n_{j}^{Z} is the atomic population of the upper state, $\Gamma_{\mathrm{jk}}^{Z,Z+1}$ is the autoionizing rate from the upper state to a state k with population n_{k}^{Z+1}, and $\langle \mathrm{DC} \rangle_{\mathrm{kj}}$ is the dielectronic capture rate from state k to the upper state j. In thermodynamic equilibrium, the populations n_{j}^{Z} and n_{k}^{Z+1} are linked via the Saha–Boltzmann equation because the states j and k belong to different ionic states, Z and $Z+1$ respectively, i.e.,

$$\frac{n_{\mathrm{j}}^{Z}}{n_{\mathrm{k}}^{Z+1}} = n_{\mathrm{e}} \cdot \frac{g_{\mathrm{j}}^{Z}}{2g_{\mathrm{k}}^{Z+1}} \cdot \left(\frac{2\pi\hbar^2}{m_{\mathrm{e}} k T_{\mathrm{e}}} \right)^{3/2} \cdot \exp\left(\frac{\Delta E_{\mathrm{k,j}}^{Z+1,Z}}{k T_{\mathrm{e}}} \right). \tag{5.125}$$

g_j^Z and g_k^{Z+1} are the statistical weights of the states j and k, n_e is the electron density, m_e the electron mass, and T_e the electron temperature. The energy difference $\Delta E_{k,j}^{Z+1,Z}$ is related to the so-called dielectronic capture energy E_{kj}^{DC} by

$$\Delta E_{k,j}^{Z+1,Z} = -E_{kj}^{DC}. \tag{5.126}$$

E_{kj}^{DC} is the energy of the Auger electron, if the autoionizing state j decays via autoionization to state k. Combining (5.124)–(5.126), we find the general expression for the dielectronic capture rate:

$$\langle DC\rangle_{kj} = \frac{g_j^Z}{2g_k^{Z+1}} \cdot \left(\frac{2\pi\hbar^2}{m_e}\right)^{3/2} \cdot \Gamma_{jk}^{Z,Z+1} \cdot \frac{\exp(-E_{kj}^{DC}/kT_e)}{(kT_e)^{3/2}} \tag{5.127a}$$

or, in convenient units

$$\langle DC\rangle_{kj} = 1.656 \times 10^{-22} \cdot \frac{g_j^Z}{g_k^{Z+1}} \cdot \Gamma_{jk}^{Z,Z+1} \cdot \frac{\exp\left(-E_{kj}^{DC}(eV)/T(eV)\right)}{(T_e(eV))^{3/2}} \left[\frac{cm^3}{s}\right]. \tag{5.127b}$$

If $P_{j,gr}^Z$ is the probability that the autoionizing state j of charge state Z decays to the ground state gr of the same charge state, the quantity $P_{j,gr}^Z \cdot \langle DC\rangle_{kj}$ is called the dielectronic recombination rate coefficient [$cm^3\ s^{-1}$] into state k via the intermediate state j:

$$\langle DR\rangle_{kj}^{Z+1,Z} = P_{j,gr}^Z \cdot \langle DC\rangle_{kj}^{Z+1,Z}. \tag{5.128}$$

In general, the probability $P_{j,gr}^Z$ is a function of density and temperature, i.e.,

$$P_{j,gr}^Z = P_{j,gr}^Z(n_e, T_e). \tag{5.129}$$

The probability function (5.129) has to be determined from numerical calculations of a multilevel, multicharge state atomic population kinetics that explicitly involves all necessary autoionizing states as "active levels" (means the populations of the autoionizing levels are calculated on the same footing as ground and single excited states). If collisions are negligible compared to spontaneous radiative decay rates as well as autoionizing rates, the probability $P_{j,gr}^Z$ can be approximated by the so-called satellite branching factor

$$P_{j,gr}^Z \to \sum_i B_{ji}^Z = \sum_i \left\{\frac{A_{ji}^Z}{\sum_l A_{jl}^Z + \sum_k \Gamma_{jk}^{Z,Z+1}}\right\}. \tag{5.130}$$

Let us illuminate the situation with the help of the most simple autoionizing states $2l2l'$, in particular the state $j = 2p^2\ ^1D_2$ of He-like argon. In this case, $Z = 16$,

$k = 1s\ ^2S_{1/2}$, and $i = 1s2p\ ^1P_1, i' = 1s2p\ ^3P_1,\ i'' = 1s2p\ ^3P_2$: $\Gamma_{kj}^{Z,Z+1} = 3.09\times 10^{14}\,s^{-1}$, $A_{ji}^{Z} = 1.22\times 10^{14}\,s^{-1}$, $A_{ji'}^{Z} = 1.92\times 10^{9}\,s^{-1}$, $A_{ji''}^{Z} = 6.21\times 10^{12}\,s^{-1}$. Therefore, $P_{j,gr}^{Z=16} \approx \sum_i B_{ji}^{Z=16} = 2.78\times 10^{-1} + 4.38\times 10^{-6} + 1.42\times 10^{-2} = 2.92\times 10^{-1}$. The approximation $P_{j,gr}^{Z} \approx \sum_i B_{ji}^{Z}$ assumes that all single excited states, namely $i = 1s2p\ ^1P_1$, $i' = 1s2p\ ^3P_1$, $i'' = 1s2p\ ^3P_2$, decay entirely to the ground state $gr = 1s^2\ ^1S_0$ via the radiative transitions $1s2p\ ^1P_1 \rightarrow gr$, $1s2p\ ^3P_1 \rightarrow gr$, and $1s2p\ ^3P_2 \rightarrow gr$. Because $A(1s2p\ ^1P_1 \rightarrow gr) = 1.07\times 10^{14}\,s^{-1}$, $A(1s2p\ ^3P_1 \rightarrow gr) = 1.82\times 10^{12}\,s^{-1}$, $A(1s2p\ ^3P_2 \rightarrow gr) = 3.16\times 10^{8}\,s^{-1}$, the assumption that the excited state j decays to the ground state via the intermediate states i, i', i'' is a good assumption because the sum in (5.130) is dominated by the strongest transition $j \rightarrow i$ where collisional "competition" starts to be important only for near-solid density plasmas (and contributions $j \rightarrow i'$ and $j \rightarrow i''$ are small). Therefore, the dielectronic recombination rate can be approximated by the following expression:

$$\langle \mathrm{DR}\rangle_{kj}^{Z+1,Z} \approx \sum_i \left\{ \frac{A_{ji}^{Z}}{\sum_l A_{jl}^{Z} + \sum_k \Gamma_{jk}^{Z,Z+1}} \cdot \langle \mathrm{DC}\rangle_{kj}^{Z+1,Z} \right\}. \tag{5.131}$$

With the help of (5.125), (5.131) can be written as follows:

$$\langle \mathrm{DR}\rangle_{kj}^{Z+1,Z} \approx \frac{1}{2g_k^{Z+1}} \cdot \left(\frac{2\pi\hbar^2}{m_e}\right)^{3/2} \cdot \frac{\exp(-E_{kj}^{\mathrm{DC}}/kT_e)}{(kT_e)^{3/2}} \cdot \sum_i \left\{ \frac{g_j^{Z} \cdot \Gamma_{jk}^{Z,Z+1} \cdot A_{ji}^{Z}}{\sum_l A_{jl}^{Z} + \sum_k \Gamma_{jk}^{Z,Z+1}} \right\}. \tag{5.132}$$

The term in parenthesis is the so-called dielectronic satellite intensity factor

$$Q_{k,ji}^{Z+1,Z} = \frac{g_j^{Z} \cdot \Gamma_{jk}^{Z,Z+1} \cdot A_{ji}^{Z}}{\sum_l A_{jl}^{Z} + \sum_k \Gamma_{jk}^{Z,Z+1}}. \tag{5.133}$$

Therefore, under the assumptions made in (5.130), the dielectronic recombination due to the autoionizing states $2l2l'$ is given by the sum of the dielectronic satellite intensity factors, for the present example of Ar, numerical calculations (including intermediate coupling and configuration interaction) provide $\sum_{j,i} Q_{k,ji} = 8.29\times 10^{14}\,s^{-1}$ and $E_{k,ji=2l2l'}^{\mathrm{DC}} \approx 2.302\times 10^{3}$ eV. For the autoionizing states $2l3l'$, we obtain $\sum_{j,i} Q_{k,ji} = 7.95\times 10^{14}\,s^{-1}$ and $E_{k,ji=2l3l'}^{\mathrm{DC}} \approx 2.875\times 10^{3}$ eV, for the $2l4l'$ states $\sum_{j,i} Q_{k,ji} = 4.77\times 10^{14}\,s^{-1}$ and $E_{k,ji=2l4l'}^{\mathrm{DC}} \approx 3.072\times 10^{3}$ eV, for the $2l5l'$ states $\sum_{j,i} Q_{k,ji} = 2.96\times 10^{14}\,s^{-1}$ and $E_{k,ji=2l5l'}^{\mathrm{DC}} \approx 3.16\times 10^{3}$ eV, for the $2l6l'$ states $\sum_{j,i} Q_{k,ji} = 1.89\times 10^{14}\,s^{-1}$ and $E_{k,ji=2l6l'}^{\mathrm{DC}} \approx 3.21\times 10^{3}$ eV, for the $2l7l'$ states $\sum_{j,i} Q_{k,ji} = 1.29\times 10^{14}\,s^{-1}$ and $E_{k,ji=2l7l'}^{\mathrm{DC}} \approx 3.24\times 10^{3}$ eV. One can see that the convergence for high n-spectator electrons is not quite rapid and follows approximately the scaling law $\sum_j Q_{k,ji=2lnl'}^{\mathrm{DC}} \propto 1/n^3$.

Despite of the most simple configurations $2lnl'$ for the dielectronic recombination, one can see that the numerical calculations are rather cumbersome: Very large quantum numbers nl' have to be involved in the numerical calculations to reach convergence. For large quantum numbers, however, convergence is difficult to achieve in purely quantum numerical calculations and quasi-classical approaches are mandatory to practically solve the problem.

Next, to obtain the total dielectronic recombination rate from H-like to He-like ions, one needs to invoke all possible intermediate states $j = 3lnl'; 4lnl'; 5lnl', \ldots$ One can easily understand that for more complex configurations, the number of autoionizing states to be involved becomes rapidly numerically prohibitive for purely quantum mechanical numerical calculations.

Moreover, dielectronic recombination is not only related to corresponding atomic structure calculations, but also to the collisional radiative interplay for the calculation of the probability $P_{\mathrm{j,gr}}$. In general, one needs to include explicitly all relevant autoionizing states in a collisional radiative model in order to correctly predict the ionic fractions for given temperature and density. In this case, however, the atomic state population kinetics is entirely dominated by the number of autoionizing high-n-states and numerically prohibitive. It likewise looks rather strange, to dominate an atomic state population kinetics by autoionizing states just for the purpose to calculate one recombination coefficient. It is essentially for these reasons that numerical calculations of ionic fractions are still under controversial discussion up to present days (and in particular for high-Z elements) (NIST 2019; Rubiano et al. 2007; Chung et al. 2013; Colgan et al. 2015).

Moreover, dielectronic recombination is therefore not only a theoretical subject in atomic physics, but it has important impact to the radiative properties of atoms and ions, plasma spectroscopy, and technical applications (e.g., radiation sources). Note also that historically, dielectronic recombination has been invented to understand the order of magnitude discrepancies in the ionic abundance between calculations and spectroscopic observation from the solar corona emission (Burgess 1964).

5.6.2 Total Rates of Dielectronic Recombination and Multichannel Approach

In order to obtain the total dielectronic recombination rate $\langle \mathrm{DR} \rangle_{\mathrm{tot}}^{Z+1,Z}$, all dielectronic recombination rates $\langle \mathrm{DR} \rangle_{\mathrm{kj}}^{Z+1,Z} = P_{\mathrm{j,gr}}^{Z} \cdot \langle \mathrm{DC} \rangle_{\mathrm{kj}}^{Z+1,Z}$ have to be summed with respect to the initial state k and also with respect to the intermediate states j, i.e.,

$$\langle \mathrm{DR} \rangle_{\mathrm{tot}}^{Z+1,Z} = \sum_{\mathrm{k}} \sum_{\mathrm{j}} \langle \mathrm{DR} \rangle_{\mathrm{kj}}^{Z+1,Z} = \sum_{\mathrm{k}} \sum_{\mathrm{j}} P_{\mathrm{j,gr}}^{Z} \cdot \langle \mathrm{DC} \rangle_{\mathrm{kj}}^{Z+1,Z}. \tag{5.134}$$

Because the probability $P_{\mathrm{j,gr}}^{Z}$ is a function of density and temperature [see discussion related to (5.129)], it is difficult to obtain general and closed formulas for

the dielectronic recombination rate coefficient. Only in the low-density approximation, where relation (5.130) approximately holds true, general formulas in terms of dielectronic recombination rate coefficients that depend only on temperature can be obtained.

5.6.2.1 Burgess Formulas

One of the most used general approximate empirical formula in this framework is the so-called Burgess formula (Burgess 1964) that assumes that the nl-spectator electron which is not interacting with the core is treated in the hydrogenic approximation and that the capture cross-section can be expressed in terms of the excitation cross-section for transitions $\alpha_0 \to \alpha$ using the principle of correspondence discussed above:

$$\langle \mathrm{DR} \rangle_{\mathrm{kj}}^{Z+1,Z} := D^{Z+1,Z}(\alpha_0 \to \alpha, nl). \tag{5.135}$$

For the total dielectronic recombination rate, we have

$$\langle \mathrm{DR} \rangle_{\mathrm{tot}}^{Z+1,Z} := D^{Z+1,Z} = \sum_{\alpha_0} \sum_{\alpha} \sum_{\mathrm{n}} \sum_{l=0}^{n-1} D^{Z+1,Z}(\alpha_0 \to \alpha, nl). \tag{5.136}$$

For the simplest example of autoionizing states $2l2l'$ outlined above, $\alpha_0 = 1s$ and $\alpha_1 = 2p$, i.e., the transition $\alpha_0 \to \alpha$ corresponds to the Ly-alpha transition in H-like ions. For these configurations, dielectronic recombination into the ground state is the most important one, i.e., there exists a single state $k = \alpha_0 = 1s$. α_0 coincides therefore with the atomic ground state and the sum over α_0 can be suppressed, i.e.,

$$D^{Z+1,Z} \approx \sum_{\alpha} \sum_{\mathrm{n}} \sum_{l=0}^{n-1} D^{Z+1,Z}(\alpha_0 \to \alpha, nl). \tag{5.137}$$

The dielectronic recombination rate coefficient $D^{Z+1,Z}(\alpha_0 \to \alpha, nl)$ can then be expressed via the following analytical empirical expression (Burgess 1964)

$$D^{Z+1,Z}(\alpha_0 \to \alpha, nl) = 4.8 \times 10^{-11} f_{\alpha_0 \alpha} B_{\mathrm{d}} \beta^{3/2} \mathrm{e}^{-\beta \chi_{\mathrm{d}}} \, [\mathrm{cm}^3 \, \mathrm{s}^{-1}], \tag{5.138}$$

where

$$\beta = \frac{(z+1)^2 \, \mathrm{Ry}}{k T_{\mathrm{e}}}, \tag{5.139}$$

$$\chi_{\mathrm{d}} = \frac{\chi}{1 + 0.015 \, \dfrac{z^3}{(z+1)^2}}, \tag{5.140}$$

$$\chi = \frac{\Delta \mathrm{E}(\alpha_0 \rightarrow \alpha)}{(\mathrm{z}+1)^2\,\mathrm{Ry}}\,. \tag{5.141}$$

z is the so-called spectroscopic symbol of the double excited ion after recombination. The spectroscopic symbol is given by $z = Z_\mathrm{n} - N_\mathrm{bound} + 1$, where N_bound is the number of bound electrons. For example, for neutral helium the spectroscopic symbol is $z = 1$ (He I), singly ionized helium has $z = 2$ (He II).

If the first resonance transition is a $\Delta n = 0$ transition, the branching factor B_d is given by Cowan (1981):

$$B_\mathrm{d} = \left(\frac{z\chi}{z^2+13.4}\right)^{1/2} \frac{1}{1+0.105(z+1)\chi+0.015(z+1)^2\chi^2}\,. \tag{5.142}$$

For $\Delta n \neq 0$, the branching factor is approximated by Cowan (1981):

$$B_\mathrm{d} = \left(\frac{z\chi}{z^2+13.4}\right)^{1/2} \frac{0.5}{1+0.210(z+1)\chi+0.030(z+1)^2\chi^2}\,. \tag{5.143}$$

The branching factor B_d has the following meaning: After dielectronic capture, a double excited state is formed that can decay via autoionization or radiative decay. For the dielectronic recombination, only the radiative decays contribute finally to recombination as autoionization returns the autoionizing state to the original state.

According to (5.138), α_0 is the ground state and therefore $f_{\alpha_0\alpha}$ is the dipole oscillator strength for the resonance transition $\alpha_0 \rightarrow \alpha$ with transition energy $\Delta E(\alpha_0 \rightarrow \alpha)$ in [eV]. As the oscillator strength drops rapidly with principal quantum number, it is usually sufficient to consider only the first two α-terms in the sum of (5.137) and we finally obtain the desired expression for the total dielectronic recombination [$D^{Z+1,Z}(\alpha_0 \rightarrow \alpha) := \sum_n \sum_{l=0}^{n-1} D^{Z+1,Z}(\alpha_0 \rightarrow \alpha, nl)$]:

$$D^{Z+1,Z} \approx D^{Z+1,Z}(\alpha_0 \rightarrow \alpha_1) + D^{Z+1,Z}(\alpha_0 \rightarrow \alpha_2). \tag{5.144}$$

Let us consider the dielectronic recombination into neutral helium as an example:

$$\mathrm{He}^{1+}(1s) + e \rightarrow \mathrm{He}^{0+**}(nln'l') \rightarrow \mathrm{He}^{0+}(1s^2). \tag{5.145}$$

For this example, $\alpha_0 = 1s$, $\alpha_1 = 2p$, $\alpha_2 = 3p$, …. Therefore, the oscillator strength $f_{\alpha_0\alpha_1}$ corresponds to the oscillator strength of the resonance line, namely the H-like Lyman-alpha line of singly ionized helium, $f_{\alpha_0\alpha_2}$ corresponds to the Lyman-beta line. The oscillator strengths are $f_{1s\rightarrow 2p} = 0.4164$ and $f_{1s\rightarrow 3p} = 0.07914$, respectively, and their transition energies are $\Delta E(1s \rightarrow 2p) = 40.81\,\mathrm{eV}$ and $\Delta E(1s \rightarrow 3p) = 48.37\,\mathrm{eV}$, respectively. The spectroscopic symbol is

$z = 1$ and $\Delta n \neq 0$ (therefore (5.143) applies). As one can see, higher n oscillator strengths provide almost negligible contribution to the total dielectronic recombination rate. From (5.139)–(5.143), we obtain $\beta = 4\mathrm{Ry}/kT_e$, $B_d(1s \rightarrow 2p) = 0.0825$, $B_d(1s \rightarrow 3p) = 0.0846$, $\chi_d(1s \rightarrow 2p) = 0.747$, and $\chi_d(1s \rightarrow 3p) = 0.886$. More precise quantum mechanical calculations (Sobelman and Vainshtein 2006; Wang et al. 1999) provide $B_{d,ref}(1s \rightarrow 2p) = 0.155$, $B_{d,ref}(1s \rightarrow 3p) = 0.0144$, $\chi_{d,ref}(1s \rightarrow 2p) = 0.744$, and $\chi_{d,ref}(1s \rightarrow 3p) = 0.888$. For the rate coefficient at $kT_e = \mathrm{Ry}$ ($\beta = 4$), we obtain: $D^{He1+,He0+}(1s \rightarrow 2p) = 1.65 \times 10^{-12}[\mathrm{cm^3\,s^{-1}}]$, $D^{He1+,He0+}(1s \rightarrow 3p) = 3.2 \times 10^{-13}\,[\mathrm{cm^3\,s^{-1}}]$ and for the more precise quantum mechanical calculations, $D_{ref}^{He1+,He^{0+}}(1s \rightarrow 2p) = 3.10 \times 10^{-12}\,[\mathrm{cm^3\,s^{-1}}]$, $D_{ref}^{He1+,He0+}(1s \rightarrow 3p) = 5.46 \times 10^{-14}\,[\mathrm{cm^3\,s^{-1}}]$. This confirms that the leading terms for the dielectronic recombination are indeed given by (5.144).

5.6.2.2 Multichannel Approach

The comparison of the results from formulas (5.138)–(5.143) with more precise calculations (Sobelman and Vainshtein 2006; Wang et al. 1999; Kato and Asano 1999) shows that the χ_d-values are in quite good agreement, whereas the B_d values differ strongly. For the resonance transition $1s \rightarrow 2p$, the B_d-value obtained from (5.143) is about a factor of 2 smaller than more precise values. This is a general observation: The precision of formulas (5.142), (5.143) is about a factor of 2 for the resonance transition.

For the transition $1s \rightarrow 3p$, the B_d-value obtained from (5.143) is about a factor of 6 larger than the more precise values. This large overestimation is also a general observation and related to the fact that formulas (5.142), (5.143) take into account only one autoionizing channel. For the $3lnl'$-configurations (that are related to the transition $\alpha_0 \rightarrow \alpha_2 = 1s \rightarrow 3p$), however, autoionization decays not only to the ground state but to excited states too:

$$3lnl' \rightarrow \left\{ \begin{array}{l} 1s + e_{\mathrm{Auger}} \\ 2l + e_{\mathrm{Auger}} \end{array} \right\}. \tag{5.146}$$

Numerical calculations show (Rosmej et al. 1998; Petitdemange and Rosmej 2013) that the autoionizing rates to the excited states "$2l$" are even more important than to the ground state "$1s$". This reduces considerably the branching factor for the dielectronic recombination [the B_d-factor in (5.143)]. As the more precise calculations take into account many channels of Auger decay, the branching factor is therefore systematically smaller that those of (5.142), (5.143). In fact, as one can see from (5.143) very similar branching factors are provided for the transitions $\alpha_0 \rightarrow \alpha_1 = 1s \rightarrow 2p$ and $\alpha_0 \rightarrow \alpha_2 = 1s \rightarrow 3p$ due to the consideration of one autoionizing channel only.

Table 5.2 Fitting coefficients according (5.147) for the dielectronic recombination into H-like ions originating from the $2lnl'$- and $3lnl'$-autoionizing levels, $Z = Z_n$, $m = 1$, $l_0 = 0$ in (5.147)

	$2lnl'$: $\alpha_0 = 1s \to \alpha = 2p$		$3lnl'$: $\alpha_0 = 1s \to \alpha = 3p$	
Element	B_d	χ_d	B_d	χ_d
He	3.12×10^{-4}	0.744	5.48×10^{-6}	0.888
Li	3.72×10^{-4}	0.736	6.41×10^{-6}	0.887
Be	3.67×10^{-4}	0.727	6.53×10^{-6}	0.885
B	3.42×10^{-4}	0.718	6.47×10^{-6}	0.883
C	3.13×10^{-4}	0.709	6.32×10^{-6}	0.881
N	2.85×10^{-4}	0.700	6.31×10^{-6}	0.879
O	2.58×10^{-4}	0.691	5.92×10^{-6}	0.877
F	2.33×10^{-4}	0.682	5.70×10^{-6}	0.874
Ne	2.11×10^{-4}	0.673	5.48×10^{-6}	0.872
Na	1.90×10^{-4}	0.665	5.26×10^{-6}	0.870
Mg	1.72×10^{-4}	0.657	5.04×10^{-6}	0.868
Al	1.56×10^{-4}	0.649	4.84×10^{-6}	0.866
Si	1.41×10^{-4}	0.642	4.63×10^{-6}	0.863
P	1.27×10^{-4}	0.636	4.43×10^{-6}	0.861
S	1.15×10^{-4}	0.630	4.24×10^{-6}	0.859
Cl	1.05×10^{-4}	0.624	4.05×10^{-6}	0.857
Ar	9.50×10^{-5}	0.620	3.87×10^{-6}	0.856
K	8.61×10^{-5}	0.616	3.69×10^{-6}	0.854
C	7.82×10^{-5}	0.612	3.52×10^{-6}	0.852
Sc	7.09×10^{-5}	0.609	3.35×10^{-6}	0.851
Ti	6.45×10^{-5}	0.606	3.19×10^{-6}	0.849
V	5.85×10^{-5}	0.604	3.04×10^{-6}	0.848
Cr	5.33×10^{-5}	0.602	2.89×10^{-6}	0.847
Mn	4.85×10^{-5}	0.601	2.74×10^{-6}	0.846
Fe	4.42×10^{-5}	0.599	2.60×10^{-6}	0.845
Co	4.03×10^{-5}	0.598	2.47×10^{-6}	0.844
Ni	3.68×10^{-5}	0.598	2.34×10^{-6}	0.843
Cu	3.37×10^{-5}	0.597	2.22×10^{-6}	0.842
Zn	3.08×10^{-5}	0.597	2.10×10^{-6}	0.842
Ga	2.83×10^{-5}	0.596	1.99×10^{-6}	0.842
Ge	2.60×10^{-5}	0.596	1.88×10^{-6}	0.841
As	2.39×10^{-5}	0.596	1.78×10^{-6}	0.841
Se	2.20×10^{-5}	0.596	1.68×10^{-6}	0.841
Br	2.03×10^{-5}	0.596	1.59×10^{-6}	0.841
Kr	1.88×10^{-5}	0.596	1.50×10^{-6}	0.841
Rb	1.74×10^{-5}	0.597	1.42×10^{-6}	0.841
Sr	1.61×10^{-5}	0.597	1.34×10^{-6}	0.842
Y	1.50×10^{-5}	0.597	1.27×10^{-6}	0.842

(continued)

Table 5.2 (continued)

	$2lnl'$: $\alpha_0 = 1s \rightarrow \alpha = 2p$		$3lnl'$: $\alpha_0 = 1s \rightarrow \alpha = 3p$	
Element	B_d	χ_d	B_d	χ_d
Zr	1.39×10^{-5}	0.598	1.20×10^{-6}	0.842
Nb	1.30×10^{-5}	0.599	1.13×10^{-6}	0.843
Mo	1.21×10^{-5}	0.599	1.07×10^{-6}	0.843

The numerical data include corrections for multidecay channels (two channels for $2l2l'$ and four channels for $3lnl'$)

Due to the existence of multichannel autoionization decay, the multichannel radiative decay and the complexity of configurations involved, quantum numerical calculations of the dielectronic recombination are very complex and the precision of the Burgess formula is difficult to determine. This is another reason why the recourse to quasi-classical methods appears to be mandatory for a comprehensive description of the dielectronic recombination phenomenon.

Below, we provide numerical data for dielectronic recombination into H-, He-, and Li-like ions taking into account multichannels for Auger and radiative decay (Beigman 1981; Shevelko and Vainshtein 1993; Vainshtein and Shevelko 1996). The numerical results have been fitted to a simple analytical expression in order to facilitate the application of these complex calculations:

$$D^{Z+1,Z}(\alpha_0 \rightarrow \alpha, nl) = 10^{-8} \cdot \frac{m}{2l_0 + 1} \cdot B_d \cdot \beta^{3/2} \cdot e^{-\beta\chi_d} \, [\mathrm{cm^3\,s^{-1}}], \tag{5.147a}$$

$$\beta = \frac{Z^2 \cdot \mathrm{Ry}}{kT_e}, \tag{5.147b}$$

where Ry = 13,606 eV, kT_e is the electron temperature in [eV], m is the number of equivalent electrons of state α_0, Z is the charge of the ion where the core transition $\alpha_0 \rightarrow \alpha$ takes place (e.g., for the $2lnl'$-autoionizing states of He-like argon the core transition is the $1s \rightarrow 2p$ transition in H-like argon, $Z = 18$), l_0 is the corresponding orbital momentum of state α_0. The physical meaning of the parameter χ_d is related to the fact that all contributions of the configuration with different spectator electrons nl have to be summed up for the total dielectronic recombination rate with different energies [see (5.16)]. The parameter χ_d provides a fit to the numerical results to replace the sum of different energies in a best manner by an average energy $\chi_d \cdot \beta$. Finally, the total sum is replaced by an average amplitude B_d to provide a simple analytical expression without any summation.

Table 5.2 presents the numerical calculation of the total dielectronic recombination rate into H-like ions for the core transitions $1s$–$2p$ and $1s$–$3p$ for all elements from He ($Z = 2$) (see also Annex 3) until Mo ($Z = 42$) and the corresponding fitting parameters according (5.147). It can be seen that for low-Z elements, the dielectronic recombination related to the core transition $1s$–$2p$ is dominating, for large Z-values, the relative contribution of the dielectronic recombination with the core

Table 5.3 Fitting coefficients according to (5.147) for the dielectronic recombination into He-like ions originating from the $1s2lnl'$- and $1s3lnl'$-autoionizing levels, $Z = Z_n - 1$, $m = 2$, $l_0 = 0$ in (5.147)

	$1s2lnl'$: $\alpha_0 = 1s^2 \rightarrow \alpha = 1s2p$		$1s3lnl'$: $\alpha_0 = 1s^2 \rightarrow \alpha = 1s3p$	
Element	B_d	χ_d	B_d	χ_d
Li	3.39×10^{-5}	1.11	1.57×10^{-6}	1.27
Be	9.94×10^{-5}	0.961	2.12×10^{-6}	1.14
B	1.53×10^{-4}	0.891	2.51×10^{-6}	1.07
C	1.93×10^{-4}	0.848	2.98×10^{-6}	1.03
N	2.17×10^{-4}	0.818	3.40×10^{-6}	1.00
O	2.34×10^{-4}	0.795	3.92×10^{-6}	0.983
F	2.17×10^{-4}	0.775	4.23×10^{-6}	0.967
Ne	2.05×10^{-4}	0.757	4.50×10^{-6}	0.956
Na	1.88×10^{-4}	0.740	4.56×10^{-6}	0.945
Mg	1.72×10^{-4}	0.726	4.54×10^{-6}	0.937
Al	1.57×10^{-4}	0.713	4.47×10^{-6}	0.929
Si	1.43×10^{-4}	0.701	4.36×10^{-6}	0.922
P	1.30×10^{-4}	0.690	4.22×10^{-6}	0.916
S	1.18×10^{-4}	0.681	4.07×10^{-6}	0.910
Cl	1.07×10^{-4}	0.672	3.92×10^{-6}	0.905
Ar	9.72×10^{-5}	0.664	3.76×10^{-6}	0.901
K	8.83×10^{-5}	0.658	3.61×10^{-6}	0.897
C	8.02×10^{-5}	0.652	3.45×10^{-6}	0.893
Sc	7.28×10^{-5}	0.647	3.30×10^{-6}	0.889
Ti	6.62×10^{-5}	0.642	3.15×10^{-6}	0.886
V	6.02×10^{-5}	0.638	3.01×10^{-6}	0.883
Cr	5.47×10^{-5}	0.635	2.87×10^{-6}	0.880
Mn	4.98×10^{-5}	0.632	2.73×10^{-6}	0.877
Fe	4.54×10^{-5}	0.629	2.60×10^{-6}	0.875
Co	4.14×10^{-5}	0.627	2.47×10^{-6}	0.873
Ni	3.78×10^{-5}	0.625	2.35×10^{-6}	0.871
Cu	3.46×10^{-5}	0.623	2.23×10^{-6}	0.869
Zn	3.16×10^{-5}	0.622	2.11×10^{-6}	0.868
Ga	2.90×10^{-5}	0.620	2.00×10^{-6}	0.867
Ge	2.67×10^{-5}	0.619	1.90×10^{-6}	0.865
As	2.45×10^{-5}	0.619	1.80×10^{-6}	0.864
Se	2.26×10^{-5}	0.618	1.70×10^{-6}	0.864
Br	2.08×10^{-5}	0.617	1.61×10^{-6}	0.863
Kr	1.93×10^{-5}	0.617	1.52×10^{-6}	0.862
Rb	1.78×10^{-5}	0.616	1.44×10^{-6}	0.862
Sr	1.65×10^{-5}	0.616	1.36×10^{-6}	0.861

(continued)

Table 5.3 (continued)

	$1s2lnl'$: $\alpha_0 = 1s^2 \rightarrow \alpha = 1s2p$		$1s3lnl'$: $\alpha_0 = 1s^2 \rightarrow \alpha = 1s3p$	
Element	B_d	χ_d	B_d	χ_d
Y	1.53×10^{-5}	0.616	1.29×10^{-6}	0.861
Zr	1.43×10^{-5}	0.616	1.22×10^{-6}	0.861
Nb	1.33×10^{-5}	0.616	1.15×10^{-6}	0.861
Mo	1.24×10^{-5}	0.616	1.09×10^{-6}	0.861

The numerical data include corrections for multidecay channels (two channels for $1s2lnl'$ and four channels for $1s3lnl'$)

transition $1s$–$3p$ increases. The Burgess formula provides amplitudes B_d that are about a factor of 3 smaller than the present numerical calculations. For the $3lnl'$-states, the Burgess formula considerably overestimates the dielectronic recombination rate because it does not take into account the multichannel radiative and Auger decay. This is of particular importance for low-Z elements. The one channel approximation, e.g., for C provides $B_d = 6.75 \times 10^{-5}$, whereas the four-channel approximation provides $B_d = 6.32 \times 10^{-6}$, i.e., a reduction by a factor of 10. The multichannel decay is much less important for higher Z-values, e.g., for Fe $B_d = 5.13 \times 10^{-6}$ whereas the four-channel approximation provides $B_d = 2.60 \times 10^{-6}$.

Table 5.3 presents the numerical calculation of the total dielectronic recombination rate into He-like ions for the core transitions $1s$-$2p$ and $1s$-$3p$ for all elements from He ($Z = 2$) until Mo ($Z = 42$) and the corresponding fitting parameters according (5.147). It can be seen that for low-Z elements, the dielectronic recombination related to the core transition $1s$-$2p$ is dominating, for large Z-values, the relative contribution of the dielectronic recombination with the core transition $1s$-$3p$ increases. The Burgess formula provides amplitudes B_d that are about a factor of 3 smaller than the present numerical calculations. For the $1s3lnl'$-states, the Burgess formula considerably overestimates the dielectronic recombination rate because it does not take into account the multichannel radiative and Auger decay. This is of particular importance for low-Z elements. The one channel approximation, e.g., for C provides $B_d = 6.76 \times 10^{-5}$, whereas the four-channel approximation provides $B_d = 2.98 \times 10^{-6}$, i.e., a reduction by a factor of 20. The multichannel decay is much less important for higher Z-values, e.g., for Fe $B_d = 5.34 \times 10^{-6}$ whereas the four-channel approximation provides $B_d = 2.60 \times 10^{-6}$.

Table 5.4 provides the numerical results of dielectronic recombination into Li-like ions related to a core transition $2s$-$2p$, i.e., the core transition is a $\Delta n = 0$ transition. Therefore, the fitting parameter χ_d is rather small and the associated exponential factor for the dielectronic recombination does not vary much. In addition, the configurations $1s^2 2lnl'$ are only autoionizing for rather high principal quantum numbers. This is quite different for the dielectronic recombination related to the core transition $2s$–$3p$: The states are autoionizing for rather low quantum numbers nl and the temperature dependence is much different due to an order of

Table 5.4 Fitting coefficients according to (5.147) for the dielectronic recombination into Li-like ions originating from the $1s^2 2lnl'$- and $1s^2 3lnl'$-autoionizing levels, $Z = Z_n - 2$, $m = 1$, $l_0 = 0$ in (5.147)

	$1s^2 2lnl'$: $\alpha_0 = 1s^2 2s \rightarrow \alpha = 1s^2 2p$		$1s^2 3lnl'$: $\alpha_0 = 1s^2 2s \rightarrow \alpha = 1s^2 3p$	
Element	B_d	χ_d	B_d	χ_d
Be	8.09×10^{-5}	0.0571	1.97×10^{-6}	0.197
B	6.86×10^{-5}	0.0400	2.85×10^{-6}	0.173
C	5.18×10^{-5}	0.0306	6.61×10^{-6}	0.161
N	3.95×10^{-5}	0.0248	1.06×10^{-5}	0.153
O	3.09×10^{-5}	0.0207	1.47×10^{-5}	0.149
F	2.47×10^{-5}	0.0179	1.85×10^{-5}	0.145
Ne	2.02×10^{-5}	0.0156	2.17×10^{-5}	0.142
Na	1.69×10^{-5}	0.0139	2.41×10^{-5}	0.140
Mg	1.43×10^{-5}	0.0126	2.57×10^{-5}	0.138
Al	1.23×10^{-5}	0.0115	2.67×10^{-5}	0.136
Si	1.07×10^{-5}	0.0105	2.71×10^{-5}	0.135
P	9.43×10^{-6}	0.00981	2.69×10^{-5}	0.133
S	8.41×10^{-6}	0.00914	2.60×10^{-5}	0.131
Cl	7.57×10^{-6}	0.00858	2.53×10^{-5}	0.130
Ar	6.87×10^{-6}	0.00809	2.42×10^{-5}	0.128
K	6.25×10^{-6}	0.00772	2.31×10^{-5}	0.127
C	5.76×10^{-6}	0.00736	2.19×10^{-5}	0.126
Sc	5.35×10^{-6}	0.00704	2.09×10^{-5}	0.124
Ti	5.00×10^{-6}	0.00677	1.97×10^{-5}	0.123
V	4.67×10^{-6}	0.00658	1.86×10^{-5}	0.122
Cr	4.42×10^{-6}	0.00637	1.76×10^{-5}	0.120
Mn	4.20×10^{-6}	0.00620	1.66×10^{-5}	0.119
Fe	4.02×10^{-6}	0.00605	1.57×10^{-5}	0.118
Co	3.86×10^{-6}	0.00592	1.48×10^{-5}	0.117
Ni	3.72×10^{-6}	0.00581	1.40×10^{-5}	0.116
Cu	3.61×10^{-6}	0.00571	1.32×10^{-5}	0.115
Zn	3.51×10^{-6}	0.00564	1.25×10^{-5}	0.114
Ga	3.42×10^{-6}	0.00558	1.18×10^{-5}	0.113
Ge	3.35×10^{-6}	0.00553	1.11×10^{-5}	0.112
As	3.25×10^{-6}	0.00556	1.05×10^{-5}	0.111
Se	3.20×10^{-6}	0.00554	9.96×10^{-6}	0.110
Br	3.20×10^{-6}	0.00546	9.43×10^{-6}	0.109
Kr	3.17×10^{-6}	0.00546	8.92×10^{-6}	0.108
Rb	3.15×10^{-6}	0.00547	8.45×10^{-6}	0.107
Sr	3.13×10^{-6}	0.00548	8.01×10^{-6}	0.106
Y	3.12×10^{-6}	0.00551	7.59×10^{-6}	0.105
Zr	3.11×10^{-6}	0.00554	7.20×10^{-6}	0.105
Nb	3.11×10^{-6}	0.00558	6.83×10^{-6}	0.104
Mo	3.11×10^{-6}	0.00563	6.48×10^{-6}	0.103

The numerical data include corrections for multidecay channels (one channel for $1s^2 2lnl'$ and four channels for $1s^2 3lnl'$)

Table 5.5 B_d-factors according to (5.147) for the dielectronic recombination into Li-like ions originating from the $1s^2nln'l'$-autoionizing levels, $Z = Z_n - 2$, $m = 1$, $l_0 = 0$ in (5.147)

Element	$1s^22lnl'$: $\alpha_0 = 1s^22s \rightarrow \alpha = 1s^22p$		
	B_d (one channel)	B_d (multichannel)	B_d (Burgess)
Be	8.09×10^{-5}	–	1.34×10^{-4}
C	5.18×10^{-5}	–	7.99×10^{-5}
Mg	1.34×10^{-5}	–	1.94×10^{-5}
Ar	6.87×10^{-6}	–	8.65×10^{-6}
Fe	4.02×10^{-6}	–	4.88×10^{-6}
Mo	3.11×10^{-6}	–	3.87×10^{-6}
	$1s^23lnl'$: $\alpha_0 = 1s^22s \rightarrow \alpha = 1s^23p$		
Be	3.44×10^{-5}	1.97×10^{-6}	2.88×10^{-5}
C	6.45×10^{-5}	6.61×10^{-6}	6.98×10^{-5}
Mg	6.43×10^{-5}	2.57×10^{-5}	6.96×10^{-5}
Ar	4.55×10^{-5}	2.42×10^{-5}	5.15×10^{-5}
Fe	2.61×10^{-5}	1.57×10^{-5}	3.54×10^{-5}
Mo	8.61×10^{-6}	6.48×10^{-6}	1.89×10^{-5}
	$1s^24lnl'$: $\alpha_0 = 1s^22s \rightarrow \alpha = 1s^24p$		
Be	1.60×10^{-5}	3.47×10^{-7}	1.10×10^{-5}
C	2.52×10^{-5}	3.39×10^{-7}	2.23×10^{-5}
Mg	2.06×10^{-5}	1.30×10^{-6}	1.87×10^{-5}
Ar	1.29×10^{-5}	2.05×10^{-6}	1.27×10^{-5}
Fe	6.54×10^{-6}	2.00×10^{-6}	8.01×10^{-6}
Mo	1.87×10^{-6}	1.17×10^{-6}	3.82×10^{-6}

The numerical data show single- and multiple-channel approximation as well as corresponding factors according the theory of Burgess (note that the different numerical coefficients in (5.138) compared to (5.147a) have been included in the value for B_d-Burgess for comparison of the different methods)

magnitude different χ_d-factor. Unlike the dielectronic recombination into H- and He-like ions (Tables 5.2 and 5.3), the dielectronic recombination related to the $n = 3$ core transition is very important compared to the $2s$–$2p$ related recombination. Due to this reason, the temperature dependence of the total recombination rate (being the sum of the $2s$–$2p$, $2s$–$3p$,… transitions) is complex and differs qualitatively from the dielectronic recombination into H- and He-like ions that are dominated by a single exponential factor.

The influence of multichannel Auger and radiative decay on the dielectronic recombination related to the $2s$–$3p$ core transition is likewise important for low-Z elements. For Be atoms, the multichannel decay reduces the B_d—factor by more than a factor of 10, whereas for Ar the multichannel decay decreases the dielectronic recombination only by a factor of 2.

It is interesting to discuss the influence of the various mechanisms related to the dielectronic recombination with the core hole transition $2s$–$4p$. The single channel approximation leads to a wrong estimation of the importance of high-order

Table 5.6 Fitting coefficients according to (5.147) for the dielectronic recombination into excited states of Li-like ions originating from the $1s^2 3lnl'$- and $1s^2 4lnl'$-autoionizing levels, $Z = Z_n - 2$, $m = 1$, $l_0 = 1$ in (5.147)

	$1s^2 3lnl'$: $\alpha_0 = 1s^2 2p \rightarrow \alpha = 1s^2 3d$		$1s^2 4lnl'$: $\alpha_0 = 1s^2 2p \rightarrow \alpha = 1s^2 4d$	
Element	B_d	χ_d	B_d	χ_d
Be	1.78×10^{-4}	0.140	1.88×10^{-5}	0.190
B	2.99×10^{-4}	0.137	2.01×10^{-5}	0.189
C	3.74×10^{-4}	0.135	2.04×10^{-5}	0.188
N	4.44×10^{-4}	0.133	2.18×10^{-5}	0.187
O	5.15×10^{-4}	0.131	2.35×10^{-5}	0.187
F	5.52×10^{-4}	0.130	2.53×10^{-5}	0.186
Ne	5.65×10^{-4}	0.128	2.67×10^{-5}	0.185
Na	5.76×10^{-4}	0.127	2.88×10^{-5}	0.181
Mg	5.73×10^{-4}	0.125	3.28×10^{-5}	0.174
Al	5.61×10^{-4}	0.124	3.32×10^{-5}	0.172
Si	5.39×10^{-4}	0.122	3.33×10^{-5}	0.171
P	5.19×10^{-4}	0.120	3.48×10^{-5}	0.167
S	4.96×10^{-4}	0.119	3.46×10^{-5}	0.165
Cl	4.71×10^{-4}	0.117	3.44×10^{-5}	0.164
Ar	4.48×10^{-4}	0.115	3.41×10^{-5}	0.163
K	4.25×10^{-4}	0.114	3.38×10^{-5}	0.161
C	4.04×10^{-4}	0.112	3.34×10^{-5}	0.160
Sc	3.83×10^{-4}	0.110	3.30×10^{-5}	0.159
Ti	3.64×10^{-4}	0.109	3.25×10^{-5}	0.158
V	3.45×10^{-4}	0.107	3.20×10^{-5}	0.157
Cr	3.27×10^{-4}	0.105	3.14×10^{-5}	0.156
Mn	3.11×10^{-4}	0.104	3.08×10^{-5}	0.156
Fe	2.95×10^{-4}	0.102	3.02×10^{-5}	0.155
Co	2.80×10^{-4}	0.101	2.95×10^{-5}	0.154
Ni	2.66×10^{-4}	0.0992	2.88×10^{-5}	0.154
Cu	2.53×10^{-4}	0.0978	2.80×10^{-5}	0.153
Zn	2.40×10^{-4}	0.0964	2.72×10^{-5}	0.153
Ga	2.28×10^{-4}	0.0951	2.64×10^{-5}	0.153
Ge	2.17×10^{-4}	0.0939	2.56×10^{-5}	0.152
As	2.06×10^{-4}	0.0927	2.47×10^{-5}	0.152
Se	1.96×10^{-4}	0.0916	2.39×10^{-5}	0.152
Br	1.86×10^{-4}	0.0905	2.30×10^{-5}	0.152
Kr	1.77×10^{-4}	0.0895	2.22×10^{-5}	0.152
Rb	1.68×10^{-4}	0.0885	2.14×10^{-5}	0.152
Sr	1.60×10^{-4}	0.0876	2.05×10^{-5}	0.152
Y	1.52×10^{-4}	0.0867	1.97×10^{-5}	0.152
Zr	1.45×10^{-4}	0.0859	1.89×10^{-5}	0.152
Nb	1.38×10^{-4}	0.0851	1.82×10^{-5}	0.152
Mo	1.31×10^{-4}	0.0844	1.74×10^{-5}	0.152

The numerical data include corrections for multidecay channels (three channels for $1s^2 3lnl'$ and six channels for $1s^2 4lnl'$)

dielectronic recombination rates. For example, the numerical calculations in the single channel approximation for Be atoms give $B_{\mathrm{d}}^{(1\,\mathrm{Channel})}(2s-3p) = 3.4 \times 10^{-5}$, whereas $B_{\mathrm{d}}^{(1\,\mathrm{Channel})}(2s-4p) = 1.6 \times 10^{-5}$, i.e., 2*s*-4*p* transitions are only reduced by a factor of about 2 compared to the 2*s*-3*p* transitions. Numerical calculation including the multichannel decay provide an entirely different picture: $B_{\mathrm{d}}^{(6\,\mathrm{Channel})}(2s-3p) = 2.0 \times 10^{-6}$ but $B_{\mathrm{d}}^{(6\,\mathrm{Channel})}(2s-4p) = 3.5 \times 10^{-7}$, i.e., the numerical calculations including the multichannel decay indicate that higher-order dielectronic recombination rates are strongly suppressed.

This is a general observation that multichannel decay reduces the dielectronic recombination. Table 5.5 shows the numerical calculation for the dielectronic recombination B_{d}-factors for single- and multiple- channel decay into Li-like ions for different orders and elements in comparison to the standard Burgess formula. One observes that the Burgess formula is in reasonable agreement with the numerical results for the one-channel decay although it might differ up to a factor of 3 in some cases. Comparing, however, the numerical calculations for the multi-channel decay (which is the most correct approach as discussed above) discovers extremely large overestimations of the dielectronic recombination by the Burgess formula. In particular for light elements, the overestimation might be as large as 1–2 orders of magnitude, e.g., for the dielectronic recombination related to the autoionizing states $1s^2 4lnl'$ of Be, we have $B_{\mathrm{d}}^{(\mathrm{multi-channel})}(2s-4p) = 3.47 \times 10^{-7}$, whereas $B_{\mathrm{d}}^{(\mathrm{Burgess})}(2s-4s) = 1.10 \times 10^{-5}$, i.e., an overestimation by more than factor of 30 compared to the Burgess formula. It is therefore *not* recommended (Rosmej et al. 2020) to calculate higher-order contributions to the dielectronic recombination via the Burgess approach.

5.6.2.3 Excited State-Driven Dielectronic Recombination

Table 5.6 shows the dielectronic recombination rates related to the excited states $1s^2 2p$ of Li-like ions. It can be seen from a comparison of the numerical data from Tables 5.4 and 5.6 that the excited state contribution is even more important than the ground state contribution. For example, for Be, $B_{\mathrm{d}}(2s-3p) = 1.97 \times 10^{-6}$, whereas $B_{\mathrm{d}}(2p-3d) = 1.78 \times 10^{-4}$ and $B_{\mathrm{d}}(2p-4d) = 1.88 \times 10^{-5}$. This means the excited state contribution is up to 2 orders of magnitude more important than the ground state contribution. Therefore, even for rather moderate densities with small population of the excited states, their contribution to dielectronic recombination can be important.

Particular important cases are encountered if the first excited states are related to $\Delta n = 0$ radiative transitions. Because these transition probabilities are by orders of magnitude lower than those for $\Delta n > 0$ transitions, Boltzmann populations with respect to the ground state are already achieved for rather low electron densities. For example, for Be, at densities of about 10^{15} cm^{-3}, the population of the excited states $1s^2 2p$ is more important than those of the ground state $1s^2 2s$ (Rosmej 1994).

Therefore, all excited state contributions of Beryllium, e.g., for tokamaks at typical divertor densities have larger contribution than the ground state.

The excited state contribution could be even important for very low densities if the excited states are metastable states. Therefore, in heavy ions, where we met excited states that are close to ground states, either related by a dipole-allowed radiative transition or by multipole transitions, the dielectronic recombination is extremely complex even for rather low densities. This is the main reason that up to present days, ionic balance calculations of heavy elements differ strongly from one method to another and that dielectronic recombination remains an active field of research and of considerable interest for applications (nuclear fusion, astrophysics, radiation sources, and spectroscopic diagnostics).

In conclusion, the excited state contribution is driven by atomic kinetics that can have much more important impact, than any other sophisticated effects related to ground state contributions. This points again to the great practical importance of quasi-classical methods (albeit of limited precision) that provide the possibility to obtain numerical data even for large quantum numbers that are important for the dielectronic recombination. It is important to emphasize that the inclusion of excited state contributions for the dielectronic recombination up to high quantum numbers for the corresponding core transitions may exceed ground state contributions by many orders of magnitude and it is for this reason that it is more precise to include as much as possible excited state contributions with the limited precision rather than improve via sophisticated atomic structure calculations the simplest core-transition-related dielectronic recombination but ignoring higher-order and excited states contributions.

5.6.3 Dense Plasma and Electric Field Effects on Dielectronic Recombination

Dense plasma effects are of multiple origins. The first one (as discussed above in relation with Table 5.6) is related to the atomic population kinetics where highly populated excited states directly contribute to the recombination process (Rosmej 1994). The second one is related to the shift of bound states into the continuum, and the third one concerns the change of atomic processes itself (cross-sections) due to the plasma electric microfield.

5.6.3.1 Atomic Population Kinetics

Let us begin with the atomic population kinetics and the existence of a critical principal quantum number, where collisional processes start to dominate over radiative ones [see discussion related to (5.52)–(5.57)]. The physical meaning of this critical quantum number $N_{\max}$ (5.52) is that above this principal quantum number,

the population kinetics is essentially governed by the Saha–Boltzmann relation between highly excited states and the next ionization stage and any single recombination processes (whatever its magnitude is) are rapidly assimilated via collisions that effectively suppress the recombination processes. In fact, the analytical formulas for total dielectronic recombination and also for total radiative recombination assume that finally all excited states effectively recombine (via radiative cascading to the ground state). As has been demonstrated (Rosmej et al. 2006; Rosmej 2012), even the large rates of charge exchange recombination processes from excited states are effectively assimilated by collisions [although the collision limit itself changes (Rosmej 2012)] so that there exists a critical quantum number where the Saha–Boltzmann relations hold true and where recombination into higher states does not effectively contribute to recombination (see also Sect. 10.3.1).

5.6.3.2 Limitation of Bound States

The second phenomenon is related to the fact that the plasma electric microfield limits the number of bound states. Electric field ionization starts at the critical field strength F_{crit} that is given by Bethe and Salpeter (1977)

$$F_{\mathrm{crit}} = 6.8 \times 10^8 \frac{\mathrm{V}}{\mathrm{cm}} \cdot \frac{Z_{\mathrm{eff}}^3}{n_{\mathrm{F}}^4}, \tag{5.148}$$

where Z_{eff} is the effective ion charge and n_{F} the principal quantum number from which on field ionization starts. In order to estimate the limited number of quantum states that take effectively part in the recombination process, we identify the critical field strength F_{crit} with the Holtsmark field

$$F = 1.3 \times 10^{-6} \cdot Z_{\mathrm{i}} \cdot N_{\mathrm{i}}^{2/3}(\mathrm{cm}^{-3}) \frac{\mathrm{V}}{\mathrm{cm}}, \tag{5.149}$$

and the principal quantum number n_{F} with the maximum quantum number, i.e.,

$$n_{\max} \approx 4.8 \times 10^3 \cdot \frac{Z_{\mathrm{eff}}^{3/4}}{Z_{\mathrm{i}}^{1/4} \cdot N_{\mathrm{i}}^{1/6}(\mathrm{cm}^{-3})}. \tag{5.150}$$

Let us compare the maximum quantum number from (5.150) with the critical quantum number of (5.57) assuming that $n_{\mathrm{e,crit}} = N_{\mathrm{i}} \cdot Z_{\mathrm{i}}$ and $kT_{\mathrm{e}}(\mathrm{eV}) = \alpha \cdot Z_{\mathrm{eff}}^2 \mathrm{Ry}$, where α is a constant (of the order of $\alpha \approx 0.1 - 1$):

$$n_{\mathrm{crit}} \approx 373 \cdot \alpha^{1/14} \cdot \frac{Z_{\mathrm{eff}}}{Z_{\mathrm{i}}^{1/7} \cdot N_{\mathrm{i}}^{1/7}}. \tag{5.151}$$

With the help of (5.149) and (5.150), we find

$$\frac{n_{\max}}{n_{\mathrm{crit}}} \approx \frac{13}{\alpha^{1/14}} \cdot \frac{1}{Z_{\mathrm{eff}}^{1/4} \cdot Z_{\mathrm{i}}^{3/28} \cdot N_{\mathrm{i}}^{1/42}(\mathrm{cm}^{-3})}. \tag{5.152}$$

Let us illuminate the relation (5.152) with a typical example: near-solid density high-temperature H-like aluminum, i.e., $Z_{\mathrm{eff}} = 13$, $Z_{\mathrm{i}} = 12$, $\alpha = 0.3$, $N_{\mathrm{i}} = 10^{22}\,\mathrm{cm}^{-3}$ providing $n_{\max}/n_{\mathrm{crit}} \approx 1.7$. Therefore, for almost all practical applications, we encounter the relation

$$\frac{n_{\max}}{n_{\mathrm{crit}}} > 1. \tag{5.153}$$

The physical interpretation of relation (5.153) means that the collisional thermalization and the associated effective suppression of single recombination rates into excited states are therefore related to a large ensemble of high-n quantum numbers below those that merge into the continuum. For this reason, a detailed quantum mechanical treatment of high-n-states and their merging into the continuum appears to be not critical and quasi-classical estimates seem to be well adapted to the problem.

5.6.3.3 Effects of Angular Momentum Changing Collisions

It is evident that a strict consideration of angular momentum changing collisions requests a very extended atomic level system that includes all details of the autoionizing states in order to treat properly the collisional population redistribution effects. We restrict here ourself to a principle discussion with the help of the most frequently employed formula for dielectronic recombination proceeding from dielectronic capture from channel k and with radiative transition $j \rightarrow i$ [see also (5.131)–(5.133)]:

$$\langle \mathrm{DR} \rangle_{\mathrm{k,ji}}^{Z+1,Z} \approx \frac{1}{2g_{\mathrm{k}}^{Z+1}} \cdot \left(\frac{2\pi\hbar^2}{m_{\mathrm{e}}}\right)^{3/2} \cdot \frac{g_{\mathrm{j}}^{Z} \cdot \Gamma_{\mathrm{jk}}^{Z,Z+1} \cdot A_{\mathrm{ji}}^{Z}}{\sum_{\mathrm{l}} A_{\mathrm{jl}}^{Z} + \sum_{\mathrm{k}} \Gamma_{\mathrm{jk}}^{Z,Z+1}} \cdot \frac{\exp(-E_{\mathrm{kj}}^{\mathrm{DC}}/kT_{\mathrm{e}})}{(kT_{\mathrm{e}})^{3/2}}. \tag{5.154}$$

Let us now consider a simple illustrative example, namely the Ly-alpha dielectronic $2l2l'$-satellites of He-like ions and depict two levels, one that has very large autoionizing rate and one that has a negligible ones. For the first case, we consider the level $j' = 2p^2\ {}^1D_2$, $k = 1s\ {}^2S_{1/2}$ and the radiative transition $j' = 2p^2\ {}^1D_2 \rightarrow i' = 1s2p\ {}^1P_1$. Atomic structure calculations for carbon ($Z_{\mathrm{n}} = 6$) deliver: $\Gamma_{\mathrm{j'k}}^{Z,Z+1} = 2.5 \times 10^{14}\,\mathrm{s}^{-1}$, $A_{\mathrm{j'i'}}^{Z} = 1.4 \times 10^{12}\,\mathrm{s}^{-1}$, $\sum_{\mathrm{l}} A_{\mathrm{jl}}^{Z} = 1.4 \times 10^{12}\,\mathrm{s}^{-1}$, $\sum_{\mathrm{k}} \Gamma_{\mathrm{j'k}}^{Z,Z+1} = 2.5 \times 10^{14}\,\mathrm{s}^{-1}$. For the second case, we consider the autoionizing

configuration $j = 2p^2\ {}^3P_1$, $k = 1s\ {}^2S_{1/2}$ and the radiative transition $j = 2p^2\ {}^3P_1 \rightarrow i = 1s2p\ {}^3P_2$. Atomic structure calculations ($Z_n = 6$) provide: $\Gamma_{jk}^{Z,Z+1} = 0$, $A_{ji}^{Z} = 6.0 \times 10^{11}\,\mathrm{s}^{-1}$, $\sum_l A_{jl}^{Z} = 1.4 \times 10^{12}\,\mathrm{s}^{-1}$, $\sum_k \Gamma_{jk}^{Z,Z+1} = 0$ from which it follows $Q_{k,ji}^{Z+1,Z} = 0$.

Assuming a two-level system where only dielectronic capture and angular momentum changing collisions (characterized by the rate coefficient $C_{j'j}$) contribute, the atomic populations n_j^Z and $n_{j'}^Z$ are given by

$$n_{j'}^{Z}\left(\sum_l A_{j'l}^{Z} + \sum_k \Gamma_{j'k}^{Z,Z+1} + n_e C_{j'j}\right) = n_k^{Z+1} \cdot n_e \cdot \langle \mathrm{DC}\rangle_{k,ji'}^{Z+1,Z} + n_e \cdot n_j^Z \cdot C_{jj'}, \tag{5.155}$$

$$n_{j}^{Z}\left(\sum_l A_{jl}^{Z} + \sum_k \Gamma_{jk}^{Z,Z+1} + n_e C_{jj'}\right) = n_k^{Z+1} \cdot n_e \cdot \langle \mathrm{DC}\rangle_{k,ji}^{Z+1,Z} + n_e \cdot n_{j'}^Z \cdot C_{j'j}, \tag{5.156}$$

where

$$\langle \mathrm{DC}\rangle_{k,q}^{Z+1,Z} = \frac{1}{2g_k^{Z+1}} \cdot \left(\frac{2\pi\hbar^2}{m_e}\right)^{3/2} \cdot g_q^Z \cdot \Gamma_{qk}^{Z,Z+1} \cdot \frac{\exp\left(-E_{kq}^{\mathrm{DC}}/kT_e\right)}{(kT_e)^{3/2}} \tag{5.157}$$

with $q = j, j'$. In the absence of collisions, (5.154)–(5.156) transform to

$$n_q^{(0),Z}\left(\sum_l A_{ql}^{Z} + \sum_k \Gamma_{qk}^{Z,Z+1}\right) = n_k^{Z+1} \cdot n_e \cdot \langle \mathrm{DC}\rangle_{q,k}^{Z+1,Z}, \tag{5.158}$$

providing

$$n_q^{(0),Z} = n_k^{Z+1} \cdot n_e \cdot \frac{1}{2g_k^{Z+1}} \cdot \left(\frac{2\pi\hbar^2}{m_e}\right)^{3/2} \cdot \frac{g_q^Z \cdot \Gamma_{qk}^{Z,Z+1}}{\sum_l A_{ql}^{Z} + \sum_k \Gamma_{qk}^{Z,Z+1}} \cdot \frac{\exp\left(-E_{kq}^{DC}/kT_e\right)}{(kT_e)^{3/2}}, \tag{5.159}$$

where the index "(0)" indicates the low-density case.

In order to understand the effect of angular momentum changing collisions on the total dielectronic recombination rate, we need to consider the sum for the two levels, i.e.,

$$\langle \mathrm{DR_{coll}} \rangle_{\mathrm{tot}}^{Z+1,Z} = \langle \mathrm{DR_{coll}} \rangle_{\mathrm{k,ji}}^{Z+1,Z} + \langle \mathrm{DR_{coll}} \rangle_{\mathrm{k,j'i'}}^{Z+1,Z}, \tag{5.160}$$

where the index "coll" for the single dielectronic recombination rates $\langle \mathrm{DR_{coll}} \rangle_{\mathrm{k,ji}}^{Z+1,Z}$ and $\langle \mathrm{DR_{coll}} \rangle_{\mathrm{k,j'i'}}^{Z+1,Z}$ indicates that these rates include the collisional processes. This has to be distinguished from (5.154) which is a low-density approximation. It is of principal interest to understand the change of the dielectronic recombination due to collisions with reference to the low-density case, i.e., we consider the ratio

$$\frac{\langle \mathrm{DR_{coll}} \rangle_{\mathrm{tot}}^{Z+1,Z}}{\langle \mathrm{DR} \rangle_{\mathrm{tot}}^{Z+1,Z}} = \frac{\langle \mathrm{DR_{coll}} \rangle_{\mathrm{k,ji}}^{Z+1,Z} + \langle \mathrm{DR_{coll}} \rangle_{\mathrm{k,j'i'}}^{Z+1,Z}}{\langle \mathrm{DR} \rangle_{\mathrm{k,ji}}^{Z+1,Z} + \langle \mathrm{DR} \rangle_{\mathrm{k,j'i'}}^{Z+1,Z}}. \tag{5.161}$$

The collisional dielectronic recombination rates cannot be determined from relations like (5.154) but need to be determined directly from the populations, i.e.,

$$\langle \mathrm{DR_{coll}} \rangle_{\mathrm{k,ji}}^{Z+1,Z} \propto n_{\mathrm{j}}^{Z} \cdot A_{\mathrm{ji}}^{Z}, \tag{5.162}$$

because the product of the level population with the radiative decay is the rate at which the excited state decays to the ground state which is equivalent to dielectronic recombination (note that the usual branching ratios that appear in formulas like those of (5.154) are already included via the equilibrium population) if the right-hand side of (5.155), (5.156) is driven by dielectronic capture and angular momentum changing collisions between the autoionizing levels under consideration. Combining the relations (5.161) and (5.162), we obtain

$$\frac{\langle \mathrm{DR_{coll}} \rangle_{\mathrm{tot}}^{Z+1,Z}}{\langle \mathrm{DR} \rangle_{\mathrm{tot}}^{Z+1,Z}} = \frac{n_{\mathrm{j}}^{Z} \cdot A_{\mathrm{ji}}^{Z} + n_{\mathrm{j'}}^{Z} \cdot A_{\mathrm{j'i'}}^{Z}}{n_{\mathrm{j}}^{(0),Z} \cdot A_{\mathrm{ji}}^{Z} + n_{\mathrm{j'}}^{(0),Z} \cdot A_{\mathrm{j'i'}}^{Z}}, \tag{5.163}$$

i.e.,

$$\frac{\langle \mathrm{DR_{coll}} \rangle_{\mathrm{tot}}^{Z+1,Z}}{\langle \mathrm{DR} \rangle_{\mathrm{tot}}^{Z+1,Z}} = \frac{\dfrac{n_{\mathrm{j'}}^{Z}}{n_{\mathrm{j'}}^{(0),Z}} + \dfrac{n_{\mathrm{j}}^{Z} \cdot A_{\mathrm{ji}}^{Z}}{n_{\mathrm{j'}}^{(0),Z} \cdot A_{\mathrm{j'i'}}^{Z}}}{\dfrac{n_{\mathrm{j}}^{(0),Z} \cdot A_{\mathrm{ji}}^{Z}}{n_{\mathrm{j'}}^{(0),Z} \cdot A_{\mathrm{j'i'}}^{Z}} + 1}. \tag{5.164}$$

Because $E_{\mathrm{kj}}^{DC} \approx E_{\mathrm{kj'}}^{DC}$, we have for the population ratio in the low-density case (for the example given above)

$$\frac{n_j^{(0),Z}}{n_{j'}^{(0),Z}} \approx \frac{g_j^Z \cdot \Gamma_{jk}^{Z,Z+1}}{g_{j'}^Z \cdot \Gamma_{j'k}^{Z,Z+1}} \cdot \frac{\sum_l A_{j'l}^Z + \sum_k \Gamma_{j'k}^{Z,Z+1}}{\sum_l A_{jl}^Z + \sum_k \Gamma_{jk}^{Z,Z+1}} \approx 0, \tag{5.165}$$

because $\Gamma_{jk}^{Z,Z+1} \ll \Gamma_{j'k}^{Z,Z+1}$. Therefore, population is essentially transferred by angular momentum changing collision form level j' to level j but not vice versa. Let us now specify the above example for the populations of (5.155), (5.156):

$$n_j^Z \left(\sum_l A_{jl}^Z + n_e C_{jj'} \right) \approx n_e \cdot n_{j'}^Z \cdot C_{j'j}, \tag{5.166}$$

and

$$n_{j'}^Z \left(\sum_l A_{j'l}^Z + \sum_k \Gamma_{j'k}^{Z,Z+1} \right) \approx n_k^{Z+1} \cdot n_e \cdot \langle \mathrm{DC} \rangle_{k,j'}^{Z+1,Z}, \tag{5.167}$$

Equations (5.155), (5.156), (5.158) indicate that for autoionizing levels with very large autoionizing rates, the populations are close to the low-density case. Equation (5.167) corresponds therefore to the case of low density (5.158), i.e.,

$$n_{j'}^Z \approx n_{j'}^{(0),Z}. \tag{5.168}$$

Injecting relations (5.165), (5.166), (5.168) into (5.164), we obtain

$$\frac{\langle \mathrm{DR_{coll}} \rangle_{tot}^{Z+1,Z}}{\langle \mathrm{DR} \rangle_{tot}^{Z+1,Z}} \approx 1 + \frac{n_e \cdot C_{j'j}}{\sum_l A_{jl}^Z + n_e C_{jj'}} \cdot \frac{A_{ji}^Z}{A_{j'i'}^Z}. \tag{5.169}$$

Because $g_{j'} \cdot C_{j'j} \approx g_j \cdot C_{jj'}$ for closely spaced levels, relation (5.169) takes the form

$$\frac{\langle \mathrm{DR_{coll}} \rangle_{tot}^{Z+1,Z}}{\langle \mathrm{DR} \rangle_{tot}^{Z+1,Z}} \approx 1 + \frac{g_{j'}^Z}{g_j^Z} \cdot \frac{A_{ji}^Z}{A_{j'i'}^Z} \cdot \left(\frac{1}{1 + \sum_l A_{jl}^Z / n_e C_{jj'}} \right). \tag{5.170}$$

If $\sum_l A_{jl}^Z \approx n_e C_{jj'}$, the term in parenthesis of relation (5.170) is about one half and the relation indicates that the total dielectronic recombination rate is enhanced (i.e., $\langle \mathrm{DR_{coll}} \rangle_{tot}^{Z+1,Z} / \langle \mathrm{DR} \rangle_{tot}^{Z+1,Z} > 1$) due to angular momentum changing collisions. This can be understood in a transparent qualitative picture: For the level j' with high autoionization rate, the dielectronic capture is high and due to the large autoionizing rate, the branching factor for radiative de-excitation is small. If, however, a certain fraction of population is collisionally transferred to another level before autoionization and radiative decay disintegrate the upper level j', the level j is

Table 5.7 Field-free autoionization decay rates in [s^{-1}] including intermediate coupling, configuration, and magnetic interaction

State	$Z_n = 3$	$Z_n = 6$	$Z_n = 13$	$Z_n = 18$	$Z_n = 26$	$Z_n = 42$
$2p^2\ ^1S_0$	8.4×10^{10}	5.1×10^{12}	1.3×10^{13}	1.9×10^{13}	3.4×10^{13}	7.0×10^{13}
$2p^2\ ^1D_2$	1.5×10^{14}	2.5×10^{14}	3.1×10^{14}	3.1×10^{14}	2.3×10^{14}	2.1×10^{14}
$2p^2\ ^3P_0$	2.9×10^{7}	2.3×10^{9}	2.3×10^{11}	1.2×10^{12}	3.7×10^{12}	2.8×10^{12}
$2p^2\ ^3P_1$	0	0	0	0	0	0
Breit interaction	2.6×10^{7}	6.8×10^{8}	1.9×10^{10}	7.2×10^{10}	3.2×10^{11}	2.2×10^{12}
$2p^2\ ^3P_2$	1.1×10^{9}	3.1×10^{10}	3.0×10^{12}	2.1×10^{13}	1.1×10^{14}	1.5×10^{14}

effectively populated by collisions from $j' \rightarrow j$ (because the population of the level j is small as dielectronic capture is small due to small autoionization rate). The transferred population, however, has a very favorable branching factor for the level j (e.g., in the above example $A^Z_{ji}/\left(\sum_l A^Z_{jl} + \sum_k \Gamma^{Z,Z+1}_{jk}\right) = 6.0\times 10^{11}/1.4 \times 10^{12} = 0.43$) compared to the level j' ($A^Z_{j'i'}/\left(\sum_l A^Z_{j'l} + \sum_k \Gamma^{Z,Z+1}_{j'k}\right) = 1.4 \times 10^{12}/2.6 \times 10^{14} = 0.0088$) and the transferred population is more effectively transferred to the ground state to finally contribute to the dielectronic recombination.

5.6.3.4 Electric Field Effects on Cross-Sections

The influence of the electric field on autoionization and corresponding dielectronic recombination rates was studied by (Davis and Jacobs 1975; Jacobs et al. 1976; Jacobs and Davis 1979) with the simplest atomic system of He-like autoionizing states $2l2l'$. It was realized that forbidden autoionizing processes (forbidden in *LS*-coupling scheme) become allowed by electric field mixing of autoionizing bound state wave functions. The allowed autoionization width is given by the first-order transition rate

$$\Gamma(d \rightarrow c) = \frac{2\pi}{\hbar} \cdot |\langle d|V|c\rangle|^2 \delta(E_d - E_c), \tag{5.171}$$

where V is the electrostatic interaction. Because V is a scalar operator, the autoionization vanishes unless there are available adjacent continuum states c with the same angular momentum and parity as the discrete levels d (Cowan 1981). Because of the absence of even parity P states below the second ionization threshold, the $2p^2\ ^3P$-state of He-like ions is metastable against autoionization decay. In the presence of perturbing electric fields, however, autoionization of the state $a = 2p^2\ ^3P$ may occur by a second-order process involving the field-induced transition to the nearby autoionizing state $d = 2s2p\ ^3P$. In a quasi-static ion field, the field-induced autoionization rate is given by

$$\Gamma(a \to c) = \frac{2\pi}{\hbar} \cdot \left| \sum_{\mathrm{d}} \frac{\langle a|\vec{Q} \cdot \vec{E}|d\rangle\langle d|V|c\rangle}{(E_\mathrm{a} - E_\mathrm{d}) + i\hbar(\Gamma_\mathrm{d} + A_\mathrm{d})/2} \right|^2 \delta(E_\mathrm{a} - E_\mathrm{c}), \tag{5.172}$$

where $\vec{Q}$ is the electric dipole moment operator, Γ_d and A_d are the autoionization and radiative width of the state d, respectively. Therefore, the first-order contribution from the field-induced transition decays directly into the non-resonant continuum $c = 1s\epsilon p\ ^3P$.

It should be noted that for practical applications, not only field-induced transitions have to be considered, but intermediate coupling, configuration, and magnetic interactions too. In particular for highly charged ions, these "non-electric field effects" may have likewise a considerable contribution to the forbidden autoionization width, as is demonstrated in the following Table 5.7. In addition, the Breit interaction induces an autoionization rate for the $2p^2\ ^3P_1$—state (see second line for the state $2p^2\ ^3P_1$ in Table 5.7).

Table 5.7 shows also the general effect that if the nuclear charge increases, the autoionizing widths are more and more distributed over the levels. Therefore, electric field effects are best studied for low-Z elements.

From the relationship between the corresponding capture and autoionizing rates, it follows that the electric field can induce dielectronic recombination through normally inaccessible high angular momentum states which have large statistical weights (Jacobs et al. 1976). In fact, in a plasma, the angular momentum l is no longer a good quantum number, because the presence of an electric field destroys the spherical symmetry. However, the projection m which is defined with respect to the direction of the electric field remains a good quantum number. For nonzero quantum numbers m, this results in a twofold degeneracy of the outer electron in addition to the twofold degeneracy due to the spin. The appropriate transformation of the field-free substates l has the form

$$|n\lambda m\rangle = \sum_{l=|m|}^{n-1} |nlm\rangle\langle nlm \mid n\lambda m\rangle, \tag{5.173}$$

where the quantum number λ, which replaces l in the presence of the electric field, can have integer values from $\lambda = 0 \ldots (n - |m| - 1)$. The calculations demonstrate (Jacobs et al. 1976; Jacobs and Davis 1979; Bureyeva et al. 2001, 2002) that the dependence of the autoionization rates on the quantum number λ is rather smooth in contrast to the field-free case where the autoionization rates decrease rapidly with quantum number l. Due to this reason, dielectronic capture in the presence of electric field increases because it is proportional to the autoionizing rate and the statistical weight, i.e., $\langle \mathrm{DC}\rangle_{\mathrm{k,j}}^{Z+1,Z} \propto g_\mathrm{j}^Z \cdot \Gamma_\mathrm{jk}^{Z,Z+1}$. Because the dielectronic recombination is proportional to the dielectronic capture [see (5.154)], this results in a considerable increase of the total dielectronic recombination rate. For example, for the autoionizing states $1s^2 2pnl$ in Be-like Fe^{22+} an about threefold increase of the

dielectronic recombination rate was found even for densities as low as 10^{14} cm^{-3} (Jacobs et al. 1976). This dramatic increase for rather low densities is particularly connected with the fact that for the $1s^2 2pnl$-configuration, the resonance spontaneous transition probability $2p$–$2s$ is not very large and high-n-states have autoionizing rates larger than radiative decay rates for n-quantum numbers up to about 100. In consequence, high-n-states contribute considerably to the dielectronic recombination rate. As high-n-states are likewise strongly affected by rather small electric fields, a considerable impact on the total recombination rate is encountered even for rather low plasma densities (being of importance for typical densities of solar corona or magnetic fusion plasmas).

The interaction with an electric field makes atomic structure calculations extremely complex, and it is difficult to derive general conclusions. It has been, however, demonstrated (Bureyeva et al. 2001, 2002) that the quasi-classical approach combined with a transformation to parabolic quantum numbers (5.173) provides results that are in surprisingly good agreement with extremely complex numerical calculations (Robicheaux and Pindzola 1997). Moreover, the quasi-classical approach combined with the transformation to parabolic quantum numbers allowed deriving a closed expression for the autoionization rate in an electric field:

$$\Gamma(n,\lambda,m) = \int_{l_{\min}}^{l_{\max}} P(nl;\lambda m)\cdot\Gamma(nl)\cdot \mathrm{d}l, \tag{5.174}$$

with

$$l_{\min}^2 = \frac{1}{2}\left\{\left[(n-1)^2+m^2-\lambda^2\right] - \sqrt{\left[(n-1)^2+m^2-\lambda^2\right]^2 - 4(n-1)^2 m^2}\right\} \tag{5.175}$$

and

$$l_{\max}^2 = \frac{1}{2}\left\{\left[(n-1)^2+m^2-\lambda^2\right] + \sqrt{\left[(n-1)^2+m^2-\lambda^2\right]^2 - 4(n-1)^2 m^2}\right\}. \tag{5.176}$$

$\Gamma(nl)$ is the standard autoionizing rate in spherical coordinates and $P(nl;\lambda m)$ is a joint probability (with normalization equal to one) for the appearance of spherical (nl) and parabolic (λm) quantum numbers that can be expressed in terms of Clebsch–Gordan coefficients. For large quantum numbers and the condition $m < l \ll n$ (quasi-classical limit of Clebsch–Gordan coefficients that is of practical interest), the joint probability can be approximated by Bureyeva et al. (2002)

$$P(nl;\lambda m) \approx \frac{1}{\pi}\cdot\left\{\frac{2l}{\sqrt{\left(l^2-l_{\min}^2\right)\cdot\left(l_{\max}^2-l^2\right)}}\right\}. \tag{5.177}$$

Substituting quasi-classical values for the autoionization rate $\Gamma(nl)$ into (5.174) and using (5.173), we obtain an autoionizing rate in parabolic quantum numbers expressed in terms of universal functions ($t = l/l_{\text{eff}}$, $l_{\text{eff}} = (3Z^2/\omega)^{1/3}$):

$$\Gamma(n,\lambda,m) = \frac{f_{\text{ij}}}{\pi\cdot n^3}\cdot I(t_{\min},t_{\max}), \tag{5.178}$$

$$I(\mathrm{t}_{\min},\mathrm{t}_{\max}) \approx \frac{2}{l_{\max}}\cdot\left(\frac{3Z^2}{\omega}\right)^{2/3}\cdot \mathrm{Y}\left(l_{\min}\cdot(\omega/3Z^2)^{1/3}\right), \tag{5.179}$$

$$Y(x) \approx 0.284\cdot\exp\left(-2x^3\right). \tag{5.180}$$

f_{ij} is the oscillator strength of the core transition with charge Z (e.g., the oscillator strength corresponding to the transition $1s-2p$ in H-like Al for the He-like $2lnl'$-satellites, $Z = 13$). The formulas (5.174)–(5.180) demonstrate likewise a broad distribution over the electric quantum number λ that finally results in an increase of the dielectronic recombination rate.

References

V.A. Astapenko, Impact ionization of atoms: calculation in the Born-Compton approximation. Laser Phys. **11**, 1336 (2001)

V.A. Astapenko, *Polarization Bremsstrahlung on Atoms, Plasmas, Nanostructures and Solids* (Springer, Berlin, 2013)

V.A. Astapenko, A. Eletskii, V. Kudrya, P. Ventzek, Calculation of the cross-sections for electron impact excitation of magnesium. Laser Phys. **10**, 1220 (2000)

V.A. Astapenko, V.S. Lisitsa, *Collisional Processes in low Temperature Plasma* (MIPT-Textbook, Moscow, 2007). (in Russian)

J.G. Baker, D.H. Menzel, Physical processes in gazeous nebulae. Astrophys. J. **88**, 52 (1938)

V.A. Bazylev, M.I. Chibisov, Excitation and ionization of multicharged ions by electron collisions. Phys.-Usp. **24**, 276 (1981)

I.L. Beigman, L.A. Vainshtein, B.N. Chichkov, Dielectron recombination. JETP **53**, 490 (1981)

I.L. Beigman, L.A. Vainshtein, M. Brix, A. Pospieszczyk, I. Bray, D.B. Fursa, YuV Ralchenko, Excitation and ionization cross-sections for HeI from normalized Born and *K*-matrix calculations: $\Delta S = 0$ transitions from $n = 2,3$ excited states. ADNDT **74**, 123 (2000)

V.B. Berestetskii, L.P. Pitaevskii, E.M. Lifshitz, *Quantum Electrodynamics* (Elsevier, Oxford, 1982)

H.A. Bethe, E.E. Salpeter, *Quantum Mechanics of One- and Two-Electron Atoms* (Plenum Publishing, New York, 1977)

D. Braunstein, S. Shuker, X-ray laser without inversion in a three-level ladder system. Phys. Rev. A **68**, 013812 (2003)

L.A. Bureyeva, T. Kato, V.S. Lisitsa, C. Namba, Quasiclassical representation of autoionization decay reates in parabolic coordinates. J. Phys. B: At. Mol. Opt. Phys. **34**, 3909 (2001)
L.A. Bureyeva, T. Kato, V.S. Lisitsa, C. Namba, Quasiclassical theory of dielecronic recombination in plasmas. Phys. Rev. A **65**, 032702 (2002)
A. Burgess, Dielectronic recombination and the temperature of the solar corona. Astrophys. J. **139**, 776 (1964)
H.K. Chung, C. Bowen, C.J. Fontes, S.B. Hansen, Yu. Ralchenko, Comparison and analysis of collisional-radiative models at the NLTE-7 workshop. HEDP **9**, 645 (2013)
J. Colgan, C.J. Fontes, H. Zhang, J. Abdallah Jr., Collisional-radiative modeling of Tungsten at temperatures of 1200–2400 eV. Atoms **3**, 76 (2015). https://doi.org/10.3390/atoms3020076
R.D. Cowan, Resonant-scattering (autoionisation) contributions to excitation rates in O^{4+} and similar ions. J. Phys. B: At. Mol. Opt. Phys. **13**, 1471 (1980)
R.D. Cowan, *The Theory of Atomic Structure and Spectra* (California University Press, 1981)
R.D. Cowan, Effects of autoionising levels in highly ionized atoms. Phys. Scr. **T3**, 200 (1983)
J. Davis, V.L. Jabobs, Effects of plasma microfields on radiative transitions from atomic levels above the ionization threshold. Phys. Rev. A **12**, 2017 (1975)
B. Deschaud, O. Peyrusse, F.B. Rosmej, Generalized atomic physics processes when intense femtosecond XUV- and X-ray radiation is interacting with solids. Europhys. Lett. **108**, 53001 (2014)
B. Deschaud, O. Peyrusse, F.B. Rosmej, Atomic kinetics for isochoric heating of solid aluminum under short intense XUV free electron laser irradiation. HEDP **15**, 22 (2015)
R.C. Elton, *X-Ray Lasers* (Academic Press, New York, 1990)
E. Fermi, Über die Theorie des Stoßes zwischen Atomen und elektrisch geladenen Teilchen. Zeitschrift für Physik **29**, 315 (1924)
V. Fischer, V. Bernshtam, H. Golten, Y. Maron, Electron-impact excitation cross-sections for allowed transitions in atoms. Phys. Rev. A **53**, 2425 (1996)
M.N. Gailitis, The use of the Bethe approximation in calculating the excitation cross-section of an ion by electrons (in Russian), in *Atomic Collisions* (Latvian State University, Riga, 1963), p. 93
J.N. Gau, R.J.W. Henry, Excitation of lithumlike ions by electron impact. Phys. Rev. A **16**, 986 (1977)
M. Gryzinski, Classical theory of electronic and ionic inelastic collisions. Phys. Rev. **115**, 374 (1959)
M. Gryzinski, Two particle collisions. I. General relations for collisions in the laboratory system. Phys. Rev. **138**, A305 (1965a)
M. Gryzinski, Two particle collisions. II. Coulomb collisions in the laboratory system of coordinates. Phys. Rev. **138**, A322 (1965b)
M. Gryzinski, Classical theory of atomic collisions. I. Theory of inelastic collisions. Phys. Rev. **138**, A336 (1965c)
Y. Hahn, Plasma density effects on the three-body recombination rate coefficients. Phys. Lett. A **231**, 82 (1997)
Y. Hahn, J. Li, Transient behavior of nonequilibrium plasma formed by merged beams. Zeitschrift für Physik **D36**, 85 (1996)
W. Heitler, *The Quantum Theory of Radiation* (Dover, New York, 1984)
J. Jackson, *Classical Electrodynamics*, 3rd ed. (Wiley, 1998), ISBN: 978-0-471-30932-1
V.J. Jacobs, J. Davis, Properties of Rydberg autoionizing states in electric field. Phys. Rev. A **19**, 776 (1979)
V.J. Jacobs, J. Davis, P.C. Kepple, Enhancement of dielectronic recombination by plasma electric microfields. Phys. Rev. Lett. **37**, 1390 (1976)
T. Kato, E. Asano, Comparison of recombination rate coefficients given by empirical formulas for ions from hydrogen through nickel. NIFS-DATA-54 (June 1999)
T. Kato, K. Masai, M. Arnaud, Comparison of ionization rate coefficients of ions from hydrogen through nickel. NIFS-DATA-14 (Sept. 1991)
D.P. Kilcrease, S. Brookes, Correction of near threshold behavior of electron collisional excitation cross-sections in the plane-wave Born approximation. HEDP **9**, 722 (2013)
Y.-K. Kim, M.E. Rudd, Binary-encounter-dipole model for electron-impact ionization. Phys. Rev. A **50**, 3954 (1994)

V.I. Kogan, A.B. Kukushkin, V.S. Lisitsa, Kramers electrodynamics and electron-atomic radiative-collisional processes. Phys. Rep. **213**, 1 (1992)
L.D. Landau, E.M. Lifschitz, *The Classical Theory of Fields* (Pergamon, Oxford, 2003)
L.D. Landau, E.M. Lifschitz, *Mechanics* (Elsevier, Oxford, 2005)
W. Lotz, Electron impact-ionization cross-sections for atoms up to $Z = 108$. Zeitschrift für Physik **232**, 101 (1970)
R. Loudon, *The Quantum Theory of Light*, 3rd ed. (Oxford Science Publications, 2000)
P. Mansbach, J. Keck, Monte Carlo Trajectory calculations of atomic excitation and ionization by thermal electrons. Phys. Rev. **181**, 275 (1969)
S.A. Mayorov, A.N. Tkachev, S.I. Yakovlenko, Metastable supercooled plasma. Physics Uspekhi **37**, 279 (1994)
NIST (2019). http://www.nist.gov
I.C. Percival, M.J. Seaton, The polarization of atomic line radiation excited by electron impact. Philos. Trans. Royal Soc. London Ser. A Math. Phys. Sci. **251**, 113 (1958)
F. Petitdemange, F.B. Rosmej, Dielectronic satellites and Auger electron heating: irradiation of solids by intense XUV-free electron laser radiation, in *New Trends in Atomic & Molecular Physics—Advanced Technological Applications*, vol. 76, ed. by Mohan (Springer, 2013), pp. 91–114, ISBN 978-3-642-38166-9
H. Van Regemorter, Rate of collisional excitation in stellar atmospheres. Astrophys. J. **136**, 906 (1962)
F. Robicheaux, M.S. Pindzola, Enhanced dielectronic recombination in crossed electric and magnetic fields. Phys. Rev. Lett. **79**, 2237 (1997)
F.B. Rosmej, Diagnostic properties of Be-like and Li-like satellites in dense transient plasmas under the action of highly energetic electrons. JQSRT **51**, 319 (1994)
F.B. Rosmej, The He_β-emission in dense non-Maxwellian plasmas. J. Phys. B Lett: At. Mol. Opt. Phys. **33**, L1 (2000)
F.B. Rosmej, X-ray emission spectroscopy and diagnostics of non-equilibrium fusion and laser produced plasmas, in *Highly Charged Ion Spectroscopic Research*, ed. by Y. Zou, R. Hutton (Taylor and Francis 2012), pp. 267–341, ISBN: 978-1-4200-7904-3
F.B. Rosmej, A.Ya. Faenov, T.A. Pikuz, F. Flora, P. Di Lazzaro, S. Bollanti, N. Lizi, T. Letardi, A. Reale, L. Palladino, O. Batani, S. Bossi, A. Bornardinello, A. Scafati, L. Reale, Line formation of high intensity He_β-Rydberg dielectronic satellites $1s3lnl'$ in laser produced plasmas. J. Phys. B Lett.: At. Mol. Opt. Phys. **31**, L921 (1998)
F.B. Rosmej, R. Stamm, V.S. Lisitsa, Convergent coupling of Helium to the H/D background in magnetically confined plasmas. Europhys. Lett. **73**, 342 (2006)
F.B. Rosmej, V.A. Astapenko, V.S. Lisitsa, L.A. Vainshtein, *Dielectronic recombination in non-LTE plasmas*, Matter and Radiation at Extremes (Review) **5**, 064601 (2020). https://doi.org/10.1063/5.0014158
J.G. Rubiano, R. Florido, C. Bowen, R.W. Lee, Yu. Ralchenko, Review of the 4th NLTE Code Comparison Workshop. HEDP **3**, 225 (2007)
V.P. Shevelko, L.A. Vainshtein, *Atomic Physics for Hot Plasmas* (IOP Publishing, Bristol, 1993)
I.I. Sobelman, A.V. Vinogradov, On the problem of extreme UV and X-ray lasers, in *Advances in Atomic and Molecular Physics*, vol. 20, 327, ed. by S.D. Bates, B. Bederson (Academic Press, New York, 1985)
I.I. Sobelman, L.A. Vainshtein, *Excitation of Atomic Spectra* (Alpha Science, 2006)
V.N. Thytovich, I.M. Oiringel, *Polarization Bremsstrahlung of Particles and Atoms* (Plenum, New York, 1991)
L.A. Vainshtein, V.P. Shevelko, *Program ATOM*, Preprint No. 43, (Lebedev Physical Institute, Moscow, 1996)
G.S. Voronov, A practical fit formula for ionization rate coefficients of atoms and ions by electron impact: $Z = 1$–28. ADNDT **65**, 1 (1997)
J.G. Wang, T. Kato, I. Murakami, in Dielectronic Recombination Rate Coefficients to Excited States of He from He^+. NIFS-DATA-53 (1999)